UNIVERSITÀ
DEGLI STUDI
DI PADOVA

Sede Amministrativa: Università degli Studi di Padova

Dipartimento di Scienze Chimiche

CORSO DI DOTTORATO DI RICERCA IN: SCIENZE MOLECOLARI
CURRICOLO: SCIENZE CHIMICHE
CICLO: XXXII

SUPRAMOLECULAR CHEMOSENSORS FOR THE DETECTION OF PHENETHYLAMINES

Coordinatore: Prof. Leonard J. Prins
Supervisore: Prof. Fabrizio Mancin

Dottorando: Daniele Rosa-Gastaldo

CONTACTS:

Dipartimento di Scienze Chimiche
Università degli Studi di Padova
Via Francesco Marzolo, 1
35131 Padova – Italy
https://www.chimica.unipd.it/

Daniele Rosa-Gastaldo
daniele.rosag@gmail.com
ORCID: 0000-0002-6396-6035

Prof. Fabrizio Mancin
fabrizio.mancin@unipd.it
ORCID: 0000-0003-0786-0364

Ai miei genitori

Learn from yesterday,

live for today,

look to tomorrow,

rest this afternoon.

Charles M. Schulz

Sommario

In questa tesi ho descritto e discusso i risultati ottenuti nell'ambito di un progetto di ricerca focalizzato sull'applicazione e lo sviluppo della tecnica dell'NMR-chemosensing. Questa tecnica è basata sulla combinazione di nanoparticelle d'oro da 2 nm di diametro passivate con opportuni tioli e di particolari esperimenti NMR e consente di "estrarre" dallo spettro NMR di una miscela di composti lo spettro NMR dell'analita riconosciuto dalla nanoparticella. In particolare, lo scopo primario del mio lavoro è stato dimostrare come questa tecnica possa essere usata con successo per il rilevamento delle cosiddette "designer drugs".

La maggior parte delle nuove droghe immesse sul mercato ogni anno altro non sono che analoghi strutturali di droghe già diffuse. Ciò rappresenta un grave problema di salute pubblica, perché non essendo queste nuove sostanze mai state studiate, non se ne conoscono i potenziali rischi e gli effetti a lungo termine. In più, non esistendo standard di riferimento, la loro rilevazione con tecniche tradizionali risulta difficoltosa. La tecnica che verrà descritta è stata testata e funziona anche su campioni reali, senza bisogno di pretrattamento del campione, e dà la possibilità di arrivare dal sequestro alla caratterizzazione strutturale della sostanza stupefacente nel giro di poche ore.

Dimostrerò anche che per migliorare le potenzialità dell'NMR chemosensing in termini sia di sensibilità che versatilità si può agire su un doppio fronte. Da un lato, è possibile migliorare la struttura del tiolo che ricopre le nanoparticelle, ottenendo un monostrato con maggior affinità e maggior capacità di trasferimento della magnetizzazione, entrambi aspetti fondamentali della tecnica. Dall'altro, è possibile migliorare la sensibilità agendo direttamente sul tipo di esperimento utilizzato, anche in abbinamento ad astuzie che possano aumentare l'efficienza del trasferimento di magnetizzazione, quali ad esempio usare l'acqua intrappolata nel monostrato come fonte supplementare di magnetizzazione oppure sfruttare la capacità delle nanoparticelle d'oro di autoassemblarsi su nanosfere di silice per aumentare le dimensioni del nanorecettore.

Combinando tutte queste accortezze, dimostrerò come sia possibile analizzare con questa tecnica anche specie inorganiche, come K^+, che di per sé non possiedono alcun segnale NMR.

Infine, visto che l'NMR non è, per ora, una tecnica di facile applicazione per analisi sul campo, nell'ultima parte di questo lavoro di tesi mi sono occupato anche un sensore point-of-care sviluppato sotto forma di cartina indicatrice, in cui un recettore supramolecolare autoassemblato composto da un cucurbiturile e un colorante può indicare selettivamente la presenza o meno di sostanza stupefacenti in modo rapido, sicuro ed economico.

Abstract

In this work I described and discussed the results of a research project which focused on both development and application of the NMR-chemosensing technique. This technique is based on the combination of gold nanoparticles 2 nm in diameter coated with specific thiols and particular NMR experiments, and it allows to "extract" from the NMR spectrum of a mixture of substances the single NMR spectrum of the analyte bound by the nanoparticle. Specifically, the main goal of my work was to demonstrate how this technique can be successfully used for designer-drug detection.

The majority of the new drugs that appear on the market every year belong to this category, i.e. they are structural analogs of already well-known drugs. Designer drugs represent a big health issue, because no studies on them are available, therefore the risks and potential long-term adverse effects are not known. Moreover, as reference standards are not available, their sensing with routine techniques is difficult. The technique that I will describe also works on real street samples, with no pretreatment, thus giving the possibility to get from the seizure of the powder to the characterization of the substance in a few hours.

I'll also show that to improve the potentialities of NMR chemosensing in terms of detection limit and sensitivity one can work from two sides. First, it is possible to improve the design of the coating thiol, obtaining a monolayer with different affinities and different capability of magnetization transfer, both crucial aspects for the technique. On the other hand, it is possible to improve sensitivity by acting directly on the type of NMR experiment used as well, also in combination with tricks that exploit magnetization enhancement, such as using the water trapped in the monolayer as an additional magnetization source or using the capability of gold nanoparticles to self-assemble on silica nanospheres, in order to enhance the nanoreceptor's size. Combining all the various things, I will demonstrate how it is possible to sense inorganic species too, such as K^+, which do not have an NMR signal per se.

Finally, as NMR is not, as of now, a technique that is easy to apply for on-field analysis, in the last part of this paper I propose a point-of-care sensor developed in the form of an indicator strip in which a self-assembled supramolecu-

lar receptor composed of a cucurbituril and a dye can selectively sense the presence, or not, of a drug in a quick, safe and cheap way.

Table of contents

4 Enhanced detection of analytes by water-STD

5 Colorimetric supramolecular sensor for quick detection of N-BOMes

1

General introduction

1.1 Supramolecular chemistry, complementarity and self-assembly

"Supramolecular chemistry is the chemistry of intermolecular bond, covering the structures and functions of the entities formed by association of two or more chemical species"

This is the definition of supramolecular chemistry that Jean Marie Lehn, Nobel Prize in Chemistry in 1987, gave in his Nobel Lecture.[1] The first key concept here is "intermolecular bond"; supramolecular chemistry involves more than a molecule at the same time. These molecules interact and form an "entity", the supramolecular complex, given by their association. Supramolecular chemistry is characterized by non-covalent interactions, such as electrostatic interactions, hydrophobic interactions, coordination bonds, hydrogen and halogen bonds, π-stacking and more. These interactions all have different characteristics: for example, if the electrostatic interaction is strong and non-directional, hydrogen bond is direction dependent and it occurs only between specific moieties; both are medium dependent, but not in the same way. All

these interactions must be considered by the supramolecular chemist as building blocks to create complementarity, the second key point of supramolecular chemistry.

If we want a successful interaction between two molecules, they need to have complementary interaction sites. One should be a good donor, or in supramolecular terms a host, the other a good acceptor, a guest. The effectiveness of these sites can be improved using a third key concept: cooperativity. As a general rule, non-covalent interactions are weaker than covalent bonds, but by pairing two or more cooperative interactions one can sum up their strength in a multipoint interaction. This kind of interaction can be highly specific, but reversible. If we think about an enzyme and its substrate, we can have an example of what a supramolecular interaction is. In the binding pocket, highly specific for the substrate, multiple interactions allow the specific binding with a molecule that has complementary interaction sites.

The last key concept of supramolecular chemistry is self-assembly: the information encoded in the combination of the weak interactions can lead to spontaneous assembly. Self-assembled structures are highly ordered and thermodynamically stable. The building block of a self-assembled structure can be a molecule, but also a nanostructure.

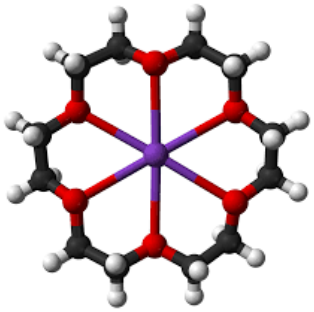

Figure 1.1. Example of supramolecular complex: multipoint interaction between K^+ and 18-crown-6.

The key concepts expressed above, the foundation of supramolecular chemistry, can be also applied to another category: sensors. If we associate the terms complementarity, specificity, and reversibility to a sensor, they look familiar.

In the rest of the chapter we will have a small journey in how supramolecular chemistry has been used -effectively- for the development of chemical sensors.

1.2 Chemical sensors

A sensor is a device that detects the value of a measurable physical property, or its changes. It can be mechanical, electronical or of a different nature: even if we don't realise it, we deal with sensors in our everyday life. Sensors are part of our routine because they are useful in many fields: for example, one can find sensors in the thermostat that is regulating the temperature of the living room; a sensor prevents the washing machine and dishwasher from starting if the door is not properly closed; there's a sensor in the differential switch that turns off the electricity if there is a failure in the electric plant at home; a sensor reminds you to fasten your seatbelt before driving, with its loud and persistent beeping.

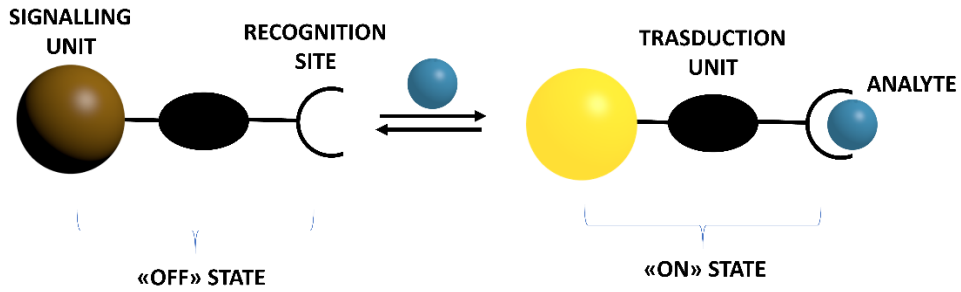

Figure 1.2. Schematic representation of a generic sensor with its components

The broad definition above also encompasses a different category of sensors, less known to the general public but still useful and very used: molecular sensors. To quote Czarnik's definition,[2] a molecular sensor is defined as "*a molecule of abiotic origin that signals the presence of energy or matter*" hence, a su-

pramolecular receptor capable of selectively form (with just a single analyte, or category of analytes of interest) a bond (that is reversible, covalent or non-covalent) which induces a change of a property of the sensor itself.[3] It's the measure of this change that allows the detection and quantification of the presence of the analyte in systems that can even be complex, such as body fluids, cells or living organisms. The molecular sensors synthesized in a lab are called chemical sensors, the ones built from biological materials are called biosensors: both are in the category of chemosensors. Molecular sensors usually exhibit a change in the magnetic or electronic properties while going from their "on" to "off" state and vice versa. These properties are of particular interest because they can be modulated by changing an external source (the analyte), that can be an ion, a small molecule, a protein but also - simply - light. A sensor has basically two main functions: the first one is to form selective interactions with the target (the analyte of interest) in such a way that the latter can be distinguished from other species, even those with similar properties or similar structure. The part responsible for this function is the recognition unit, or receptor. The second function of a sensor is crucial, because it allows the user to understand if the recognition has occurred or not, through a signal that can be easily registered or analyzed. The moiety designed for this function is the signalling unit, or reporter. A mechanism for signal transduction guarantees the communication between these two units.

Molecular receptors, hosts in supramolecular chemistry, are defined as organic structures kept together by covalent bonds, capable to bind, in a selective way, ionic or neutral substrates using one or multiple interactions and thus leading to the formation of a supramolecule. Hence, the chemistry of an artificial receptor represents a chemical generalization of coordination chemistry, one that does not limit its applications to transition metal ions, but it is extended to all substrates: cationic, anionic or neutral of organic, inorganic or biological nature. To guarantee a high degree of recognition, while designing the receptor one should consider the number, nature and position of covalent and noncovalent interactions that will take place between the receptor and

the analyte of interest, modulating them accordingly to the molecule of interest: its therefore necessary to apply the design principles of supramolecular chemistry to the receptor, with the aim of obtaining the desired molecular interaction, increasing the stability of the host-guest complex using multiple cooperating interactions. The reporter is chosen carefully according to its electrochemical or spectroscopical properties and to the possible transduction mechanism, that ensures that the reported properties are modified by the nearby host-guest interaction.

1.3 The classical approach to sensors

Historically, the oldest type of sensors is called fluorescent intrinsic, i.e. systems in which the analyte bounds to a recognition site that is part of a π-system of the fluorophore. In these systems there is therefore a direct interaction between the substrate and the fluorescent probe, that produces a modification of the fundamental or excited state and consequently a variation in its emission spectrum.

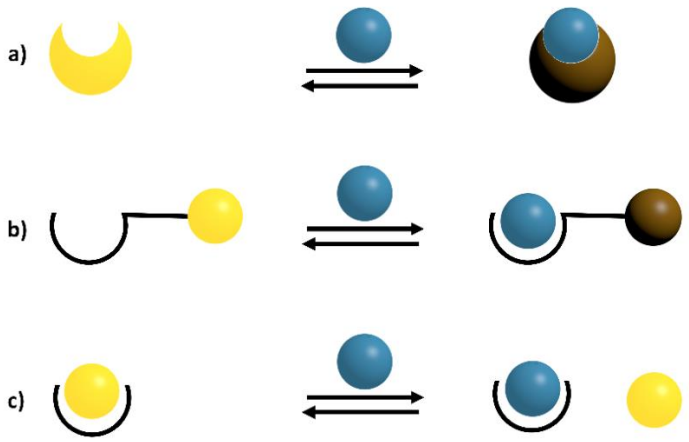

Figure 1.3. schematic representation of the structures of the sensors discussed in this chapter: a) classical; b) intrinsic c) self-assembled.

A fluorescent reporter is a convenient choice because fluorescence spectroscopy is a sensitive method with high spatial and temporal resolution, fast, relatively cheap, and easy to set up. Fluorescent emission is a versatile method because it can be monitored as emission itself or as quenching of emission, as variation of the maximum or shape of the emission spectrum, or also as a lifetime measurement. Moreover, some species that are non-emissive can become fluorescent upon derivatization or complexation. An intrinsic receptor has the advantage to grant a direct interaction between the bound analyte and the fluorophore, that leads to a modification of the emission properties of the latter. In this case, the transduction mechanism is directly connected (intrinsic) with the structure of the chemosensor. It must be said that a structure designed in such a way is not versatile, because modifications of the receptor to adapt it to different analytes can consequently modify the properties of the reporter, and vice versa.

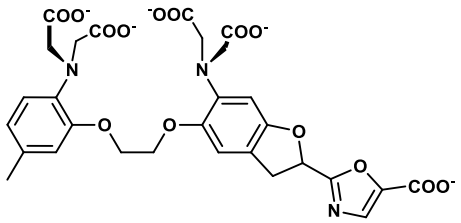

Figure 1.4: chemical structure of Fura 2, as developed by Tsien and co-workers in 1985.

For example in *Figure 1.4* is shown the structure of Fura-2, developed by Tsien[4] and co-workers in the early eighties and largely used since then in biology to determine the level of Ca^{2+} ions inside living cells. As a consequence of the complexation of the metallic cation, that involves also the aniline-type nitrogen conjugated with the π-system of the fluorophore, the electronic distribution is altered with a consequent increase of the fluorescence emission intensity. Similar sensors are available for Na^{+}, Mg^{2+}, Zn^{2+}.

Another category of fluorescent sensors, of recent development, but just as important as the previous one, are the so-called "conjugated fluorescent sensors". In these sensors, the receptor is electronically isolated from the π-system of the fluorophore by a spacer. The two subunits can hence be de-

signed and optimized separately, and then connected only as a last step: the main advantage of this approach is therefore the flexibility. On the other hand, this kind of design requires the presence of a signal transduction mechanism from receptor to reporter, and its individuation is usually trickier than in the case discussed above.

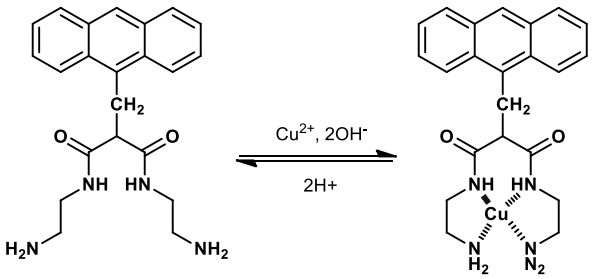

Figure 1.5. Structure of the selective Cu^{2+} sensor.

A classic example of conjugated fluorescent sensor is the molecule reported in *Figure 1.5* developed by Fabbrizzi et al.[5] In this case a selective ligand for Cu^{2+} ions, that is not fluorescent by itself, is connected by a methyl group (as electronic insulating linker) to an anthracene, the fluorescent reporter. The complexation of Cu^{2+} induces the quenching of the fluorescence emission of the reporter by electron or energy transfer from the dye to the metal ion. The decrease in emission is function of the concentration of metal ions, it is linear, and it is possible to sense copper concentrations down to the 0.1 μM. Using similar principles, it has been possible to realize many sensors for transition metals, for anions (mainly halogen halides) and for some organic molecules.

In the last decade a third design, named "self-assembled fluorescent sensors", has also been developed. In this third type of sensors, receptor and reporter are two separate molecules, distinct from each other, that must self-assemble in solution to generate the supramolecular sensing system. This approach has many advantages compared to the previous ones: optimization and modification of a sensor are pretty simple because they can be done independently for each unit. However, the identification of an effective way for the transduction of the signal between them may be a difficult task; moreover, the design of the sensor itself is not trivial and can be limited by the need of specific interac-

tions among the two units. The self-assembly of the organized system – supramolecular sensor- can be assisted by a templating agent such as a surfactant, a monolayer, a glass surface or a nanomaterial. It has to be noted that even in the final assembled system, the two subunits don't interact with each other directly but only through space vicinity.

The first example of self-assembled fluorescent sensor has been presented by Anslyn et al and it uses a strategy called "chemosensing ensemble" (now called "indicator displacement approach"). The system self-assembles using ion-ion interactions: the reporter is displaced from the binding site of the receptor by the entrance of the analyte and this variation of the chemical environment leads to a partial quenching of the fluorescence as shown in *Figure 1.6*. More in detail, Anslyn and co-workers[6] use carboxyfluorescein as reporter for the detection of citrate anion. After calibration it was possible to quantitatively determine the citrate concentration in soft drinks like Coca-Cola.

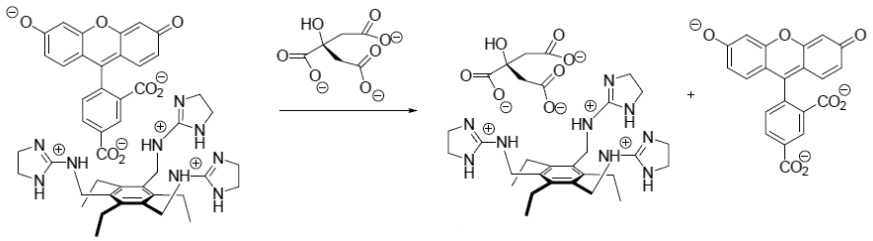

Figure 1.5. Practical application of a chemosensing ensemble, citrate quantification in lemonades

The main problem related to this approach to fluorescent as well as other class of molecular sensors is that the signal generated by the reporter is of on-off type, related to a property or a variation of a property –the emission- of the reporter itself and not of the analyte, the real target of the analysis. The analyte is identified by relying only on the specific interactions that it establishes with the receptor, or, in other words, relying only on the selectivity of the receptor: if there is an interferent in the sample to be analysed, one capable of interacting with the receptor with the same or even greater strength

than the analyte, the reporter will generate just the same signal while bonding with the former and with the latter. A situation like this is not desirable because it generates what we call a false positive signal, i.e. a signal not generated by the analyte but indistinguishable from that. This problem is considerably amplified when the selectivity of the receptor is diminished on purpose, with the aim to get more versatile sensors –not for a single target but for a class of analytes: the greater the number of species capable of interacting with the receptor, the higher the risk of false positives.

1.4 The advantages of NMR

All sensors described in the previous section are based on fluorescence. However, similar system can be based on absorbance, electric potential, as well as other spectroscopic properties. Among all the spectroscopic and analytical techniques, nuclear magnetic resonance –NMR- is a powerful alternative because it provides a lot of information on the composition and even structure of the system under analysis. An NMR signal is strongly and directly related to the molecular structure that generates it, and with the notable exception of enantiomers, all molecules have a characteristic and unique spectrum. Moreover, no pre-treatment is usually needed to analyse the sample. The limited sensitivity of the technique is going to be improved with the availability of higher magnetic fields and cryoprobes, as well as more sophisticated experimental schemes and pulse sequences. Unlike optical spectroscopies, NMR, especially in its imaging approach MRI, can also be used in vivo, since the radiofrequencies used to detect a spectrum are permeable to body tissues, which makes it non-invasive and non-destructive. Moreover, the applicability of NMR to sensing is not limited to ^{1}H nucleus, but it can effectively be applied to other nuclei, in particular ^{31}P or ^{19}F. In NMR sensors many ob-

servables can be used to follow the recognition of the analyte: upon interaction of a host with a guest, the change in the chemical neighbourhood of the two species induces a perturbation in chemical shift. This can be observed relatively to the host signals, the guest signals, or to the appearance of the supramolecule signals for the host-guest complex. From the number of the signals present upon complexation and the direction of the shift it is possible to have an insight on the dynamics of the binding. The recognition can occur in fast exchange regime on the NMR time scale, so that the signal of the supramolecular complex will be an average between the signal of the free analyte and the complexed one; or it can occur in slow exchange regime, where the signals of the supramolecular complex are clearly rising as a separate set of signals in the spectrum. Both cases are useful and bring different information (detailed information will be provided in next two chapters). In the case of chemical shift modification, the feasibility is not limited to ^{1}H, it is even more useful when other nuclei, for example ^{19}F, are used. In the first case, the region of interest is limited to 10 ppm, in the second the useful range is spread on 400 ppm, so small differences in chemical shift are more easily appreciated and there is limited possibility of superimposing. But the difference in chemical shift is not the sole observable. Upon complexation, if the receptor is big enough –as proteins or nanoparticles- or has paramagnetic properties –as gadolinium- the longitudinal and transversal relaxation rates T_1 and T_2 of the analyte can be perturbed. In the same situation, perturbation of diffusion coefficients or differences in NOE map patterns amongst the involved molecules are often found. In the next two paragraphs I will discuss two categories of NMR approach to sensors, which are relevant for the goal of this thesis: discriminative sensing, and NMR-chemosensing.

1.5 Discriminative sensing

The first examples of NMR discriminative sensing come from the works of the groups of Swager[7–10] and Shiller[11,12]. A particularly nice example is a ^{19}F based detector for identification of neutral organic compounds: aliphatic and aromatic organic nitriles[7]. A good check list for a discriminative receptor is the following: the recognition event has to produce a supramolecular complex with NMR properties that differ from those of both the analyte and the receptor. At least one of the signals of the supramolecular complex has to be different from that of the guest alone. This happens only if the complex is formed in slow exchange with the free species. Since a discriminative sensor is used to detect a whole category of similar molecules, one signal rising from the sensor might not be enough for an unambiguous discrimination, so there must be the possibility to either build several sensors with analogue structure and different signals, or one sensor with multiple non-equivalent signals. As a third and last requirement, the chemical shift induced by the complexation on ^{19}F signals must be related only to spatial proximity, so that one can gather information on both the binding event and chemical structure.

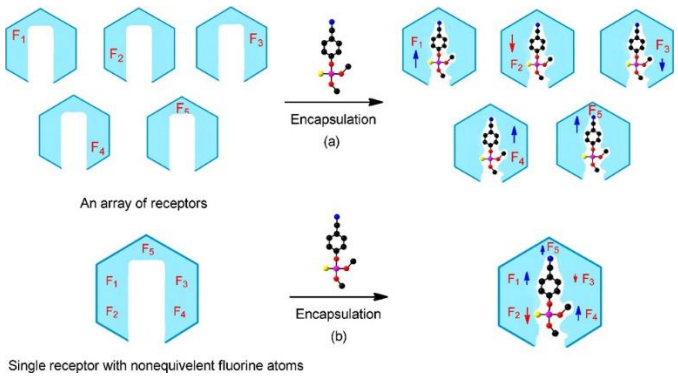

Figure 1.6. Schematic illustration of nitrile sensing with a calix[4]arene tungsten imido complex: a) discrimination through multiple non-equivalent fluorinated sensors; b) discrimination through a single sensor with multiple non-equivalent fluorines. Image from Zhao et al.[7]

One sensor that fulfils all the above requirements is a calix[4]arene tungsten-imido complex decorated with a fluorine atom on the upper rim. The encapsulation of a nitrile moiety (the analyte) induces a change in the environment inside the calixarene, displacing the coordinated molecules of solvent. This reflects on a change of chemical shift of the fluorine atom bound to the calixarene. Multiple receptors can be thus obtained by synthesizing a series of different calixarenes with the fluorine atom in different non-equivalent positions, or a single receptor with multiple fluorine atoms in non-equivalent position as depicted in *Figure 1.6*.

The sensing experiments are performed by adding a series of different nitriles, relevant for pesticides and pharmaceutical industries, to a solution of chloroform containing the calix[4]arene tungsten-imido complex. The recognition event happens when nitrile forms a coordination bond with the tungsten atom. As shown in *Figure 1.7* every different analyte (in slow exchange regime) produces a different signal in the fluorine spectrum. This means that the structure of each nitrile influences the magnetic environment around the fluorine atom in a different way, thus producing a downfield shift the entity of which (0.2- 0.9 ppm) is directly related to each structure. Of course, a mixture of the receptor with all the analytes gives a spectrum that is the sum of the spectra of the single analytes. In this case the peaks are all well separated and this can lead to a precise identification of the components of a mixture. It must be noted that in case of fast exchange the peak position would be a weighted average between the peak of the bound specie and the peak of the free specie, and in this case the system would not be discriminative.

Just like in the classical approach, here as well the signal does not stem directly from the analyte; in this case though, it does carry information about the analyte (the chemical shift) and it's not a mere concentration-related on-off. By building a library of analytes, one can understand exactly which molecule is interacting with the sensor.

The system described until now can be further complicated in order to get a better discrimination. The position (and nature) of the fluorine atom can be changed. If for the first receptor trifluoromethoxy groups were used to decorate the meta position of a benzene ring, for a second receptor ortho- or meta-trifluoromethyl groups can be used. The concept behind the differences in chemical shift is the same, but it has been noted that in case of ortho-trifluoromethyl groups, alkyl nitriles give a downfield shift and benzyl nitriles an upfield shift. The data obtained from the two receptors can be combined leading to a 2D plot in which the discrimination of nitriles is even more accurate than before (*Figure 1.8*).

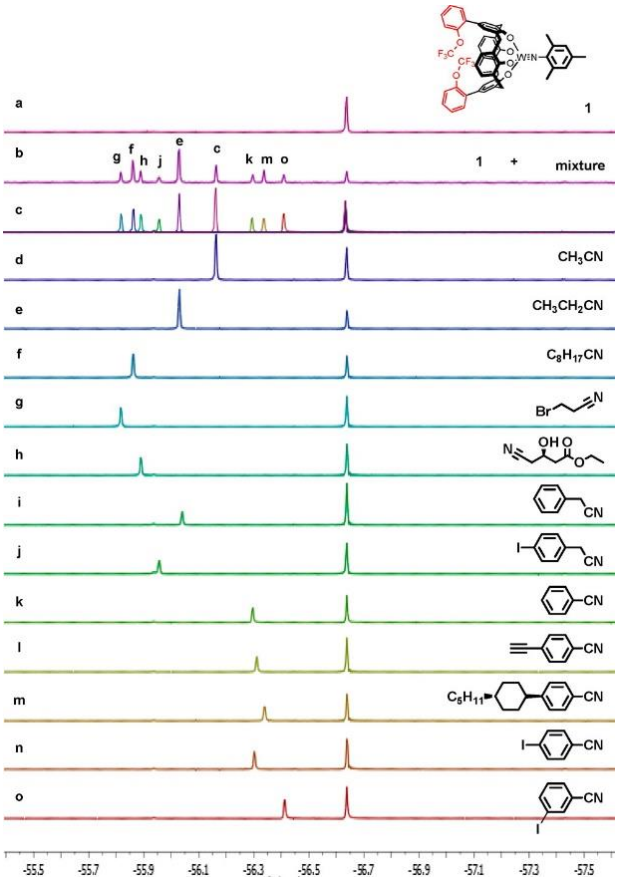

Figure 1.7. ^{19}F NMR spectra (64 scans) of the fluorinated calix[4]arene tungsten-imido complex**1** alone (a) and mixtures of complex **1** (1.0 mM in $CDCl_3$) and different analytes (2.0 mM): (a) complex **1** alone, (b) nine nitriles added to a solution of **1** in CDCl3, (c) superimposition of the spectra of complex **1** with each of the nine nitriles from (b) collected independently, (d)–(o) complex **1** bound to various nitriles. Image by Zhao et al.[7]

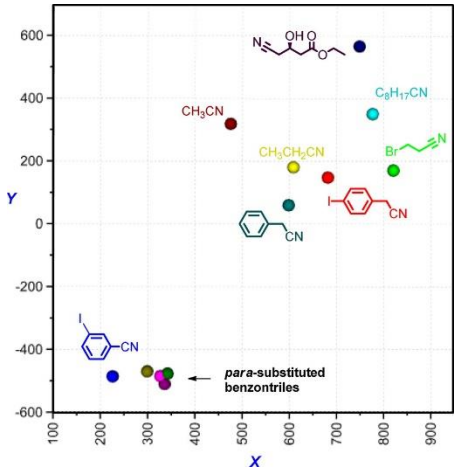

Figure 1.8. 2D scatter of the detected analytes using the ^{19}F resonances shift upon binding. On every axis, a signal from a different receptor is reported. Image by Zhao et al.[7]

The case of a single receptor with multiple non-equivalent fluorine atoms is of particular interest. In this case, a single binding event produces a pattern of variations in chemical shift that is specific and characteristic of just that analyte, because all the fluorine nuclei will be affected in a different way. Therefore, the resulting spectrum is a unique fingerprint of the specific nitrile that is interacting. Mapping the positions of different signals, it is possible to generate a multidimensional plot (3D if three different signals are used) as in *Figure 1.9*. The results obtained regard 100 µm samples with 24 min of acquisition in a 400 MHz spectrometer. With the same principle, using chiral palladium-based pincher ligands, Zhao and Swager[10] reached the simultaneous resolution and differentiation of a mixture of twelve chiral amines

The second example is a nanoparticle based boronate receptor for dopamine and 1,2-dihydroxyphenyl derivatives presented by Gabrielli et al.[13] It is well known that any molecule bound to a gold nanoparticle experiences a variation on longitudinal relaxation time T_2 that reflects on the shape of the NMR signals, with a line broadening. If the nanoparticle is big enough, the signal can even not be visible in the spectrum. The modulation of T_2 induced by the nanoparticle interaction, together with the chemical shift perturbation, are used to detect dopamine.

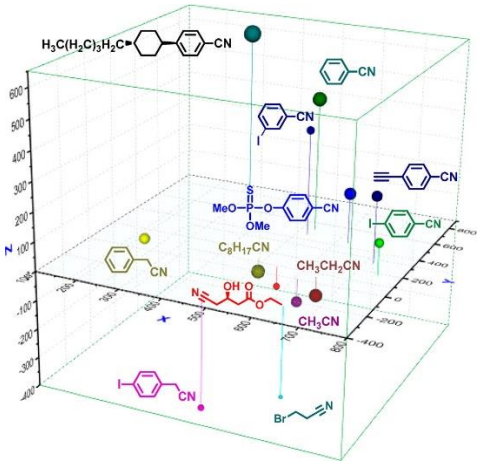

Figure 1.9. 3D scatter of the detected analytes using the ^{19}F resonances shift upon binding. On every axis, a signal from a different receptor is reported. Image by Zhao et al.[7]

A gold nanoparticle of 2 nm of diameter decorated with a monolayer of thioundecyl-α-D-glucopiranoside or thioundecyl-β-glucopiranoside is combined with a fluorophenylboronic acid so to obtain a boronate ester complex as in *Figure 1.10*. The boronate ester formed on the nanoparticle monolayer produces a signal that is not visible, because it acquires the T_2 of the nanoparticle, while when unbound - as a boronic acid, free to move in solution – it displays a sharp peak in ^{19}F NMR. When the analyte is added, this causes the displacement of the reporter from the nanoparticle and the production of a reporter-analyte complex that has again a longer relaxation times and sharper signals. So, the analyte recognition results in an increase of the correlation time of the reporter and in the sharpening of the signals. Moreover, the boronate ester that is formed gives rise to a signal that is characteristic of that analyte.

The modulation of T_2 allows the detection of the signal also by MRI, extending the potentialities of the method also to in-vivo imaging. Like in the previously reported example by Swager and co-workers, here too multianalyte detection is possible, since every different analyte generates a boronate ester with the reporter - with ^{19}F with characteristic position. In *Figure 1.11* is reported the case of dopamine, catechol and galactose. Moreover, if simple discrimination is not the only goal, this system offers the possibility of barcoding as well. It is

sufficient to use three different reporters (a thing as simple as mixing the glucose decorated gold nanoparticle with three different aromatic boronate ester reporters) to obtain a set of three independent characteristic signals from each analyte added.

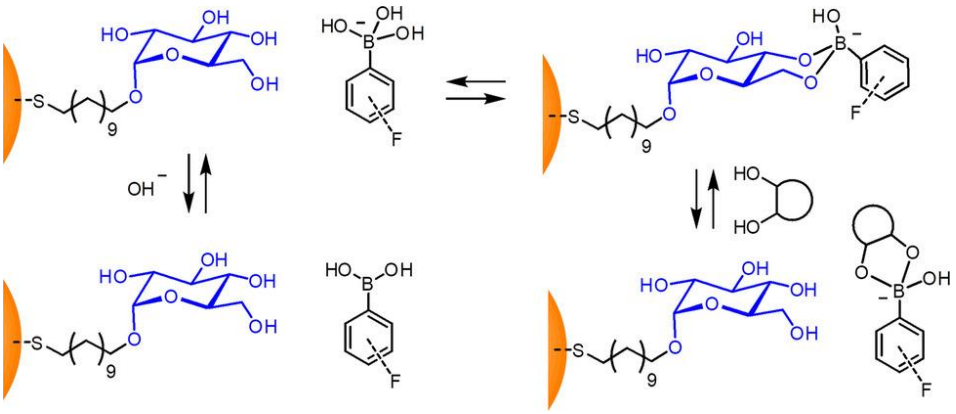

Figure 1.10. Equilibria between receptor, reporter and analyte. Image by Gabrielli et al.[13]

With the system described by Gabrielli et al,[13] it is possible to perform quantitative determination as well. In their example, a simple titration experiment of the adduct nanoparticle-reporter with increasing concentrations of dopamine, the integrated area of the signal of the adduct dopamine reporter increases linearly with the concentration of the reporter, so building a calibration curve allows quantitative determination. It has been shown that quantification is possible even in the presence of sugars like glucose and galactose, and even in urine, with a detection limit of 10 um with 50 minutes of acquisition time.

The two examples described in this chapter have one thing in common: the discriminative chemosensor, compared to the classical chemosensors can succeed in their task also when multiple and similar analytes are present in solution, and even when the concentration of interferents is above their detection concentration. This happens because the signal from the analyte carries information on which molecule is interacting with the receptor. This di-

minishes the issue of false positives. Still, if an unknown analyte is interacting whit the system, there is not an immediate way to identify it.

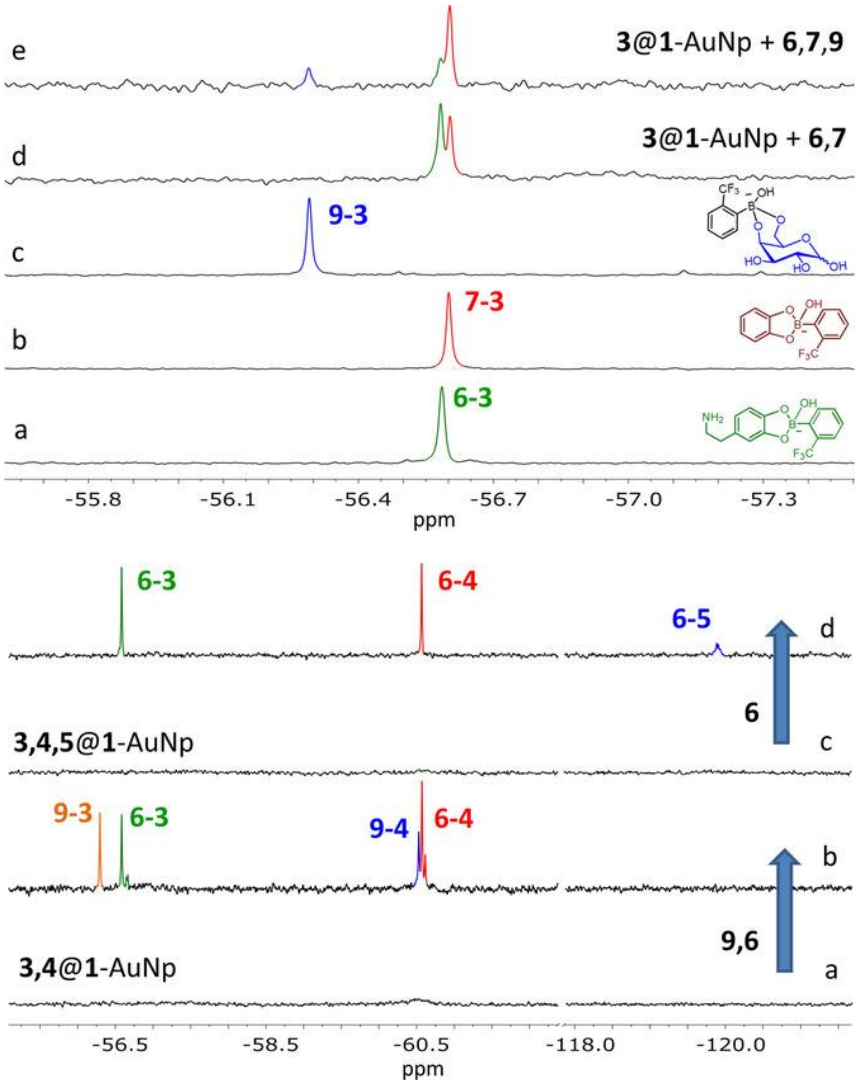

Figure 1.11 ^{19}F-NMR detection of dopamine (**6**) with **3@1**-AuNp and **4@1**-AuNP. a) Spectrum of **1-AuNp** and **3** (7.14 and 170 μM, respectively) in[D_6]DMSO; b) spectrum of the same mixture after the addition of NaOD (0.001%);c) spectrum of the same mixture after the addition of **6** (200 μM); d) spectrum of a mixture of **3** and **6** (170 and 300 μM, respectively)in [D_6]DMSO/NaOD (0.001%); e) spectrum of **1-AuNp** and **4** (7.14 and 170 μM, respectively) in [D_6]DMSO; f) spectrum of the same mixture after the addition of NaOD (0.001%); g) spectrum of the same mixture after the addition of **6** (200 μM); h) spectrum of a mixture of **4** and **6** (170 and 300 μM, respectively) in [D_6]DMSO/NaOD (0.001%). Image and caption adapted from Gabrielli et al.[13]

1.6 NMR-chemosensing

To overcome the problem of false positives, and to sense and recognize unknown molecules as well, a technique called NMR chemosensing has been developed by Mancin and co-workers. As discussed earlier, NMR spectroscopy is a very powerful and versatile technique. However, it fails when attempting to detect a single molecule in a complex mixture. The NMR chemosensing technique allows the virtual separation of the spectrum of these substances and gives the possibility to assign the structure of the analyte.

Indeed, the signal generated is not coming from a property of the sensor, but it's the full NMR spectrum of the analyte. By using the structural information given as response, it is possible to understand which exact analyte is interacting and it is possible to detect false positives because a potential interferent will have a different NMR spectrum with respect to the analyte itself. Hence, it is possible to build a non-specific sensor, capable of interacting and binding not just one, but a whole category of analytes. The lack of selectivity of the sensor is compensated by specific properties of the signal, that in this case carries structural information. In chapter two of this thesis, we will use this strategy to build an NMR sensor for amphetamines.

NMR-chemosensing relies on the combination of monolayer coated gold nanoparticles and a peculiar NMR experiment called NOE-pumping. that recalls the NOE-pumping experiment originally proposed by Shapiro. This experiment, that will be discussed in full detail in the next chapter, exploits the magnetization (or saturation) transfer from a system of large dimension (the nanoparticle) to single molecules of small dimensions (the analytes) that interact with it. This way, only the magnetization of the interacting analytes will be retained at the end of the experiment, and their signals will be the only ones visible.

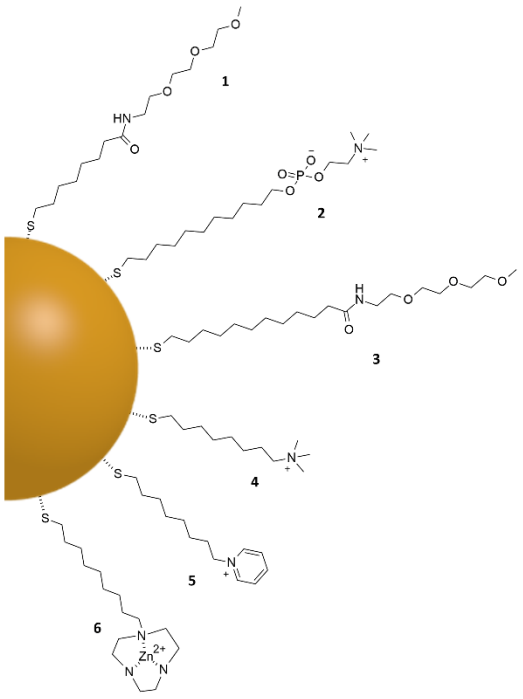

Figure 1.12. coating thiols for the gold nanoparticles discussed in this section. Each thiol coats a different batch of nanoparticles.

The technique described so far has been used by Perrone et al[14] to analyse a mixture of sodium salicylate and other hydroxybenzoates or sulfobenzoates. The distinction of these analytes by simple ^{1}H-NMR spectroscopy is not trivial. However, with the NMR-chemosensing protocol using 2 nm gold nanoparticles passivated with thiol **1** in *Figure 1.12* it is possible to isolate just the signals coming from sodium salicylate. If a calibration curve is built, it is then possible to integrate the signal of the analyte for quantitative determination. The source of selectivity in this case is the hydrophobic interaction between the coating monolayer on the nanoparticle surface and the salicylate, which is characterized by the highest octanol-water partition coefficient among the studied analytes. The use of nanoparticles covered by thiols **2** (zwitterionic) and **3** (longer hydrophobic section with respect to thiol **1**) leads to a general decrease of selectivity. However, thiol **3** has higher selectivity than **2**, suggesting that the idrophobicity given by the alkyl spacer is not the only driving

force for the recognition, but also that the terminal hydrophilic moiety does not play the only role of granting the nanoparticle solubility in water.

Since salicylate is negatively charged, the natural improvement in sensing ability would be adding a positive charge in the coating monolayer. This possibility is explored by Salvia et al with the synthesis of thiols **4** and **5** in *Figure 1.12* bearing charged ammonium groups at the end. As expected, this second interaction favours the binding of the analyte and nanoparticles coated with thiol **4** provide a sensing system more sensitive than with thiol **1**: in particular, with a concentration of nanoparticles of 15μM the reported detection limit is 0.5mM in 4 h of experiment.

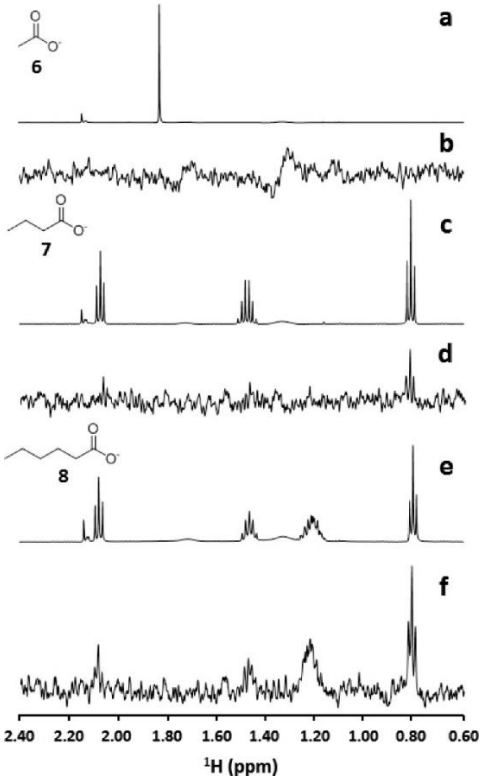

Figure 1.13: a) ^{1}H-NMR spectrum of sodium acetate (**6**). b) NOE-pumping spectrum of the same sample with gold nanoparticles coated with the thiol **4** c) ^{1}H-NMR spectrum of sodium butanoate (**7**). d) NOE-pumping spectrum of the same sample with gold nanoparticles with thiol **4**. e) ^{1}H-NMR spectrum of sodium hexanoate (**8**). d) NOE-pumping spectrum of the same sample with gold nanoparticles coated with the thiol **4**. Experimental conditions: [carboxilates]=2 mM, [AuNPs]=15 μM, carbonate buffer 20 mM, pD=10. Image by Salvia et al.[15]

Comparing the results of **4** and **1**, we can see that the introduction of a second favourable interaction (the ion pairing) fosters the binding of the substrate as least as much as the first one (the hydrophobic binding), granting higher affinity and consequently lower detection limits. This point has been proved experimentally by applying the NMR chemosensing protocol to a mixture of linear carboxylic acids of different length (2mM concentration), using the nanoparticle covered by thiol **4** as a sensor. As expected, no signal is detected in the case of acetate, a weak signal for the terminal methyl of sodium butanoate and all the signals from sodium hexanoate: so, the recognition of the analyte at lower concentrations requires in this case the presence of a negative charge and at least five carbon atoms on the analyte. Therefore, the affinity of the nanoparticle for the analyte can be tuned by means as simple as a variation of the nature of the coating thiol. Also, the AuNP coated with thiol **6** has been compared with the previous ones: if the trimethylammonium and N-alkyl pyridinium moieties are only able to provide electrostatic interactions, the one bearing a Zn^{2+} triazacyclononane moiety (Zn^{2+}-TACN) can also give coordination interactions, thus improving the binding constants of the nanoparticle and the selectivity.

AuNPs coated with thiol **6** were used by Diez-Castellnou et al[16] to detect phosphates such as metabethasone sodium phosphate (Bentelan®, a steroid) in a commercial drug tablet containing also a larger amount of sodium benzoate (and other excipients such as sodium citrate, sodium bicarbonate and polyvinylpyrrolidone). In this case, since the recognition event is not in fast exchange regime, they do not use the whole NOE-pumping experiment, but just the diffusion filter part (see infra). Signals of Bentelan® are successfully extracted from the mixture because this analyte strongly binds to the nanoparticle, assuming the same diffusion coefficient and surviving the diffusion filter.

Another application of these nanoparticles, considering that the analyte interacting with them experiences a decrease of the diffusion coefficient, could be the use as a pseudo stationary phase for NMR chromatography. 2 nm na-

noparticles don't perturb the magnetic field homogeneity, therefore they can be used, as reported so far, for NMR in solution. As they are big enough to have a slow diffusion coefficient when compared to small molecules, a mixture of analytes can be resolved according to the different time that different analytes spend bound to the monolayer surface. Salvia et al[17] used this method to successfully solve a mixture of salicylate, benzoate, tosilate, and tyramine and the results are reported in *Figure 1.13*. In this case a simply DOSY experiment can't discriminate effectively the analytes, by the contrary the same experiment in presence of monolayer coated nanoparticles with thiol 2 allows the complete separation of the signals of the molecules, even when small differences in chemical shift give superimposed signals in a normal NOE-pumping experiment.

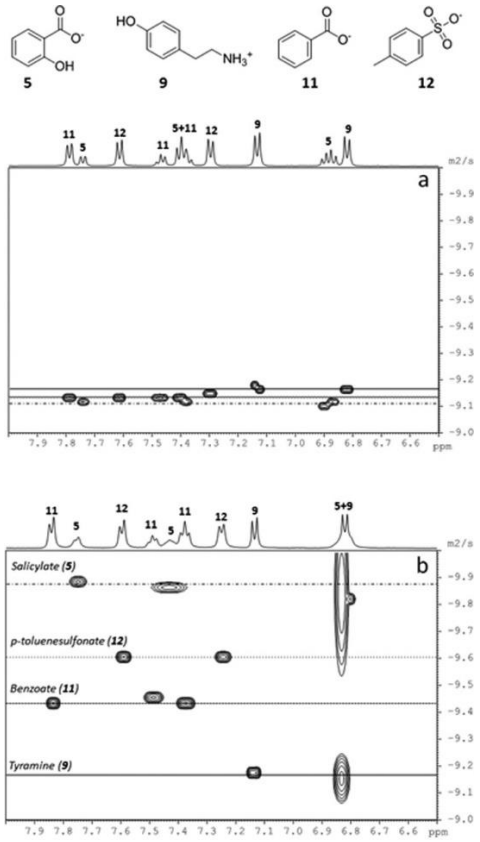

Figure 1.14: DOSY experiment on a mixture of sodium salicylate (**5**), sodium benzoate (**11**), potassium tosilate (**12**) and tyramine (**9**) in water, with (**a**) or without (**b**) the nanoparticles coated with the thiol **2**. Image by Salvia et al.[15]

1.7 Drugs of abuse, an overview

With the term drugs of abuse, we usually mean chemical substances, natural or synthetic, that are used with recreational purposes, to increase social skills, to prevent people from getting tired, to lose some inhibition or increase the excitation obtained from an experience, a party or another social activity. As opposed to that, some of drugs have the purpose to relax. In this broad definition, even alcohol (ethanol) and tobacco (nicotine) can fit. But even if the threat they pose on society is of high impact, they will be left out in the following of this thesis, mainly because they are regulated, meaning they can be sold legally, and they should be consumed accordingly to the regulations.

Illicit drugs market is in constant evolution: substances are disappearing from the market every year, and new substances appear to replace them. The increase of the drug of abuse market is confirmed also by the – more and more recurring - finding of these new substances in wastewaters. The problem here is of a double nature: first of all social, since these new substances are not tested nor produced in a controlled way. Therefore, they can be harmful not only because of the pharmacological effect per se, but also because they can contain dangerous impurities, added to enhance the effect or reduce the amount of active principle used, and also because they are not accurately dosed. The second problem, that we will discuss more deeply in the rest of the thesis, is analytical. While well-established protocols are available to detect well-known drugs, quick tests that allow fast and reliable on-field and lab monitoring and tracking are missing. When a new substance is spotted, a lot of complex procedures are required just in order to assign it a chemical structure. So, a good analytical technique for drug detection should be flexible enough to establish in the fastest and most reliable way possible if a potentially illicit drug is actually an illicit drug, and to provide identity information on the molecule present in the seized sample.

On another note, contrasting this criminal activity is just as complex as the market itself. First, the distribution of illegal drugs is different in different areas, for example if cocaine is more diffused in the south and west region of Europe, amphetamines are more diffused in the north of Europe, and controls should be done accordingly. The great infrastructures connecting all Europe are as of late used for the capillary delivery of illicit drugs, even in places where these were not known before. The global and european legislations are trying to address this problem from different angles. Bans are set on risk categories rather than on single molecules, controls are notlimited to the final product but also involvechemical precursors. For example, under control are benxyl methyl ketone (BMK), ephedrine and pseudoephedrine, piperonyl methyl ketone (PMK). These precursors, that have often drug applications themselves, can be obtained from over-the-counter medicines such as as tablet or spray preparations for cold related symptoms.

1.8 Designer drugs, the case of fentanyl

Designer drugs will be the main analytical target of this thesis as they are particularly suited to both discriminative and point of care sensing systems. A designer drug is an illegal substance obtained with small modifications of the structure of an already known active substance. On theory, the pharmacological effects of a designer drug are analogue to the ones of the parent drug, but the strength of the effects and the presence of side effects can't be known in advance. As anticipated before, designer drugs are created to improve the effect of an already existing drug, but also for legal reasons: selling an unknown substance is not forbidden, because it's not possible to ban something that is not known.

For example, fentanyl is a synthetic opioid developed in 1960s and used as a substitute of morphine, as a narcotic analgesic, as a coadjuvant in anaesthesia or for the treatment of strong pain. Fentanyl is reported to be 100 times stronger than morphine. For this reason, it is very appealing as a drug of abuse because small quantities can produce strong effects, especially if mixed with other drugs. With small modifications of the structure of fentanyl, it is possible to obtain molecules with even stronger analgesic effect. In *Figure 1.15* are reported the structures of three different opiates; carfentanyl, where to the base structure a carbomethoxy moiety is added in position 4 of the piperidine ring, is 100 times stronger than fentanyl. This means that it starts having effect from 1μg dose. Because of this, the legal use of carfentanyl is limited to veterinary treatments.

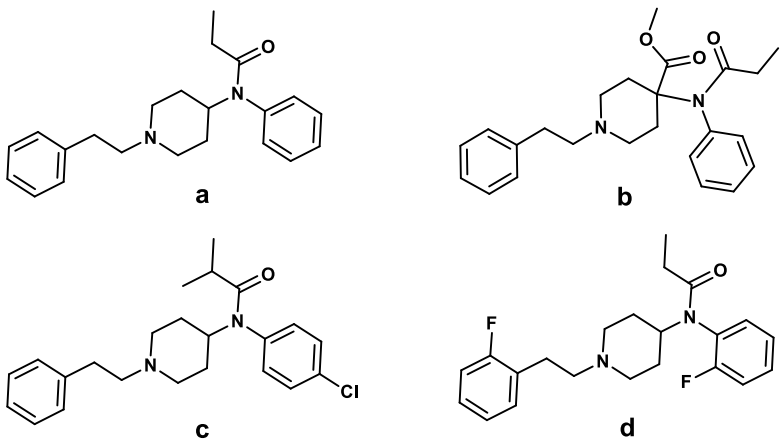

Figure 1.15: a) chemical structure of fentanyl; b) chemical structure of carfentanyl; c)-d) chemical structures of two designer-drugs based on the fentanyl chemical structure.

The other two molecules are two analogues of fentanyl that have no clinical use, but they have been reported as designer drugs seized from the illegal market. For the first one, the methyl moiety is replaced by an isopropyl, and a chlorine is inserted in position 4 of the aniline ring; for the last one, a fluorine is inserted in the meta position of both the aromatic rings. Both these molecules have been reported as cause of fatalities in Europe after overdose. It is easy to see how the potential substitutions to the fentanyl backbone are prac-

tically limitless. Indeed, more than 1400 fentanyl analogues have been reported. Every single molecule obtained has a different effective dose, different side effects and different risks. And, key point for this thesis work, as of now everyone needs a different analytical protocol to be recognized as a drug of abuse, and to be characterized. The same problems shown here for the fentanyl class of opioids, are present for other categories of drugs of abuse as well, like synthetic cannabinoids, or amphetamines and methamphetamines.

Bibliography

(1) Lehn, J. -M. Supramolecular Chemistry—Scope and Perspectives Molecules, Supermolecules, and Molecular Devices (Nobel Lecture). *Angew. Chemie Int. Ed. English* **1988**, *27* (1), 89–112.

(2) Czarnik, A. W. Supramolecular Chemistry, Fluorescence, and Sensing; 1993; pp 1–9.

(3) Bissell, R. A.; De Silva, A. P.; Gunaratne, H. Q. N.; Lynch, P. L. M.; Maguire, G. E. M.; Sandanayake, K. R. A. S. Molecular Fluorescent Signalling with "fluor-Spacer-Receptor" Systems: Approaches to Sensing and Switching Devices via Supramolecular Photophysics. *Chemical Society Reviews*. 1992, pp 187–195.

(4) Grynkiewicz, G.; Poenie, M.; Tsien, R. Y. *A New Generation of Ca2+ Indicators with Greatly Improved Fluorescence Properties*; 1985; Vol. 260.

(5) Fabbrizzi, L.; Licchelli, M.; Pallavicini, P.; Sacchi, D.; Taglietti, A. Sensing of Transition Metals through Fluorescence Quenching or Enhancement: A Review. *Analyst*. Royal Society of Chemistry 1996, pp 1763–1768.

(6) Metzger, A.; Anslyn, E. V. A Chemosensor for Citrate in Beverages. *Angew. Chemie - Int. Ed.* **1998**, *37* (5), 649–652.

(7) Zhao, Y.; Markopoulos, G.; Swager, T. M. 19F NMR Fingerprints: Identification of Neutral Organic Compounds in a Molecular Container. *J. Am. Chem. Soc.* **2014**, *136* (30), 10683–10690.

(8) Zhao, Y.; Swager, T. M. Detection and Differentiation of Neutral Organic Compounds by 19F NMR with a Tungsten Calix[4]Arene Imido Complex. *J. Am. Chem. Soc.* **2013**, *135* (50), 18770–18773.

(9) Zhao, Y.; Chen, L.; Swager, T. M. Simultaneous Identification of Neutral and Anionic Species in Complex Mixtures without Separation. *Angew. Chemie - Int. Ed.* **2016**, *55* (3), 917–921.

(10) Zhao, Y.; Swager, T. M. Simultaneous Chirality Sensing of Multiple Amines by 19F NMR. *J. Am. Chem. Soc.* **2015**, *137* (9), 3221–3224.

(11) Axthelm, J.; Görls, H.; Schubert, U. S.; Schiller, A. Fluorinated Boronic Acid-Appended Bipyridinium Salts for Diol Recognition and Discrimination via 19F NMR Barcodes. *J. Am. Chem. Soc.* **2015**, *137* (49), 15402–15405.

(12) Axthelm, J.; Askes, S. H. C.; Elstner, M.; Upendar Reddy, G.; Görls, H.; Bellstedt, P.; Schiller, A. Fluorinated Boronic Acid-Appended Pyridinium Salts and 19F NMR Spectroscopy for Diol Sensing. *J. Am. Chem. Soc.* **2017**, *139* (33), 11413–11420.

(13) Gabrielli, L.; Carril, M.; Padro, D.; Mancin, F. Multimodal 19F NMR Dopamine Detection and Imaging with a Nanoparticle-Based Displacement Assay. *Chem. - A Eur. J.* **2018**, *24* (49), 13036–13042.

(14) Perrone, B.; Springhetti, S.; Ramadori, F.; Rastrelli, F.; Mancin, F. "NMR Chemosensing" Using Monolayer-Protected Nanoparticles as Receptors. *J. Am. Chem. Soc.* **2013**, *135* (32), 11768–11771.

(15) Salvia, M. V.; Ramadori, F.; Springhetti, S.; Diez-Castellnou, M.; Perrone, B.; Rastrelli, F.; Mancin, F. Nanoparticle-Assisted NMR Detection of Organic Anions: From Chemosensing to Chromatography. *J. Am. Chem. Soc.* **2015**, *137* (2), 886–892.

(16) Diez-Castellnou, M.; Salvia, M. V.; Springhetti, S.; Rastrelli, F.; Mancin, F. Nanoparticle-Assisted Affinity NMR Spectroscopy: High Sensitivity Detection and Identification of Organic Molecules. *Chem. - A Eur. J.* **2016**, *22* (47), 16957–16963.

(17) Salvia, M. V.; Ramadori, F.; Springhetti, S.; Diez-Castellnou, M.; Perrone, B.; Rastrelli, F.; Mancin, F. Nanoparticle-Assisted NMR Detection of Organic Anions: From Chemosensing to Chromatography. *J. Am. Chem. Soc.* **2015**, *137* (2), 886–892.

2

NMR chemosensing for identification of designer drugs [a]

Summary

Properly designed monolayer-protected nanoparticles (2 nm core diameter) can be used as nanoreceptors for selective detection and identification of phenethylamine derivatives (designer drugs) in water. The molecular recognition mechanism is driven by the combination of electrostatic and hydrophobic interactions within the coating monolayer. Each nanoparticle can bind up to 30-40 analyte molecules. The affinity constants range from 10^5 to 10^6 M^{-1} and are modulated by the hydrophobicity of the aromatic moiety in the substrate. Detection of drugs candidates (as amphetamines and methamphetamines) is performed by using magnetization (NOE) or saturation (STD) transfer NMR experiments. This way, the NMR spectrum of the drug is isolated from that of the mixture, allowing broad- class multianalyte detection and even identification of unknowns. The introduction of a dimethylsilane moiety

[a]This chapter is an adapted and extended version of a manuscript which I co-authored and that has been already published during my PhD: *Detection and identification of designer drugs by nanoparticle-based NMR chemosensing*, L. Gabrielli‡, D. Rosa-Gastaldo‡ M.-V. Salvia, S. Springhetti, F. Rastrelli, and F. Mancin* Chem Sci. **2018,** 9(21), 4777–4784.

in the coating monolayer allows the performance of STD experiments in complex mixtures. This way, a detection limit of 30 μM is reached with standard instruments

2.1 Designer drugs sensing

As described in the introductive chapter, detection and identification of designer drugs is a big challenge for both forensic and customs laboratories, as they lack analytical standards and they require isolation and careful identification,[1] an expensive and time consuming procedure.

On-site detection kits are commercially available for early screening and even "in-home" quality control (i.e. Mecke, Mandelin, Marquis tests). These are based on chromogenic chemical reactions[2] or antibody-based immunoassays[3] (see chapter 4). However, they provide qualitative results which need validation by more sophisticated analysis and may easily fail in identifying new substances.[3]

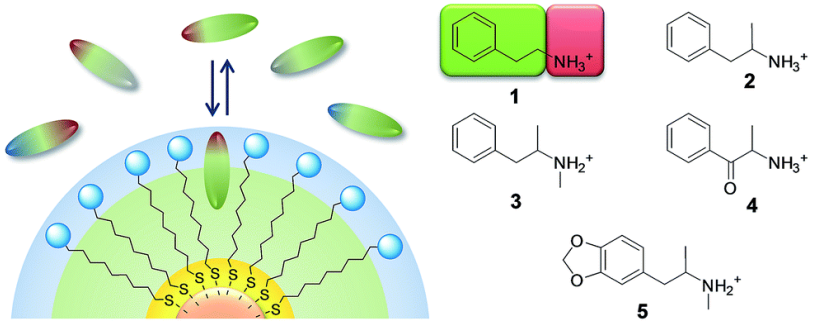

Figure 2.1. Left: Recognition of amphiphilic organic ions by MPGNs coated with amphiphilic thiols with complementary charge. Right: Chemical structure of representative psychoactive molecules of the 2-phenethylamine (**1**) family: amphetamine (**2**), methamphetamine (**3**), cathinone (**4**), MDMA (**5**). (color code: blue, negative charge; red, positive charge, grey, neutral hydrophilic, green neutral hydrophobic). Figure from the above mentioned work.[4]

Several approaches, extensively discussed in the introductive chapter, have been proposed to address the limitation of unknown samples. In the specific case of the drugs of abuse, most chemosensors are based on the host-guest chemistry of the cucurbiturils (which will be extensively discussed in chapter 4). For example. in a recent work, Hwanh, Oh, and Kim functionalized a transistor with cucurbit[7]uril that allows the detection of amphetamine (2) and methamphetamine(3) in water and human urine in the nanomolar range.[5] However, if the detection of a designer drug is thus possible, its identification is not, as the result is just a variation in current intensity. A second relevant example comes from Dalcanale and co-workers, for the detection of MDMA (3,4-methylenedioxymethamphetamine, or ecstasy) with a pyrene-derivatized tetraphosphonate cavitand selective for the N-methylammonium hydrochloride group characteristic of methamphetamines (*Figure 2.2*).

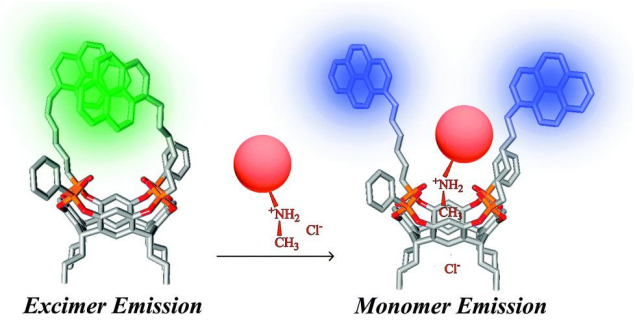

Figure 2.2. Scheme of the Dalcanale fluorescent system. Figure from Masseroni et al.[6]

The system works when loaded in pegylated silica nanoparticles as a fluorescent probe or when immobilized on AFT cantilevers (without the pyrene moieties).[7] In this case as well, if the detection of different methamphetamines is possible, the structural assignment is not, and other designer drugs such as cathinones or amphetamines (that lack of the N-methylammonium moiety) can't be detected.

To overcome this problem, in this chapter I report the design and synthesis of a family of nanoparticle receptors capable of recognizing phenethylamine-

related designer drugs, and I will demonstrate their suitability for NMR-based detection, discrimination and identification of designer drugs in water, without any pre-treatment and at micromolar concentrations.

2.2 Nanoparticle synthesis

Gold nanoparticles are synthesized using a modified Brust and Schiffrin protocol developed by Peng[8] and then Scrimin[9] and co-workers (*Figure 2.3*). Tetrachloroauric acid was transferred from an aqueous phase to toluene using tetraoctylammonium bromide. At this point, dioctylamine (DOA) is added. DOA has the double function of reducing Au(III) to Au(I) and to create small clusters of gold that will influence the final size of the nanoparticle. In particular, 20 equivalents of dioctylamine with respect to gold are needed to get a final particle cores size of about 1.8 nm, that will lead, after passivation with a thiol, to AuNPs with an average formula of $Au_{180}SR_{70}$. The second function of DOA is to coat the formed nanoparticles and prevent them from aggregation. The reductant used is sodium borohydride at 0°C. $NaBH_4$ dissolved in ice-cold water is added to the mixture: it has been noted that at this temperature the yield of the final nanoparticle is higher, compared to the synthesis at ambient temperature. The nanoparticles are left under gentle stirring and inert atmosphere for 2 h. Then, the desired coating thiol is added to passivate the particles. DOA doesn't compete with the thiols in coating the surface: the interaction between secondary amine and gold is weaker than the thiol-gold interaction. After the addition of the thiol stirring is continued from 3 to 12 h (ageing) according to the nature of the thiol and of the nanoparticles one aims to get (if the thiol added leads to immediate precipitation of the coated nanoparticles, the prolonged stirring does not affect the final result). The dilution used, the ratio of the reagents and the stirring times, just as in every nanocluster recipe, are a key point to get the desired size and stability of the gold nanoparticles (ageing). Once the coating is complete, AuNPs are usually

purified by various cycles of precipitation from organic solvents and centrifugation or by size exclusion chromatography, both really effective in the removal of the excess thiol and DOA left from the synthesis. This synthesis comes very handy when, as is the case for every thiol in this work, the thiols used for the final coating of the monolayer protected gold nanoparticles are not commercial.

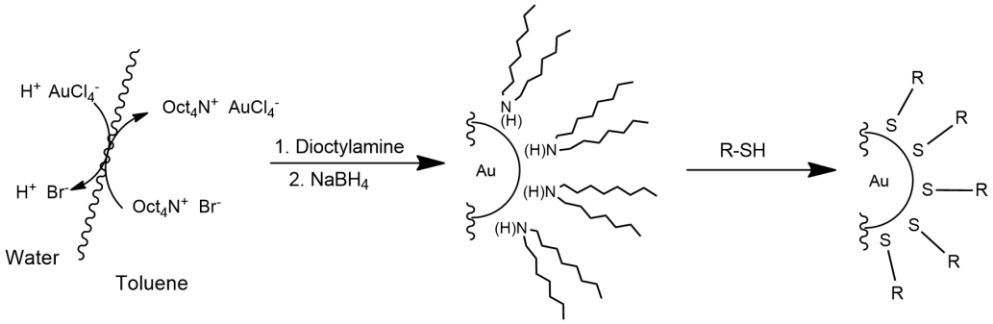

Figure 2.3. Synthesis of gold nanoparticles

Only two equivalents of thiol are needed to get a full passivation of the nanoparticle surface, instead of the 10 or more used in the classical Brust and Schiffrin approach, where the thiol has the double function of passivation agent and the size determining factor.

2.3 Nanoreceptor design

We already saw how AuNPs coated with amphiphilic thiols, featuring an hydrocarbon chain and a polar or charged end-group, can bind organic molecules with an amphiphilic structure in water.[10–13] Previous studies showed how the recognition is driven, in selected cases, by the formation of "cavitand-like" pockets in the coating monolayer.[14,15] Since the affinity for amphiphilic organic anions can be strongly enhanced by decorating the monolayer with positively charged head-groups, and since most psychoactive drugs – particu-

larly those based on the phenethylamine backbone - feature, at physiological pH, an amphiphilic structure with a positively charged ammonium group and lipophilic aromatic or carbocyclic moieties (*Figure 2.4*), I thought that decorating the monolayer with a coating thiol bearing the opposite charge could work as well for enhancing affinity.

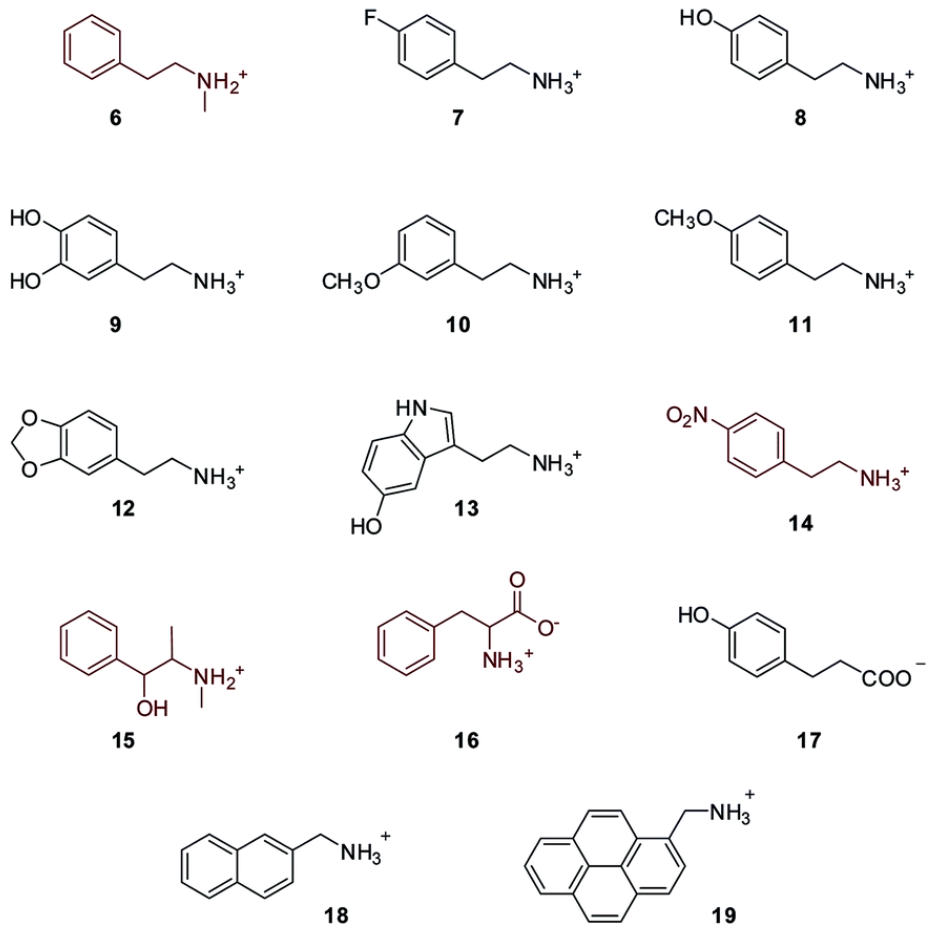

Figure 2.4. Substrates used in this chapter; substrates coloured in dark red are not luminescent. Figure from the above mentioned work.[4]

I consequently hypothesized that MPGNs coated with thiols featuring a hydrophobic portion and an anionic head-group should be able to act as broad-class receptors for phenethylamine derivatives.

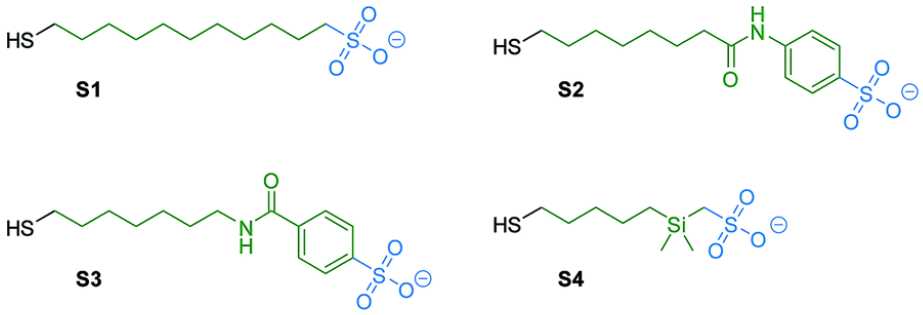

Figure 2.5. Nanoparticle coating thiols. Figure from the above mentioned work.[4]

With this in mind, I selected and synthesized thiols **S1**-**S4** (*Figure 2.5*). In **S1** the hydrophobic portion is a simple alkyl chain, while in **S2** and **S3** a phenyl moiety was added via amide linkage. In **S4** a dimethylsilane group was introduced for STD-NMR purpose, since it allows selective NPs saturation without overlapping with the analytes signals. **S1**-**S4** were used to synthesize MPGNs (**S1/S4-AuNP**) with an average gold core diameter of 1.6±0.3 nm. The average molecular formula is $Au_{140}SR_{50}$. In every case, the nanoparticles resulted well soluble in water.

2.4 Synthesis of the coating thiols

For the synthesis of thiol **S1**, both the 1,11-dibromoundecane and the 11-bromoundecene are convenient starting materials. As for the first option, since the two bromines are equivalent, it appears convenient to introduce the protected thiol in the first step, so that the disubstituted by-product can be easily separated by column chromatography. Only after this step, the sulfonate group can be introduced, by the reaction of the just-obtained thioacetate with sodium sulphite under heating. If starting from 11-bromoundecene, the sulfonate is better introduced first, since in this case the double substitu-

tion is not possible and the chromatography after the first step can be avoided. The thiol group can be added at this point, by performing a thiol-ene reaction[16] using a photoinitiator and thioacetic acid. I chose the second pathway, because it presents potentially better overall yield and less time-demanding purification. The characterization of the molecule obtained matched the one present in literature.[17]

For the synthesis of thiol **S2** the best starting materials commercially available are 8-bromoctanoic acid and sulfanilic acid, a benzene derivative substituted in positions 1 and 4 with a sulfonate and an amine moiety, that is sold in zwitterionic form. As a first step, the acetyl-protected thiol moiety is inserted the same way as for thiol **S1**. To connect the sulfanilic acid to the alkyl chain, an amide coupling seemed the best option, so after obtaining the pentafluorophenol ester of the acid, I performed the reaction with sulfanilic acid. As this was not working in standard conditions, it was necessary to perform it in DMF and higher temperature (60°C) to obtain both the complete solubilization of the reagents and the conversion to the product.

On paper, the synthesis of thiol **S3** consists in the synthesis of the reversed amide with respect to **S2**, where the amine group is on the alkyl chain and the carboxylic acid is on the ring. In this case, 4-sulfobenzoic acid is commercially available as potassium salt, but a bromoamine or an aminoalkene of the correct length (7 carbon atoms, so to have the same length of **S2**) are not available. As the thioacetate group and the amine can't coexist in the same molecule for obvious reasons, the thioacetate group must be inserted after the amide coupling with the 4-sulfobenzoic acid. So, I decided to convert to amine the 7-bromoheptene. To this purpose, many standard routes are available (i.e. Gabriel reaction) and I chose to perform the conversion of the bromide to azide and subsequent reduction to amide with lithium aluminium hydride (catalytic hydrogenation can't be used in this case to preserve the double bond). The formation of the amide linkage is not straightforward in this case, because the carboxylate and sulfonate moiety in the 4-sulfobenzoic acid have very similar reactivity when using the standard procedures. All the attempts of coupling in

standard conditions failed, mostly because of the formation of by-products (sulphonamides, adducts with EDC) of difficult purification and with yields comparable with the desired product. So, following an already reported procedure,[18] both the sulfonate and carboxylic functions were activated using $SOCl_2$, and the reaction performed at -78°C. At this temperature, only the carboxyl chloride leads to the desired product. The unreacted sulfanyl chloride has been hydrolysed with prolonged stirring in basic medium, to restore the desired negative charge. As a last step, the thiocetate has been introduced via thiol-ene reaction.

For the **S4** thiol**,** we needed two methyl groups bound to a silicon atom (so to have a singlet in a not crowded region of the ^{1}H-NMR spectrum) in between the linker (alkyl chain) and the receptor (the sulfonate moiety). I thought it could be convenient to start from a commercially available compound that has already the methyl groups bound to the silicon, and two other functions to allow the binding of the alkyl chain and the sulfonate. The obvious choice was bischloromethyl-dimethylsilane. The first idea was to substitute the chlorine atoms with an iodide, a better leaving group, and then using an alkyl alcohoxide to substitute one of them. The sulphonate introduction, as second step, would have been performed again using sodium sulphite. Since this attempt has not been successful, because the silane used is not compatible with the use of strong bases, I decided to convert the two chlorines in two alcohols (via acetate) and then doing two couplings through activation via triflate. I tried to make the triflate of the silanol to react it with an alcohol terminated alkyl chain, as well as the triflate of the alkyl chain to react it with the silyl alcohol. None of the reactions led to the right product. So I decided to change the approach: it's known from literature procedures that in the chloro(chloromethyl)dimethylsilane only the chlorine atom directly bound to the silicon can undergo attack by a Grignard reagent.[19] So I chose the alkene of the desired length (shorter than the previous thiols, such as to improve the magnetization transfer via STD experiments, see next paragraphs), performed the synthesis of the Grignard and obtained the desired molecule. To introduce

the sulfonate moiety, I decided to convert the chlorine atom to a better leaving group (bromide derivative) and then to have it reacting with sodium sulphite in the usual pathway. As a last step, in this case as well, I performed the thiol-ene reaction.

All the four thiocetates obtained have been converted to thiols by Zemplén methanolysis using MeONa in dry methanol.

2.5 The NOE-pumping experiment

The basic experiment to use nanoparticles to detect molecular targets in mixtures is the diffusion filter, or 1D-DOSY. The key point is that when a nanoparticle receptor is present in solution, it will interact only with the analyte (or analytes) of interest. This, upon interaction with the nanoparticle, experiences a modification of its diffusion coefficient. This happens because, for the time of the interaction, the analyte is part of the nanoparticle as a host-guest complex, it assumes the size of the nanoparticle, and consequently the diffusion coefficient of the nanoparticle. This way, applying a diffusion filter, it is possible to separate quite easily the bound analyte from the analytes not interacting with the receptor. Obviously, for this to work, the difference in diffusion coefficients between the nanoparticle and the analyte has to be big enough. If the recognition event is in fast exchange regime on the NMR timescale, however, the apparent diffusion coefficient of the interacting analyte is a weighted average of the one of the free analyte (higher) and one the bound analyte (lower, the same as the nanoparticle), so the difference of the two coefficients may be not enough to differentiate the analytes with just a diffusion filter. In addition, the signals of the nanoparticles are also retained in the spectrum and they are the most intense one.

A more complex and elegant experiment is: NOE-pumping[20–22] (*Figure 2.6*).

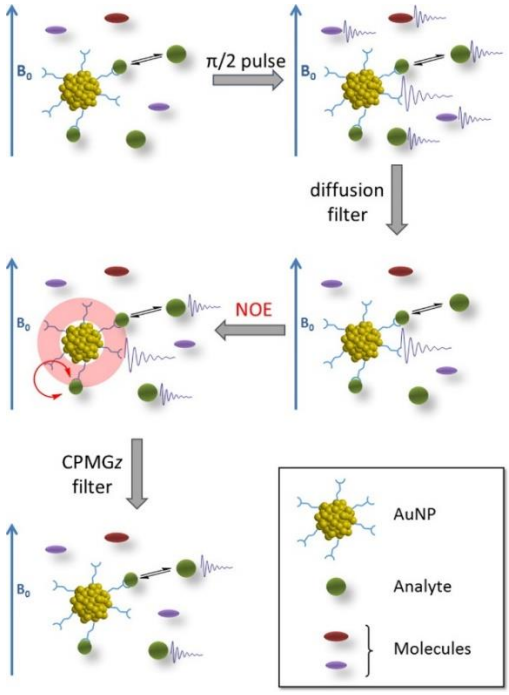

Figure2. 6. NOE-pumping scheme. Figure by Salvia et al.[22]

Looking at the pulse sequence (*Figure 2.7*), the first part of a NOE-pumping experiment is still a diffusion filter: after a non-selective 90° pulse, two gradient pulses with the same strength, but opposite in sign, separated by a delay Δ are used. Only the molecules that, in this interval Δ, are not moving (or move very slowly) inside the sample get an overall zero gradient (for our purpose, the nanoparticles). All the other molecules, instead, get an overall non-zero gradient, proportional to the distance they travelled in the sample during Δ. This way, the only magnetization not losing phase coherence is the one of the nanoparticles. A spectrum acquired at this point would show only the signals of the thiols coating the AuNP. Then, a classic NOE experiment is performed: two 90° pulses separated by a mixing time T_m. During T_m (1.2 seconds in this case) the magnetization is transferred thanks to the nuclear Overhauser effect from the nanoparticle to the analyte bound to it. A spectrum acquired at this point shows the residual but attenuated (due to their faster relaxation) signals of the nanoparticles together with the signals of the analyte interacting with it.

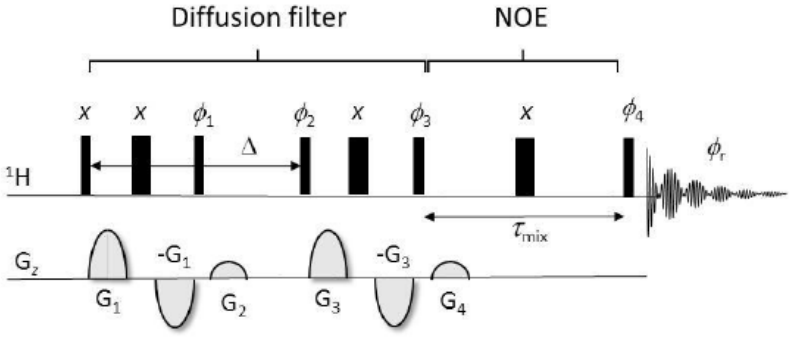

Figure 2.7. the NOE-pumping pulse sequence. Figure by Salvia et al.[23]

The longer the T_m, the more effective the magnetization transfer, the less intense the signals of the nanoparticle and the more intense the signals of the analyte. However, T_m can't be prolonged too much, because this would generate an overall intensity decrease of all the signals, with loss of sensitivity. It has to be stressed that the experiment works only if the recognition is in fast exchange regime: indeed the signal produced not only arises from the analyte bound to the nanoparticle, but also (and mostly) from the analytes that are free in solution at the moment of the acquisition, but that have been previously bound to the nanoparticle and therefore preserve the magnetization received from the nanoparticle. A single receptor pocket on the nanoparticle can transfer magnetization to more than one analyte during the experiment, producing multiple recognition events. From the experiment dynamics we just examined comes the "NOE-pumping" name, meaning the increment of the signal by pumping magnetization on the analytes via nuclear Overhauser effect. At the end of the NOE-pumping experiment, it can optionally be inserted a T_2 filter to improve the quality of the spectrum by decreasing the intensity of the residual signals of the nanoparticle that could make the interpretation or integration of the analyte signals in the spectrum difficult. This clearing is possible because the T_2 of the nanoparticles is shorter than the one of the analytes (molecular weight difference is two-three orders of magnitude). The sequence used recalls the CPMG sequence, in a modified version by Rastrelli et al, called CPMGz for the reduction of spectral artefacts.[24]

2.6 Molecular recognition ability

I selected the simplest **S1-AuNP** as a front-line candidate to test the ability of anionic nanoparticles to detect phenethylamine derivatives. The nanoparticles, at 15 μM concentration (corresponding to 1 mM concentration of coating molecules), were mixed with 2.0 mM phenethylamine (**1**) in deuterated water buffered at pD = 7.0. Then, a "NOE pumping-CPMGz" experiment was performed (*Figure 2.8a*).

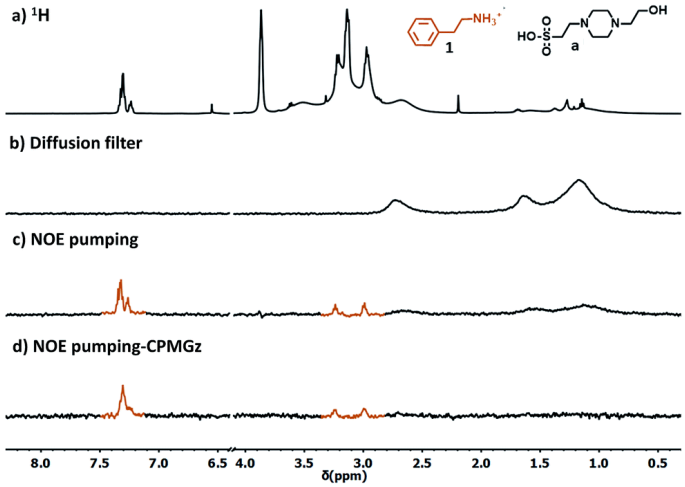

Figure 2.8. (a) ^{1}H-NMR spectrum of phenethylamine (**7**) and **S1-AuNP** in HEPES buffered D_2O. (b) diffusion filter spectrum of the same sample (640 scan, 40 min). (c) NOE-pumping spectrum of the same sample (3072 scan, 4 h). (c) NOE-pumping-CPMGz spectrum of the same sample (60 ms CPMGz filter, 3072 scans, 4 h). Conditions: [**7**] = 2.0 mM, [**S1-AuNP**] = 15 μM, HEPES buffer 10 mM, pD = 7.0. Figure from the above mentioned work.[4]

As stated before, the diffusion filter dephases the magnetization of all the fast diffusing species in the sample but not that of the slow-diffusing nanoparticles (*Figure 2.8b*). During the following NOE step, part of the residual magnetisation is transferred from the nanoparticles to any molecular species interacting (in a fast exchange regime) with them (*Figure 2.8c*). Eventually, the T_2 relaxation filter attenuates the signal of the slowly tumbling and conformationally hindered nanoparticle-coating ligands. As a result, only the signals of the molecules recognised by the nanoparticle receptor are present in the spectrum (*Figure 2.8d*).

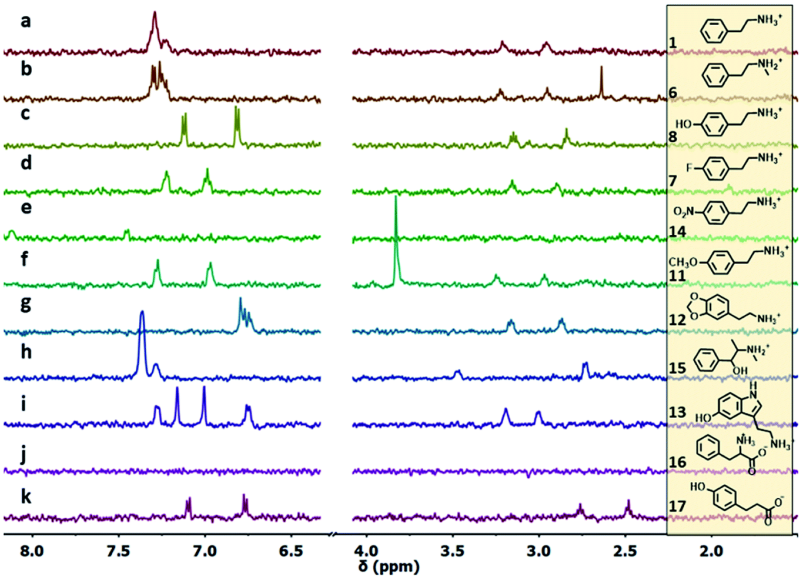

Figure 2.9. ^{1}H-NMR spectra NOE pumping-CPMGz (3072 scan, 4 h) of **AuNP-S1** (14 μM in D_2O), HEPES buffer (10.0 mM) and different analytes (2 mM): (**a**) – (**k**). For 4-nitrophenethylamine (**e**) NOE pumping spectrum is shown. For 12 (**g**) and 15 (**h**) signals respectively at 5.11 and 1.04 ppm at are not shown for figure clarity. Regions between 4,2 and 6.3 ppm and below 1,6 ppm are not displayed. Figure from the above mentioned work.[4]

The results reported in *Figure 2.8* confirmed the ability of **S1-AuNP** to recognize and detect phenethylamine. The four signals belonging to the five groups of magnetically equivalent protons in the substrate (two of them overlap at 7.3 ppm) are the only ones present in the NOE pumping-CPMGz spectrum and allow the easy identification of the detected molecule. Interestingly enough, the signals of other species present in the sample such as water, residual solvents, and in particular the HEPES buffer, are not present in the final spectrum. Consequently, the two triplets at 2.9 and 3.2 ppm arising from the ethyl residue of **1**, which are not visible in the ^{1}H-NMR spectrum due to the overlap of the broad and intense HEPES signals, are clearly extracted in the final spectrum.

The ability of **S1-AuNP** nanoparticles to recognise the cationic amphiphilic structure of many designer drugs was confirmed by investigating the detection of other molecules with similar structure (*Figure 2.9*), including some neurotransmitters and drug precursors. Phenethylamine derivatives such as

N-methylphenethylamine (**6**), 4-fluoro-phenethylamine (**7**), tyramine (**8**), dopamine (**9**), 3-methoxyphenethylamine (**10**), 4- methoxyphenethylamine (**11**), 3,4-methylenedioxyphenethyl amine (**12**), serotonine (**13**), 4-nitro-phenethylamine (**14**) and ephedrine (**15**) were all detected and identified thanks to their distinctive ^{1}H-NMR signals. On the other hand, molecules with similar structure but without the cationic head group, such as phenylalanine (**16**), as well as hydrophilic organic molecules, such as HEPES, glucose and lactose (not shown), did not produce any signal in the NOE pumping experiments.

Surprisingly enough, phloretic acid (**17**) is detected, even if with lower sensitivity. This suggests that the electrostatic repulsion between the anionic headgroups of the nanoparticles and the carboxylate moiety of the amphiphilic substrate may not be sufficient to completely prevent the interaction. Moreover, it is well known that a nanoparticle can perturb the pH of the water close to the monolayer. In this case, the pH next to a negatively charged nanoparticle can be up to one unit lower than the actual pH of the solution; furthermore, a relevant percentage of the phloretate can be protonated. Indeed, performing the same experiment in a more basic environment prevents the system from detecting the phloretate. Still, even if the NMR spectrum of **17** is quite similar to that of the corresponding phenethylamine **8**, the identification of the compound as a carboxylate is quite simple, since the signals of the aliphatic methylenes shift from the region typical of phenethylamines (2.7-3.3 ppm) to that of phenethylcarboxylates (2.3-2.7 ppm).

2.7 Affinity measurements

To get more insight into the recognition properties of **S1-AuNP**, we measured their affinity for different analytes by fluorescence titrations, taking advantage of the luminescence properties of molecules **7**-**13** and **17**-**19**. The

experiments were performed by adding increasing amounts of analytes to a 1.4 μM (0.1 mM concentration of coating molecules) solution of **S1-AuNP** in water at pH 7 (HEPES buffer 10 mM). Gold nanoparticles effectively quench the emission of the dyes bound to the coating monolayer. When the affinity of the analytes for **S1-AuNP** was high enough, an initial quenching of the emission was observed (indicating the binding of the dye to the AuNPs) followed by a linear emission increase after saturation was reached. In *Figure 2.10* is reported the emission spectra obtained during the titration of **S1-AuNP** with serotonin (**13**). Each spectrum was recorded three times, and, for each set, the average fluorescence intensity at 335nm was plotted against the concentration of **13** added (*Figure 2.11*). Fitting of the data with a 1:1 binding model gave the desired binding constants.

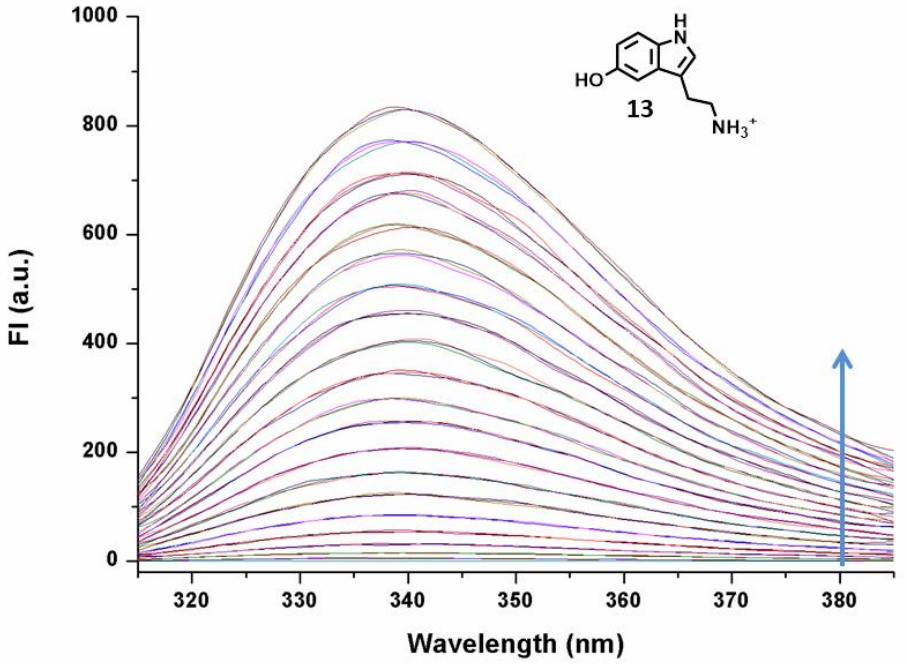

Figure 2.10. Fluorescence spectra obtained from the titration of **S1-AuNPs** (0.1mM) with serotonin (solution 3mM, 2μL additions) at 25°C in water. Every spectrum was recorded three times.

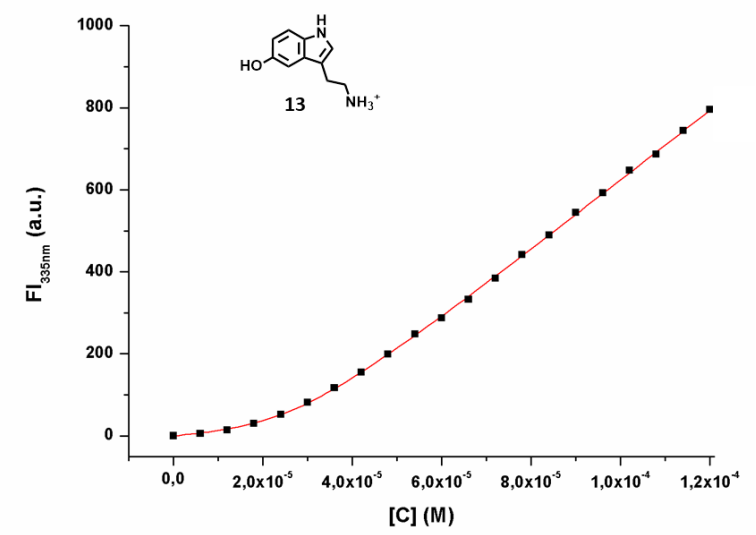

Figure 2.11. Plot of fluorescence intensities vs concentration of serotonin (**13**) added. In red, the fitting curve obtained from DynaFit. Conditions **S1-AuNP**s 0.1 mM, HEPES 2mM.

Table 1. Binding parameters of analytes **1** and **7**-**19** to **AuNP-1** in water (values in red are estimated). Errors are derived from fitting errors from estimation of K_a

Analyte	*K, M^{-1}*	*[binding sites], M*	*Log D (pH 7.4)*[b]
1	3.6×10^{5} [c,d]	- [c]	-0.84
	$[(7.9\pm0.8)\times10^{5}]$ [e]	$[(3.8\pm0.1)\times10^{-5}]$ [e]	
7	$(2.6\pm0.6)\times10^{5}$	$(4.5\pm0.3)\times10^{-5}$	-0.85
	$[(4.1\pm0.4)\times10^{5}]$ [e]	$[(4.2\pm0.1)\times10^{-5}]$ [e]	
8	$(1.3\pm0.2)\times10^{5}$	$(3.5\pm0.2)\times10^{-5}$	-2.01
9	$(1.2\pm0.2)\times10^{5}$	$(2.8\pm0.2)\times10^{-5}$	-2.18
10	$(4.1\pm0.4)\times10^{5}$	$(4.2\pm0.1)\times10^{-5}$	-1.04
11	$(4.8\pm0.5)\times10^{5}$	$(3.9\pm0.1)\times10^{-5}$	-1.04
12	$(3.9\pm0.3)\times10^{5}$	$(4.1\pm0.1)\times10^{-5}$	-0.87
13	$(2.7\pm0.3)\times10^{5}$	$(2.9\pm0.1)\times10^{-5}$	-1.71
14	4.6×10^{5} [c,d]	- [c]	-0.43
15	3.7×10^{5} [c,d]	- [c]	-0.75
16	- [c]	- [c]	-1.46
17	- [f]	- [f]	-1.24
18	$(6.1\pm1.4)\times10^{5}$	$(3.3\pm0.1)\times10^{-5}$	0.55
19	$(2.2\pm0.1)\times10^{6}$	$(5.5\pm0.1)\times10^{-5}$	2.16

[1-AuNP] = 10×10-5 M, pH = 7.0 (HEPES buffer 10 mM); b) Predicted with the ACD/Labs Percepta module, www.chemspider.com. c) not measurable as substrate is not fluorescent; d) estimated from the plot in **Figure 2.13**; e) values obtained by **9**-displacement titration; f) no binding observed.

It is important to point out that this model assumes that multiple, equivalent and independent binding sites are present in the nanoparticle-coating mono-

layer. The results of the fittings are summarised in *Table 1*. Binding constants (K) values in the range 1×10^5 - 1.3×10^6 M^{-1} were found. Such values are consistent with those previously measured for the interaction of cationic nanoparticles with organic anions[23].

In a few cases, namely compounds **1**, **14**, and **15** we could not determine the affinity of the nanoparticles since these compounds are not luminescent. In addition, in the case of compound **17**, we did not observe any interaction with the nanoparticles in the fluorescence titration. However, in this case NOE pumping experiments indicates that the molecule is indeed recognised by the nanoparticles. We decided to perform a series of simulations to determine which is the minimum affinity that allows the detection of the interaction, and the determination of the binding constant, in the fluorescence titrations. Results are reported in *Figure 2.12*. Analysis of the figure indicates that binding constants smaller than $5\cdot10^4$ M^{-1} (curve reported in red) are hardly measurable with this technique. On the other hand, the NOE pumping experiment, in the conditions used in *Figure 2.9*, is capable to detect the analyte with binding constants as small as $1\cdot10^2$ M^{-1}, and this explains the apparent disagreement between fluorescence and NMR experiments with derivative **17**.

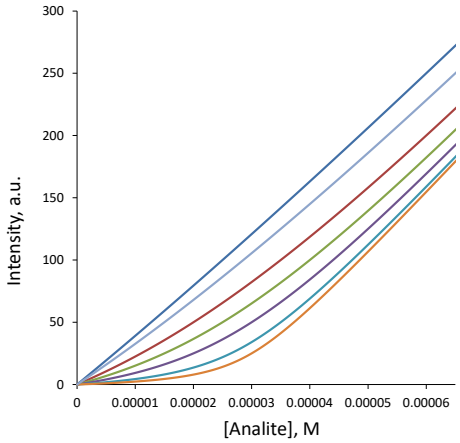

Figure 2.12. Simulated titration experiments for different binding constants ([binding sites] = 3×10^{-5} M). From the bottom: K = 1×10^6 M^{-1}, 5×10^5 M^{-1}, 2×10^5 M^{-1}, 1×10^5 M^{-1}, 5×10^4 M^{-1}, 2×10^4 M^{-1}, 1×10^4 M^{-1}. Inspection of the plot clearly indicates that binding constants smaller than 5×10^4 M^{-1} (red) are difficult to be measured in these experimental conditions.

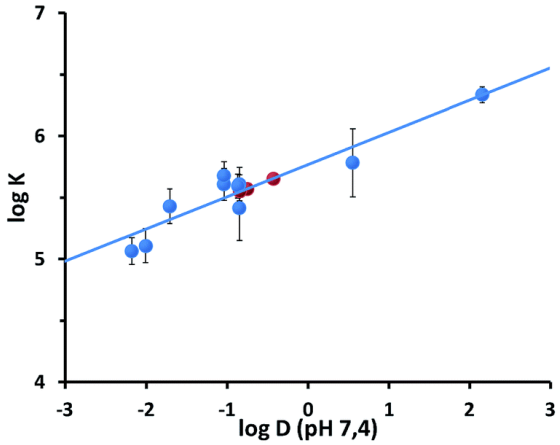

Figure 2.13. Plot of the log K vs log D (pH = 7.4) values relative to the binding of the luminescent analytes 8-13 and 17-19 to S1-AuNP. The lines represent the linear fit of the data (R=0.885). Red circles report the affinity values estimated for substrates 1, 14 and 15 on the basis of their log D values and the fitting parameters. The error bars reported are the confidence value of 3σ according to the errors on K reported in Table 1. Figure from the above mentioned work.[4]

Remarkably, a good linear correlation (*Figure 2.13*) was found between log(K) values of the different analytes and their n-octanol/water partition coefficients computationally predicted at pH 7.4 (log D). This confirms that the interaction between the nanoparticles and the analytes is modulated by the accommodation of the aromatic moiety in the hydrophobic portion of the monolayer (being the ion-pairing headgroups interaction similar in all the cases). The relatively small slope (0.26) suggests that hydrophobic "stabilization" provided by the alkyl chains in the monolayer is less effective than n-octanol solvation. The linear plot of *Figure 2.10* may in principle be used to extrapolate affinities for non-fluorescent analytes as **1**, **14** and 15 (*Table 1*).

The number of binding sites in **S1-AuNPs** estimated with the luminescence titrations is in most cases comprised between 30% and 40% of the number of coating thiols (*Table 1*), suggesting that each binding pocket in the monolayer is formed by about 3 thiols and that each nanoparticle can bind between 20 and 30 analyte molecules. A displacement titration performed with **7** (*Table 1*) in the presence of **9** provided a number of binding sites similar to that obtained with the direct titration. This suggests that the incoming guest mole-

cules occupy the same binding pockets of the leaving ones. However, the affinity constant measured with the displacement experiment is almost double than that obtained with direct titration. A similar result was obtained with **1** (*Table 1*) which, in the displacement titration, again provided a K value two-fold larger than the one estimated on the basis of the log D. Such a discrepancy may be justified by noting that in direct and displacement titrations the **S1-AuNP** are in different states. In the direct titration, the nanoparticles are progressively loaded with the guest. If the binding constant for each site is influenced by the occupancy state of the surrounding ones, the K value measured will be an average of the ones corresponding to the different possible states. Binding sites surrounded by unoccupied ones will prevail in the first part of the titration, and binding sites surrounded by occupied ones will predominate in the final part. On the contrary, during the displacement experiment each binding site is surrounded only by occupied sites. Consequently, only the binding constant relative to this state is measured. Finding a larger binding constant in the displacement titrations may hence suggest a small allosteric effect, with the guest-saturated nanoparticles having a stronger affinity for their guests than the empty ones.

2.8 The DOSY experiment

To verify the reliability of the correlation and of the estimated data, we investigated the affinity of these analytes for **S1-AuNPs** by diffusion-ordered NMR spectroscopy (DOSY). As discussed, the success of these experiments is based on the ability of the bulky nanoparticles to effectively perturb the apparent diffusion coefficients of the interacting analytes. In particular, being in a fast exchange regime on the NMR time scale, the apparent diffusion coefficient of each analyte will be the average between those of the free species and of the nanoparticles, weighted on the relative populations of bound and unbound analyte.

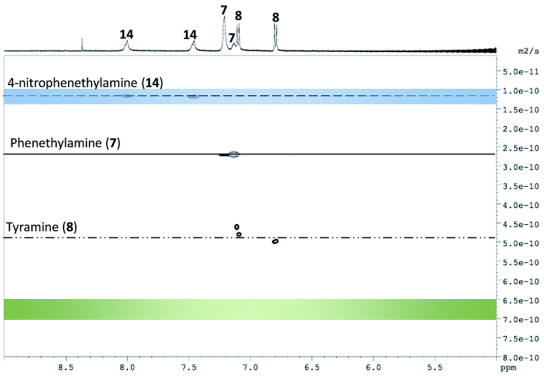

Figure 2.14. DOSY experiment performed on a mixture of phenethylamine (**7**), tyramine (**8**) and 4-nitro-phenethylamine (**14**) in water in the presence of **S1-AuNP** (32 transients, 64 scan per transient, 2 h). Conditions: [analytes]= 0.5 mM, [AuNP] = 45 μM, HEPES buffer 10 mM, pD = 7.0. The blue and green bars represent the diffusion coefficients respectively of the nanoparticles and the unbound analytes in the experimental conditions used. Figure from the above mentioned work.[4]

According to the estimated values of the binding constants, the affinity of the three analytes for S1-AuNP should follow the order **14** > **1** > **7** (*Table 1*). When the mixture of the three molecules, each at 0.5 mM concentration, was analysed by DOSY-NMR in the presence of **S1-AuNPs** (45 μM), the three components were nicely separated according to their apparent diffusion coefficients, which decrease in perfect agreement with the predicted affinity order (*Figure 2.14*). Nicely enough, the DOSY experiment reported in *Figure 2.14* also proves that **S1-AuNP** allows a multianalyte detection by solution-state "chromatographic NMR" as well.[25–27]

2.9 Affinity tuning

NOE-pumping NMR and fluorescence titrations on selected analytes where then used to investigate the different recognition ability of **S1**-, **S2**-, **S3**- and **S4-AuNPs** (*Figure 2.15,* data in *Table 2*).

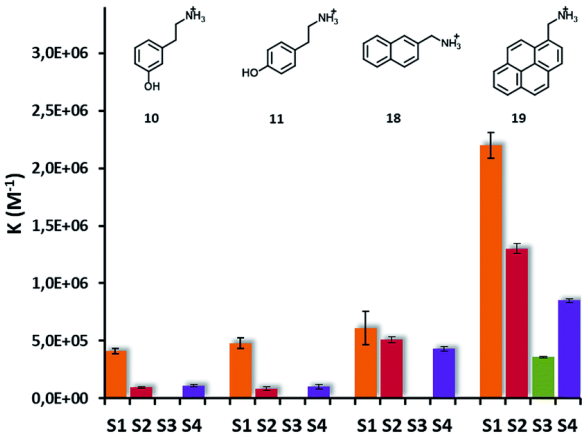

Figure 2.15. Graphical representation of binding constants of analytes **10**, **11**, **18**, **19** and **S1**-, **S2**-, **S3**- and **S4-AuNPs**. Figure from the above mentioned work.[4]

Table 2. Data of *Figure 2.15*. Binding parameters of analytes **10**, **11**, **18**, **19** to **S1**, **S2**, **S3**, **S4**-AuNPs in water. The errors reported are derived from fitting errors from estimation of K. Figure from the above mentioned work.[4]

Analyte	*AuNp*	*K ,M^{-1}*	*[binding sites], M*
10	**S1**	**(4.1±0.4)×10^5**	**(4.2±0.1)×10^5**
	S2	**(9.3±1.2)×10^4**	**(4.0±0.3)×10^5**
	S3	**-** [b]	**-** [b]
	S4	**(1.1±0.2)×10^5**	**(2.4±0.2)×10^5**
11	**S1**	**(4.8±0.5)×10^5**	**(3.9±0.1)×10^5**
	S2	**(8.5±1.5)×10^4**	**(4.7±0.4)×10^5**
	S3	**-** [b]	**-** [b]
	S4	**(1.0±0.2)×10^5**	**(2.3±0.3)×10^5**
18	**S1**	**(6.1±1.4)×10^5**	**(3.3±0.1)×10^5**
	S2	**(5.1±0.3)×10^5**	**(4.1±0.1)×10^5**
	S3	**-** [b]	**-** [b]
	S4	**(4.3±0.2)×10^5**	**(3.1±0.1)×10^5**
19	**S1**	**(2.2±0.1)×10^6**	**(5.5±0.1)×10^5**
	S2	**(1.3±0.1)×10^6**	**(5.7±0.1)×10^5**
	S3	**(3.6±0.1)×10^5**	**(4.7±0.1)×10^5**
	S4	**(8.5±0.1)×10^5**	**(5.4±0.1)×10^5**

a) [AuNp] = 10×10^{-5} M, pH 7.0 (HEPES buffer 10 mM); b) no binding observed

Modification of the nanoparticles coating thiols by introducing either aromatic or dimethylsilane moiety resulted in a reduction of the affinity for the

analytes with respect to **S1-AuNP**. Log K versus log D plots (*Figure 2.13*) remain roughly linear, even if calculated with few data points, indicating that with these nanoparticles as well the ion pairing and the hydrophobic interaction are the main, if not the sole, interactions at play. In the case of **S4-AuNP**, the slope of the plot (0.29) is very close to that obtained with **S1-AuNP** (0.26), suggesting a similar hydrophobic contribution and that the affinity decrease arises from a weaker ion pairing interaction. (*Figure 2.16*)

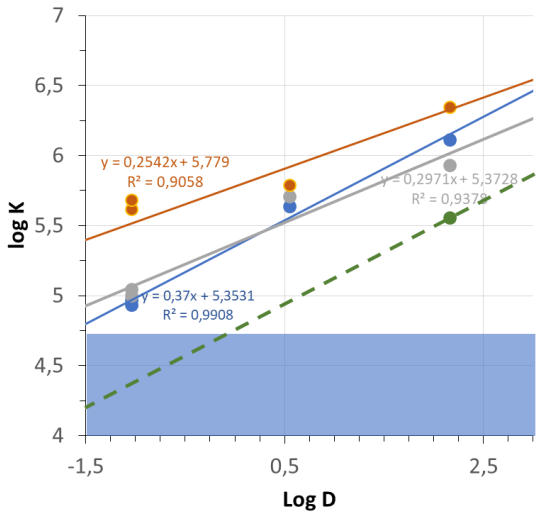

Figure 2.16. Plot of the log K *vs* log D (pH=7.4) values relative to the binding of the luminescent analytes **10**, **11, 18** and **19** to **S1/S4**-AuNp (orange: **S1**-AuNp, blue: **S2**-AuNp, green: **S3**-AuNp, grey: **S4**-AuNp). The lines represent the linear fit of the data for **S1**-AuNp, **S2**-AuNp and **S4**-AuNp, in the case of **S3**-AuNp the green dotted line is not the result of a fit and it has been drawn with the same slope of the one relative to **S2**-AuNp. The blue area represents the binding constant values which cannot be measured by fluorescence titrations.

The electron-donating propensity of the silicon atom may reduce the charge density of the sulfonate. In the case of **S2-AuNP** the slope is 0.37, indication of a stronger hydrophobic contribution. Still, affinities measured are always smaller than those of **S1-AuNPs**. The aromatic residue produces hence two different effects: on one hand it decreases, via delocalization, the charge density at the sulfonate; on the other hand, it increases the stabilization of the hydrophobic portion of the substrates. The reduction of ion pairing ability is

presumably stronger with **S3-AuNP** due to the presence of the electron-withdrawing carbonyl group in para position. Indeed, affinity generally decreases below the threshold that can be detected by fluorescence titrations, which as discussed earlier is around 5×10^4 M^{-1}. Only with substrate **19**, where the strong hydrophobic contribution maintains the affinity for the nanoparticles in the measurable interval, we could determine the binding constant to **S3-AuNPs**, which is 6-fold smaller than that for **S1-AuNP**.

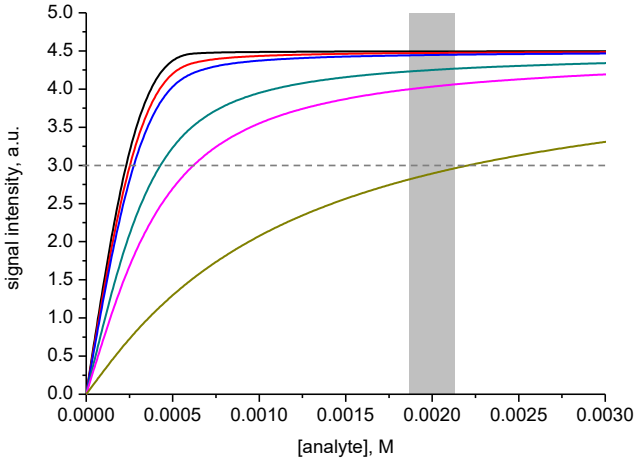

Figure 2.17. Simulated plots of the NOE pumping signal intensities for different binding constants ([binding sites] = 5×10^{-5} M). From the top: K = 5×10^5 M^{-1}, 1×10^5 M^{-1}, 5×10^4 M^{-1}, 1×10^4 M^{-1}, 5×10^3 M^{-1}, 1×10^3 M^{-1}.

The affinity reduction observed has however a small effect on the sensitivity of the NOE pumping experiments (*Figure 2.17*). This is due to the combined effect of receptor affinity and magnetization transfer efficiency, as shown in the simulation reported in *Figure 2.17*. Larger affinity for the analyte grants that the fraction bound to the nanoparticles is relatively large also at small concentrations. However, the efficiency of magnetization transfer is such that, with these nanoparticles, signal to noise (S/N) values around 4.5 are reached at saturation. It must be noted that this value is directly correlated to the amount of analyte molecules bound to the particles, and hence to the total amount of nanoparticles present in the sample. Since the detection limit is

fixed at S/N of 3, this means that about 70% of the nanoparticles binding sites must contain the analytes. For these reasons, for the nanoparticle's concentration used (1 mM thiols), detection limits changes from 0.3 mM to 0.6 mM by changing the binding constant from 5×10^5 M^{-1} to 5×10^5 M^{-1}.

On the other hand, selectivity is substantially improved. Indeed, signals of phloretic acid (**17**), which was detected in these conditions with **S1-AuNP** (*Figure 2.9*), are not present in the NOE pumping spectra with **S2-AuNP.**

Clearly, the affinity decrease brought about by thiol **S2** on the likely already small binding constant of **17** is such to prevent an effective interaction with the nanoparticles.

2.10 Field testing

Having established the ability of **S1/4-AuNPs** to bind and signal phenethylamine derivatives via diffusion and magnetization transfer NMR experiments, we turned our attention to their employability in relevant conditions. In this experiment, **S2-AuNP** were used because they proved to have better selectivity and similar detection limit with respect to **S1-AuNP**.

In the first experiment, I simulated the composition of a "designer drug" tablet by mixing in the NMR tube N-methyl-phenethylamine (**6**, 2 mM) as designer drug model, phenylalanine (**14**, 2 mM) as model masking agent, and an excess (20 mM) of glucose as a possible excipient. The resulting ^{1}H-NMR spectrum in HEPES buffered D_2O is very complex, and identification of the target compound is hampered by the severe signal crowding (*Figure 2.18a*). Upon addition of **S2-AuNP**, the NOE pumping-CPMGz sequence reveals the sole signals arising from N-methylphenethylamine (*Figure 2.18b*).

In a second experiment, a seized "street" tablet was analysed. Sample preparation was as simple as dissolving a crushed quarter tablet (60 mg) in D_2O, adding a small amount of **S2-AuNP** solution and recording the NOE pumping CPMGz-spectrum. in this case as well, the ^{1}H-NMR spectrum shows a large number of signals arising from the drug and lactose present in the tablet (*Figure 2.18c*). In contrast, the NOE pumping-CPMGz spectrum contains only a set of 9 signals (*Figure 2.18d*) whose analysis readily leads to identify the compound as MDMA (**5**), the active component of Ecstasy.

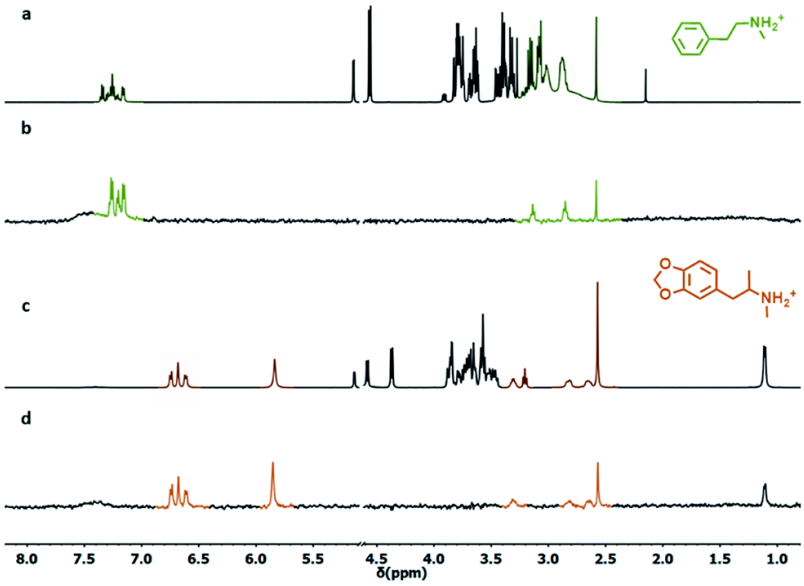

Figure 2.18. a) 1H-NMR spectrum of N-methylphenethylamine HCl (6, 2mM), phenylalanine (14, 2 mM) and glucose (20 mM) in D2O. b) NOE pumping-CPMGz spectrum of the same sample in the presence of S2-AuNP (3072 scan, 4 h). c) 1H-NMR spectrum of a drug tablet dissolved in D2O. d) NOE pumping-CPMGz spectrum of the same sample in the presence of S2-AuNP (3072 scan, 4 h). Conditions: [S2-AuNP] = 15 μM, HEPES buffer 10 mM, pD = 7.0. Figure from the above mentioned work.[4]

2.11 Saturation Transfer Difference - STD

The main limitation of NOE-based chemosensing is its low sensitivity, which results into relatively high limits of detection, as discussed earlier. Experiments of *Figure 2.18* reveals that this is not a problem in the analysis of seized samples, since the amount of drug present in just part of a single tablet is more than enough to reach the necessary concentration. On the other hand, the analysis of biological samples, where drug concentrations are in the micromolar range, is out of reach. In our first report on nanoparticle-based NMR chemosensing, we demonstrated that sensibly lower limits of detection can be reached by using Saturation Transfer Difference (STD) experiments in place of NOE pumping ones.

The STD experiment is widely used in biochemistry and it's a powerful tool to understand the interactions of small molecules with macromolecules such as proteins. Just like NOE-pumping, STD is based on the fact that magnetisation can be transferred from a receptor (the nanoparticle in this case) to the analyte through NOE. In this case, the discriminating factor is not the variation of the diffusion coefficients, but the interaction between analyte and receptor. The experiment schematised in *Figure 2.19* consists of three steps. first, a normal NMR spectrum is recorded as a reference while saturating at -20 ppm (off resonance), so in an area free of signals in the ^{1}H-NMR spectrum. This way, all the signals show their natural intensities(I_0) and they are not perturbed by the saturation. Then, a second spectrum is recorded (this time on resonance) saturating selectively one signal of the receptor. This way, the saturation is spread to the whole receptor by spin diffusion, to ultimately reach the interacting analytes. The signals of the interacting molecules, as well as the receptor ones, decrease. The loss in intensity is proportional to the efficiency of the interaction (for proximity reasons). The third phase of a STD experiment is then the subtraction from the first spectrum (I_0) of the second one (I_{sat}) to give the final STD spectrum, where only the signals of the species that interact with the nanoparticle are present. For non-interacting species,

the effect of the saturation of the nanoparticle is null, so I_0 and I_{sat} are the same, giving as a result no signal in the STD spectrum. While conceptually similar to a NOE experiment, STD provides stronger signals because, when the monolayer magnetization is saturated, any binding event generates the same enhancement. As opposite, the magnetisation transfer in the NOE experiment is efficient for analytes binding to the monolayer soon after the inversion of its magnetization, but it drops significantly for late binding events. Moreover, in this case the recognition has to occur in a fast exchange regime and the best results are obtained in excess of free analyte. One limitation of STD is that, in order to avoid the generation of artefacts, there must be no overlap between the signals of the unknown analytes and the signal of the receptor to be saturated.

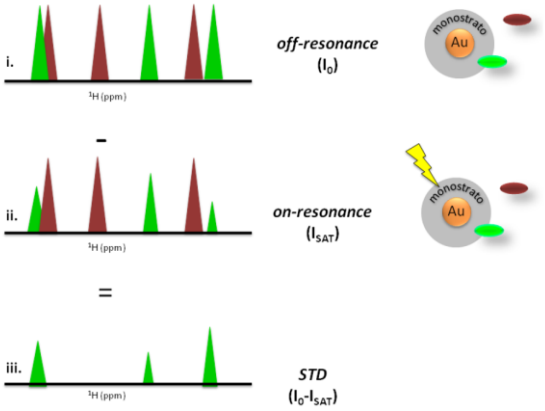

Figure 2.19. Schematic representation of the STD working principle.

In order to overcome such a limitation, **S4-AuNP** was designed, where the dimethylsilane protons resonate at 0.1 ppm. Indeed, such signal lies at the edge of the spectral window for most organic species, thus allowing a selective saturation of the nanoparticle monolayer. Effectiveness of **S4-AuNP** in the detection of drug models at low concentration was tested by analysing HEPES buffered D_2O solutions (pD 7.0) containing 1 mM phenylalanine (**14**) and 50 μM N-methylphenethylamine (**6**). The severe spectral crowding and the low signal intensity prevent the detection of 6 in the sample with a standard ^1H experiment. However, a STD spectrum featuring a 2 s saturation time

(*Figure 2.20*) selectively reveals the presence of **6**. No interference is observed from the overlapping signal of phenylalanine, even when this is in 20-fold excess.

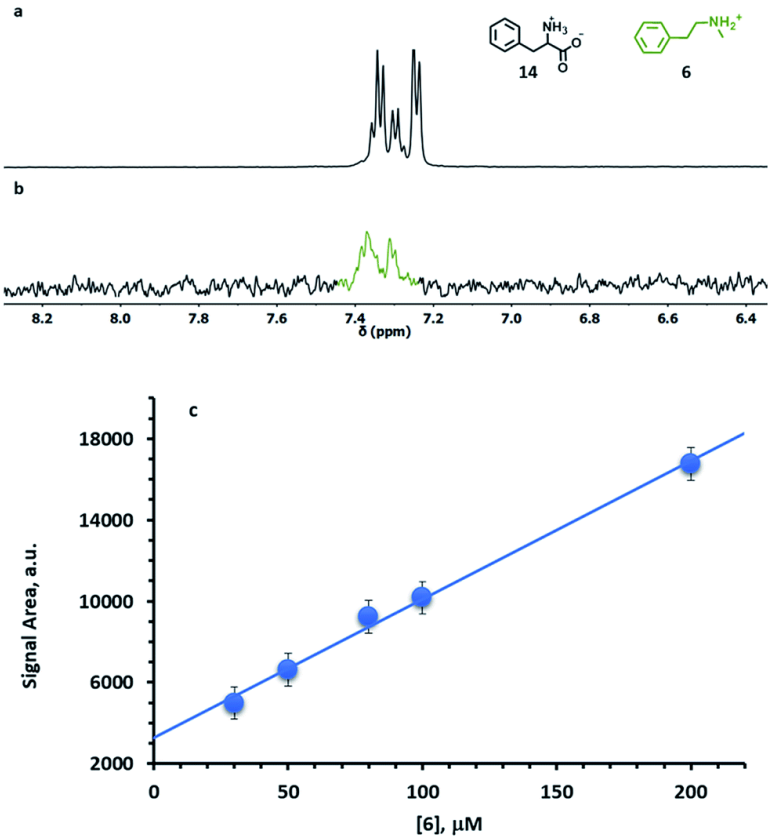

Figure 2.20. a) ^{1}H-NMR subspectrum of phenylalanine (**14**, 1 mM) and N-methylphenethylamine (**6**, 50 µM) b) STD subspectrum of the same mixture in the presence of **S4**-AuNP (1024 scans, 3 h); c) Plot of the integrated signal area of the aromatic signals of **6** in the STD spectra vs [**6**], the blue line represents the linear fit of the data (R = 0.995). Conditions: [**S4**-AuNP] = 15 µM, HEPES buffer 10 mM, pD = 7.0. Figure from the above mentioned work.[4]

Concentration-dependent STD experiments confirmed that the integrated intensities of the signal from **6** increased linearly with dopamine concentration in the physiologically relevant concentration range 0-200 µM,[28] which allows the quantitative determination of the analyte (*Figure 2.20-21*).

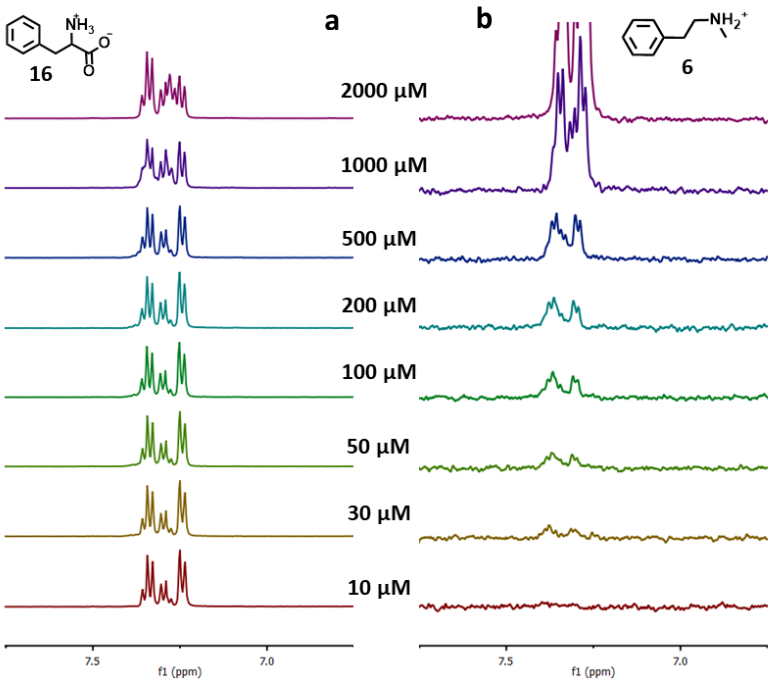

Figure 2.21. N-Methylphenetylamine detection: **S4**-AuNP (15 µM), Phenylalanine (1 mM), N-Methylphenetylamine (from bottom to the top: 10, 30, 50, 100, 200, 500, 1000, 2000 µM), HEPES (10 mM, pD 7.0), D_2O: (**a**) ^{1}H-NMR and (**b**) STD-NMR experiment (on res. 40 Hz) of the same mixtures.

The lowest concentration of **6** that can be detected in these conditions is 30 µM. Indeed, STD is expected to deliver a dramatic sensitivity boost in NMR chemosensing experiments when performed on high field spectrometers equipped with cryoprobes.

2.12 Conclusions

In this chapter, I designed monolayer-protected nanoparticles capable of broad-class recognition of amphiphilic organic cations in water by exploiting strong ion pairing and hydrophobic interactions. Association of nanoparticle-based receptors with magnetisation or saturation transfer NMR experiments allows the straightforward detection and identification of N-phenethylamine derivatives even in complex mixtures, at micromolar concentration and without any pre-treatment. "Cocktails" of different drugs can be analysed using DOSY experiments. No other chemosensing-based system can reach a similar performance. In principle, by using this protocol it should be possible to propose a tentative chemical structure of a new "designer drug" a few hours after the seizure of a single tablet. The introduction of a dimethylsilane group in proximity to the sulfonate moiety allowed the synthesis of AuNPs tailored for STD-NMR experiments, where the monolayer can be saturated without interference from the sample's signals. This approach successfully decreased the detection limit down to the low micromolar range, thus opening the way to the screening of biological fluids such as urine or blood.

Simple thiols such as those used here can be synthesized in few days and assembled on the nanoparticles in a few hours. Even if the insertion of aromatic residues apparently did not result into the establishment of additional interactions with the analyte, modifications in the hydrophobic layer resulted in a modified selectivity. This suggests that the next issue to address is to improve the design of the nanoreceptor in order to reach more sophisticated molecular recognition. More studies are needed in order to deeply understand the effect of thiol modifications on the monolayer properties and structure, and in particular how the coating molecules interact with the vicinal ones and with external analytes as well. Yet, a binding site reproducing the structure of the natural receptors could provide not only a structural but even a functional evidence against new illicit drugs.

Supplementary information

2.1 General

Solvents were purified by standard methods. All commercially available reagents and substrates were used as received.

TLC analyses were performed using Merck 60 F254 precoated silica gel glass plates. Column chromatography was carried out on Macherey-Nagel silica gel 60 (70-230 mesh).

NMR spectra were recorded using a Bruker AV III 500 spectrometer operating at 500 MHz for 1H, 125.8 MHz for 13C. Chemical shifts are reported relative to internal Me4Si. Multiplicity is given as follow: s = singlet, d = doublet, t = triplet, q = quartet, qn = quintet, m = multiplet, br = broad peak.

ESI-MS mass spectra were obtained with an Agilent Technologies LC/MSD Trap SL mass spectrometer.

HRMS mass spectra were obtained with a Mariner Applied Biosystem (API-TOF) mass spectrometer (MeOH, 0.5% formic acid).

TEM images were recorded on a Jeol 300 PX electron microscope. One drop of sample was placed on the sample grid and the solvent was allowed to evaporate. TEM images were analysed with ImageJ software to measure the diameters distribution and average values.

TGA were run on 1 mg nanoparticle samples using a Q5000 IR model TA instrument from 30 to 1000 °C under a continuous air flow.

Fluorescence spectra were recorded on a Perkin Elmer LS50B fluorimeter.

2.2 Synthesis of thiols

Thiol **S1** was prepared as reported in the following scheme:

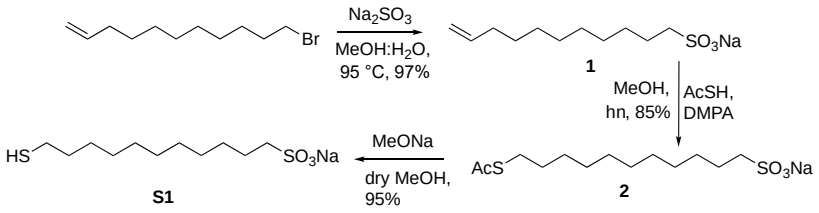

Scheme 2.1. Synthesis pathway for thiol **S1**

*Sodium undec-10-ene-1-sulfonate (**1**).*

11-bromoundec-1-ene (510 mg, 2.190 mmol, 1 equiv) was dissolved in 9 mL of H2O and 4 ml of MeOH. Na2SO3 (554 mg, 4.400 mmol, 2 equiv) was added and the mixture was stirred under reflux overnight. Then the solvent was evaporated under reduced pressure and the residue was purified by flash column chromatography (DCM:MeOH from 9:1 to 1:1), affording the desired sulfonate compound 1 (533 mg, 97%).

^{1}H-NMR (D_2O, 200 MHz): δ 1.26 (br s, 12H) 1.68 (m, 2H), 1.99 (m, 2H), 2.82 (m, 2H), 4.92 (m, 2H), 5.80 (m, 1H).

13C-NMR (D_2O, 500 MHz): δ 23.95, 27.68, 27.70, 28.12 28.24 28.40 28.46, 33.11, 51.08, 113.89, 140.46.

MS (ESI) m/z: 233.1 ([M]-)

*Sodium 11-(acetylthio)undecane-1-sulfonate (**2**).*

Sulfonate **1** (200 mg, 0.78 mmol, 1 equiv) was dissolved in 2 mL of MeOH and the solution was degased under N2 bubbling for 30 min. Then thioacetic acid (220 µl, 3.120 mmol, 4 equiv) and 2,2-dimethoxy-2-phenylacetophenone (DMPA, 20 mg, 0.078 mmol, 0.1 equiv) were added and the mixture was stirred under UV irradiation (365 nm) for 2.5 h. The solvent was evaporated

under vacuum and the crude was purified by flash column chromatography (DCM:MeOH from 9:1 to 1:1), affording the desired sulfonate compound 2 (220 mg, 85%).

^{1}H-NMR (D_2O, 200 MHz): δ 1.25 (br s, 14H), 1.39 (m, 2H), 1.64 (m, 2H), 2.31 (s, 3H, CH3-), 2.69 (m, 4H).

MS (ESI) m/z: 309.1([M]-)

*Sodium 11-mercaptoundecane-1-sulfonate (**S1**).*

The acetylated sulfonate **2** (84 mg, 0.250 mmol, 1 equiv) was dissolved in 2 mL of dry MeOH and then sodium methoxide was added (32 mg, 0.590 mmol, 2.4 equiv). After stirring for 2.5 hours under N2 atmosphere, the reaction was quenched adding IR 120H^+ resin until pH neutralization, then the resin was filtered off, the solvent was evaporated, giving the deprotected Sodium 11-mercaptoundecane-1-sulfonate S1 (70 mg, yield 95%), that was freshly used for the nanoparticles' synthesis.

^{1}H-NMR (MeOD, 300 MHz): δ 1.32 (br s, 14H), 1.57 (m, 2H), 1.78 (m, 2H), 2.49 (m, 2H), 2.79 (m, 2H).

^{13}C-NMR (MeOD, 500 MHz): δ 23.78, 23.96, 27.71, 28.10, 28.24, 28.40, 28.46, 28.55, 33.01, 51.08.

TOF ES- HRMS: [M^-] calcd. for C11H23O3S2=267.109. Found =267.113

Spectroscopic data are in agreement with those reported in literature.

Thiol **S2** was prepared as reported in the following scheme:

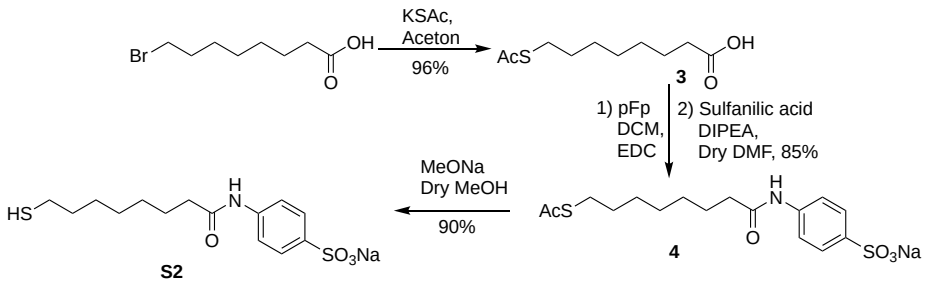

Scheme 2.2. Synthesis pathway for thiol **S2.**

*8-(Acetylthio)octanoic acid (**3**).*

8-bromooctanoic acid (4 g, 17.928 mmol, 1 eq) was dissolved in 100 mL of aceton, then KSAc (2.46 g, 21.514 mmol, 1.2 eq) was added and the mixture was stirred at room temperature overnight. Then the solvent was evaporated under reduced pressure and the residue was purified by flash column chromatography (PE:EtOAc from 8:2 to 7:3), affording the desired compound 3 (3.76 g, 96%).

^{1}H-NMR (CDCl3, 500 MHz): δ 1.35 (m, 6H), 1.58 (m, 2H), 1.64 (m, 2H), 2.30 (s, 3H), 2.36 (t, J=7.5Hz, 2H), 2,89 (t, , J=7.3Hz 2H).

^{13}C-NMR (CDCl3, 300 MHz): δ 24.54, 28.54, 28,70, 28.85, 29.07, 29.41, 30.64, 33.98, 179.98, 196.12.

*4-(8-(acetylthio)octanamido)benzenesulfonate • DIPEA (**4**).*

Compound **3** (1 g, 4.581 mmol, 1 equiv) was dissolved in 10 mL of dry DCM and then pentafluoro phenol (pFp 626 µl, 5.955 mmol, 1.3 equiv) and EDC·HCl (1.14 g, 5.955 mmol, 1.3 equiv) were added. The mixture was stirred for 20 h, then the solvent was evaporated under reduced pressure. The crude was dissolved in dry DMF (15 mL), then sulfanilic acid (937 mg, 5.406 mmol, 1.18 equiv) and DIPEA (3 mL, 17.408 mmol, 3.8 equiv) were added; the reaction

was stirred at 68°C and monitored by TLC (7:3 Tol:MeOH). After completion the solvent was evaporated and the crude was purified by flash column chromatography (Tol:MeOH 7:3), affording the desired sulfonate compound 4 (1.54 g, 85%).

^{1}H-NMR (MeOD, 500): δ 1.39 (m br, 27H), 1.57 (m br, 2H), 1.70 (m br, 2H), 2.32 (s, 3H), 2.42 (t, J=7.5 Hz, 2H), 2.88 (t, J=7.3 Hz, 2H), 3.23 (q, J=7.4 Hz, 2H), 3.72 (hept, J=6.6 Hz, 2H), 7.38, 7.76 (m, 4H)

^{13}C-NMR (MeOD, 500): 11.93, 16.03, 17.47, 25.36, 28.27, 28.47, 28.55, 28.77, 29.35, 36.63, 42.51, 54.47, 118.82, 126.31, 140.27, 140.57, 173.33, 196.06

TOF ES- HRMS: [M $^{-}$] calcd. for C16H22O5NS2=372.094 Found =372.102.

*Sodium 4-(8-mercaptooctanamido)benzenesulfonate (**S2**).*

The acetylated sulfonate 4 (223 mg, 0.445 mmol, 1 equiv) was dissolved in 5 mL of dry MeOH and then sodium methoxide was added (72 mg, 1.334 mmol, 3 equiv); after stirring at for 3 hours under N2 atmosphere, the reaction was quenched adding IR 120H+ resin until pH neutralization, then the resin was filtered off, the solvent was evaporated, giving the deprotected Sodium 4-(8-mercaptooctanamido)benzenesulfonate S2 (145 mg, yield 90%), that was freshly used for the nanoparticles' synthesis.

^{1}H-NMR (MeOD, 300): δ 1.36 (m, 8H), 1.56 (m br, 1H), 1.69 (m br, 2H), 2.41 (t, J=7.5 Hz, 2H), 2.88 (t, J=7.3 Hz, 2H), 7.38, 7.76 (m, 4H)

^{13}C-NMR (MeOD, 500): δ 25.29, 28.46, 28.58, 28.63, 28.97, 29.39, 33.22, 136.17, 137.76, 139.54, 141.07.

TOF ES- HRMS: [M $^{-}$] calcd. for C14H20O4NS2=330.083 Found =330.085

Thiol **S3** was prepared as reported in the following scheme:

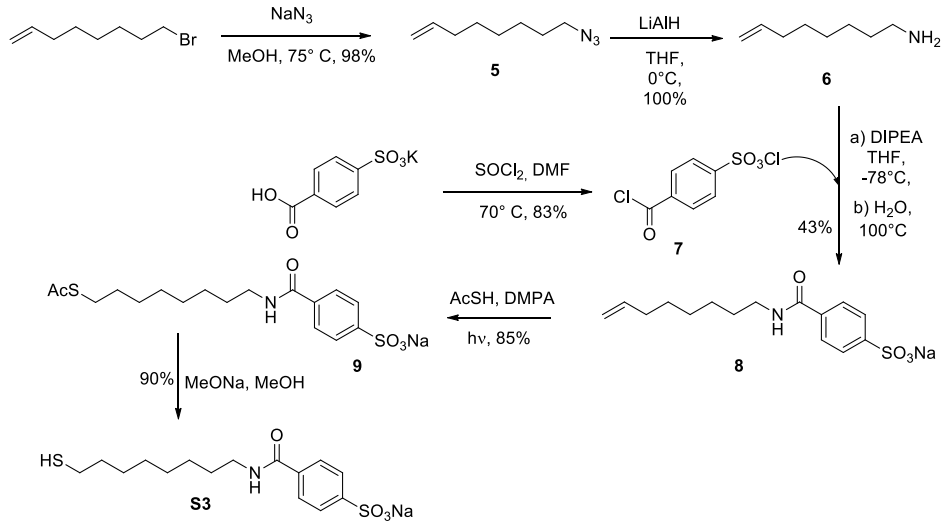

Scheme 2.3. Synthesis pathway for thiol **S3.**

*8-azidooct-1-ene (**5**).*

8-bromooct-1-ene (1 g, 5,23 mmol, 1 equiv) and NaN3 (605 mg, 9,29 mmol, 1,77 equiv) were refluxed overnight in MeOH (7 mL). Then the solvent was removed under reduced pressure and the mixture was carefully extracted in DCM/H2O. The organic layers were collected, dried over NaSO4 anhydrous concentrated, obtaining 791 mg (98% yield) of a colorless liquid.

^{1}H-NMR (CDCl3, 500 MHz): δ 1.41 (br s, 6H) 1.62 (m, 2H), 2.08 (m, 2H), 3.28 (t, J=7.0 Hz, 2H), 5.00 (m, 2H), 5.83 (m, 1H).

^{13}C-NMR (CDCl3, 500 MHz): δ 26.57, 28.60, 28.72, 28,80, 33.64, 51.46, 114.38, 138.88

*Oct-7-en-1-amine (**6**).*

In a rbf, under N2 atmosphere, 1M THF solution of $LiAlH_4$ (12 mL, 12 mmol, 2,3 equiv) was diluted with dry THF (30 mL) and the obtained solution was cooled at 0°C. Compound 5 (0,791 g, 5,13 mmol, 1 equiv) was dissolved in dry

THF (20 mL) and this solution was slowly added (over 20 min) to the stirring $LiAlH_4$ solution. The ice bath was removed and the mixture was stirred under rt for 2 hours. After reaction completion, NaOH 1% solution (40 mL) was added and the mixture was extracted three times with Et_2O (40 mL). The organic layers were collected and dried over Na_2SO_4 anhydrous. No further purifications were required and due to highly volatility of compound 6, the solution was concentrated and used for the next step as a 0,3 M Et_2O solution (17 ml, 99%).

^{1}H-NMR (CDCl3, 500 MHz): δ 1.35 (m, 6H) 1.42 (m, 2H), 2.09 (m, 2H) 2.66 (t, J=6.9 Hz, 2H), 4.97 (m, 2H), 5.85 (m, 1H).

^{13}C-NMR (CDCl3, 500 MHz): δ 26.72, 28.94, 29.00, 33.74, 33.96, 42.25, 113.82, 139.24.

MS (ESI) m/z: 128.2 ([M+H]+)

*4-(chlorosulfonyl)benzoylchloride (**7**).*

Benzensulphonic acid (1,5 g, 6,25 mmol, 1 equiv), thionyl chloride (15 mL, 76,88 mmol, 12 equiv) and dry DMF (0,1 mL) were stirred at 70°C for 4 hours. Then the mixture was concentrated under vacuum and Toluene was added. The solution was filtered, and the solvent was evaporated under vacuum, obtaining 1,31 g (87%) of compound **7**.

^{1}H-NMR (CDCl3, 500 MHz): δ 8.23 (m, 2H) 8.39 (m, 2H)

^{13}C-NMR (CDCl3, 500 MHz): δ 127.75, 132.42, 138.54, 148.99, 167.03

*Sodium 4-(oct-7-en-1-ylcarbamoyl)benzenesulfonate (**8**).*

Compound **7** (165 mg, 0,69 mmol, 1 equiv) and DIPEA (300 μl, 1,72 mmol, 2,5 equiv) were dissolved in dry THF and the resulting solution was stirred for 10 minutes under N_2 atmosphere at -78°C. Then compound 6 (1,3 mL of Et2O 0,3 M solution, 0,39 mmol, 0,58 equiv) was added in two portions over 30 minutes and the mixture was stirred for 2 hours at -78°C. Then the solution

was brought to rt and filtered. The solvent was removed under reduced pressure and the obtained crude was dissolved in 40 mL of CHCl3 and subsequently extracted with NaHCO3 saturated solution, HCl 1M and finally brine. The organic layer was dried with Na2SO4, the solvent was evaporated under reduced pressure and the mixture was purified via flash chromatography (PE:EtOAc from 9:1 to 7:3). The obtained product was dissolved in H2O and refluxed for 3 hours. Then water was evaporated under reduced pressure giving, without need of further purifications, the desired sulfonate **8** (57 mg, 43%).

^{1}H-NMR (MeOD, 200 MHz): δ 1.44 (br s, 6H, -CH2-) 1.67 (m, 2H), 2.11 (m, 2H), 3.40 (t, 2H), 5.06 (m, 2H), 5.83 (m, 1H) 7.91 (m, 4H).

MS (ESI) m/z: 333.2 ([M+Na]-)

*Sodium 4-((7-(acetylthio)heptyl)carbamoyl)benzenesulfonate (**9**).*

Compound **8** (127 mg, 0.38 mmol, 1 equiv) was dissolved in 2 mL of MeOH and the solution was degased under N2 bubbling for 30 min. Then thioacetic acid (115 μl, 1.63 mmol, 4 equiv) and 2,2-dimethoxy-2-phenylacetophenone (DMPA, 6 mg, 0.02 mmol, 0.05 equiv) were added and the mixture was transferred in UV cuvettes and stirred under UV irradiation (365 nm) for 2.5 h. The solvent was evaporated under vacuum and the crude was purified by flash column chromatography (DCM:MeOH from 9:1 to 8:2), affording the desired sulfonate compound **9** (125 mg, 85%).

^{1}H-NMR (MeOD, 200 MHz): δ 1.37 (br s), 1.59 (m, 4H), 2.29 (s, 3H), 3.38 (m, 4H), 7.89 (m, 4H).

^{13}C-NMR (MeOD, 200 MHz): δ 26.8 29.5 29.7 30.0, 30.6, 31.9, 40.2, 128.1, 129.9, 138.8, 157.9, 167.5, 195.2.

*Sodium 4-((7-mercaptoheptyl)carbamoyl)benzenesulfonate (**S3**).*

The protected thiol **9** (45 mg, 0.12 mmol, 1 equiv) was dissolved in 2.5 mL of dry MeOH and then sodium methoxide was added (20 mg, 0.35 mmol, 3 equiv); after stirring at for 3 hours under N_2 atmosphere, the reaction was quenched adding IR 120H$^+$ resin until pH neutralization, then the resin was filtered off and the solvent was evaporated. Flash chromatography purification (8:2 DCM:MeOH) gave the deprotected S3 (38 mg, yield 90%), that was freshly used for the nanoparticles' synthesis.

^{1}H-NMR (MeOD, 200 MHz): δ 1.37 (br s, 6H), 1.59 (m, 4H), 3.38 (m, 4H), 7.89 (m, 4H).

^{13}C-NMR (MeOD, 500 MHz): δ 23.55, 26.61, 27.93, 28.28, 28.29, 28.99, 33.80, 39.70, 125.73, 126.89, 136.02, 147.73, 167.94

TOF ES- HRMS: [M-] calcd. for C15H22NO4S2=344.099. Found =.344.106

Thiol **S4** was prepared as reported in the following scheme:

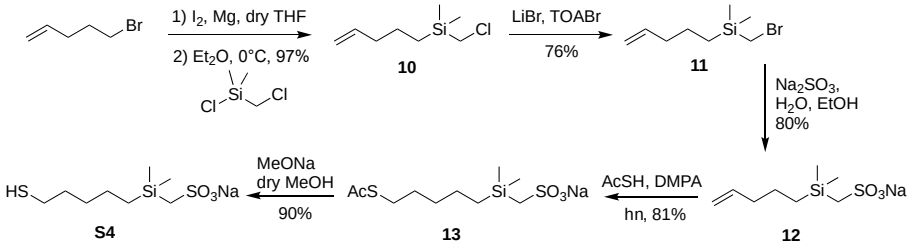

Scheme 4. Synthesis pathway for thiol **S4.**

*(Chloromethyl)dimethyl(pent-4-enyl)silane (**10**).*

Mg turnings (693 mg, 29.713 mmol, 1.1 equiv) were vigorously stirred overnight in a two neck flask under N2. Then 3 mL of dry THF and a catalytic amount of I_2 are added and the solution is heated in order to activate the Mg. Then 5-bromopent-1-ene (3.2 mL, 27.012 mmol, 1 equiv) and dry THF (57 mL) were added drop by drop. The solution was stirred under N2 at 40°C for

6 hours. Then the solution was cooled to 0°C and slowly added via canula to a 0°C solution of chloro(chloromethyl)dimethylsilane (4.3 mL, 32.414 mmol, 1.2 equiv) in dry EtO2. The obtained solution was stirred overnight at room temperature and then it was quenched by adding a saturated solution of NH_4Cl. Then the mixture was extracted with Et^2O for five times, the organic layers were collected, dried over Na_2SO_4 and then concentrated under reduced pressure. The obtained crude was purified was purified by flash column chromatography (100% PE), affording the desired compound **10** (4.7 g, 97%).

^{1}H NMR (500 MHz, CDCl3) δ 6.03 – 5.75 (m, 1H), 5.21 – 4.98 (m, 2H), 2.89 (s, 2H), 2.25 – 2.13 (m, 2H), 1.59 – 1.49 (m, 2H), 0.81 – 0.72 (m, 2H), 0.22 (s, 6H).

^{13}C NMR (126 MHz, CDCl3) δ 138.60, 114.74, 37.44, 30.34, 23.03, 13.23, -4.62.

^{29}Si NMR (99 MHz, CDCl3) δ 3.71.

*(Bromomethyl)dimethyl(pent-4-enyl)silane (**11**).*

In a Schlenk tube compound **10** (2.5 g, 14.143 mmol, 1 equiv), LiBr (previously dried at 150°C under N2, 3.69 g, 42.430 mmol, 3 equiv) and TOABr (1.50 g, 2.829 mmol, 0.2 equiv) were added and the mixture was stirred for 24 h at 60°C. The obtained crude was purified by flash column chromatography (100% PE), affording the desired compound **11** (2.37 g, 76%).

^{1}H NMR (500 MHz, CDCl3) δ 6.02 – 5.79 (m, 1H), 5.21 – 4.98 (m, 2H), 2.58 (s, 2H), 2.24 – 2.11 (m, 2H), 1.59 – 1.49 (m, 2H), 0.82 – 0.72 (m, 2H), 0.23 (s, 6H).

^{13}C NMR (126 MHz, CDCl3) δ 138.61, 114.74, 37.43, 23.07, 17.09, 13.69, -4.04.

^{29}Si NMR (99 MHz, CDCl3) δ 3.69.

*Sodium (dimethyl(pent-4-enyl)silyl)methanesulfonate (**12**).*

In a Schlenk tube compound **11** (400 mg, 1.808 mmol, 1 equiv) and Na2SO3 (456 mg, 3.616 mmol, 2 equiv) were dissolved in 13 mL of H2O:EtOH 1:1 and

the reaction was stirred for 24 h at 60°C. The obtained crude was purified by reverse phase chromatography (C18 resin, from 100% H2O to 100% MeOH), affording the desired compound **12** (352 mg, 80%).

^{1}H NMR (500 MHz, MeOD) δ 5.96 – 5.70 (m, 1H), 5.09 – 4.90 (m, 2H), 2.58 (s, 2H), 2.16 – 2.01 (m, 2H), 1.54 – 1.37 (m, 2H), 0.81 – 0.63 (m, 2H), 0.18 (s, 6H).

^{13}C NMR (126 MHz, MeOD) δ 138.5, 113.6, 41.9, 37.3, 23.0, 14.4, -4.2.

^{29}Si NMR (99 MHz, CDCl3) δ 0.85.

MS (ESI) m/z: 221.1 ([M]-)

*Sodium ((5-(acetylthio)pentyl)dimethylsilyl)methanesulfonate (**13**).*

Sulfonate **12** (221.3 mg, 1.471 mmol, 1 equiv) was dissolved in 3 mL of MeOH and the solution was degased by N2 bubbling for 30 min. Then thioacetic acid (415 μl, 5.890 mmol, 4 equiv) and 2,2-dimethoxy-2-phenylacetophenone (DMPA, 39 mg, 0.147 mmol, 0.1 equiv) were added and the mixture was stirred under UV irradiation (365 nm) for 2.5 h. The solvent was evaporated under vacuum and the crude was purified by flash column chromatography (DCM:MeOH from 9:1 to 8:2), affording the desired sulfonate compound **13** (381 mg, 81%).

^{1}H NMR (500 MHz, MeOD) δ 2.88 (t, J = 7.3 Hz, 2H), 2.59 (s, 2H), 2.32 (s, 2H), 1.64 – 1.53 (m, 2H), 1.46 – 1.35 (m, 2H), 0.78 – 0.65 (m, 2H), 0.18 (s, 6H).

^{13}C NMR (126 MHz, MeOD) δ 196.23, 41.87, 32.24, 29.11, 28.99, 28.41, 22.85, 14.67, -4.16.

^{29}Si NMR (99 MHz, MeOD) δ -0.84.

MS (ESI) m/z: 297.0 ([M]-)

*Sodium ((5-mercaptopentyl)dimethylsilyl)methanesulfonate (**S4**).*

The acetylated sulfonate **13** (30 mg, 0.0987 mmol, 1 equiv) was dissolved in 1 mL of dry MeOH and then sodium methoxide was added (16

mg, 0.296 mmol, 3 equiv). After stirring for 2.5 hours under N2 atmosphere, the reaction was quenched adding IR 120H+ resin until pH neutralization, then the resin was filtered off, the solvent was evaporated, giving the deprotected sodium 11-mercaptoundecane-1-sulfonate **S4** (25 mg, yield 90%), that was freshly used for the nanoparticles' synthesis.

^{1}H NMR (500 MHz, MeOD) δ 2.57 (s, 2H), 2.52 – 2.45 (m, 2H), 1.66 – 1.56 (m, 2H), 1.49 – 1.32 (m, 4H), 0.76 – 0.66 (m, 2H), 0.18 (s, 6H).

^{13}C NMR (126 MHz, MeOD) δ 41.90, 37.31, 33.56, 24.70, 23.30, 15.06, -4.16.

^{29}Si NMR (99 MHz, MeOD) δ -0.87.

TOF ES- HRMS: [M -] calcd. for C8H19O3S2Si=255.055. Found = 255.049.

2.3 Synthesis AuNPs

Monolayer protected gold nanoparticles (**S1**, **S2**, **S3**, **S4-AuNPs**) were prepared following a previously reported two-step procedure. A solution of $HAuCl_4 \bullet 3H_2O$ (50 mg, 0.127 mmol, 1 equiv) in water (2 mL) was extracted with a solution of tetraoctylammonium bromide (0.175 g, 0.318 mmol, 2.5 equiv) in N_2 purged toluene (125 mL). To the resulting reddish-orange organic solution dioctylamine (0.613 g, 2.539 mmol, 20 equiv) was added (the amount of dioctylamine was calculated in order to obtain 2 nm nanoparticles). The mixture is vigorously stirred under N_2 for 1,5 hours. During this period of time the colour of the mixture fades. Then the solution is cooled at 0°C and a $NaBH_4$ solution (48.0 mg, 1.269 mmol, 10 equiv) in H_2O (1 mL) is then rapidly added. The colour of the solution turns rapidly to black and after 1.5 hours of stirring at 0°C, the aqueous layer is removed. To the obtained nanoparticle solution, the desired thiol **S1-4** (0.254 mmol, 2 equiv) dissolved in 3 mL of MeOH was rapidly added. The reaction mixture was stirred for 3 hours

at 0°C. All the formed AuNPs were insoluble in toluene, hence the mixtures were centrifuged and the collected AuNPs were washed under sonication 7 times, with EtOAc and MeOH. The resulting NPs were finally purified by gel permeation chromatography with Sephadex G-25.

TEM analysis of the different samples of small nanoparticles (*Figure 2.22, 2.24, 2.26, 2.28*) yields an average diameter for **S1-AuNPs** of 1.8 ± 0.2nm, for **S2-, S3-, S4-AuNPs** of 1.6 ± 0.4 nm. This data, together with the loss of organic weigh obtained by TGA analysis (*Figure 2.30, 2.31, 2.32, 2.33*), indicate that the formula for AuNP is $Au_{127}SR_{39}$ for **S1-AuNPs**, $Au_{180}SR_{54}$ for **S2-AuNPs**, $Au_{127}SR_{55}$ for **S3-AuNPs**, $Au_{127}SR_{44}$ for **S4-AuNPs**. The gold core of AuNP was approximated as a sphere, and the weight loss considered is related to the thiol minus $NaHSO_3$ that stays as inorganic residue. NMR analysis (*Figure 34, 35, 36, 37*) indicates monolayer formation (broadening of all signals and missing of the SCH_2CH_2 protons' signals). UV-vis spectra (*Figure 38, 39, 40, 41*) were recorded.

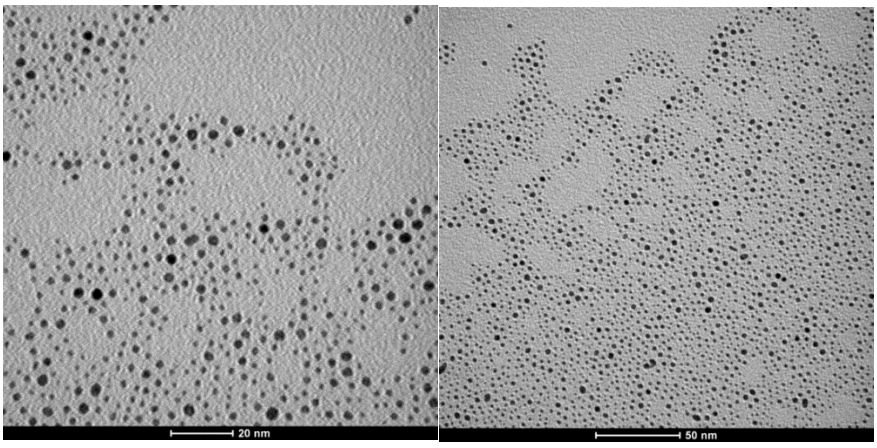

Figure 2.22: TEM of S1-AuNPs.

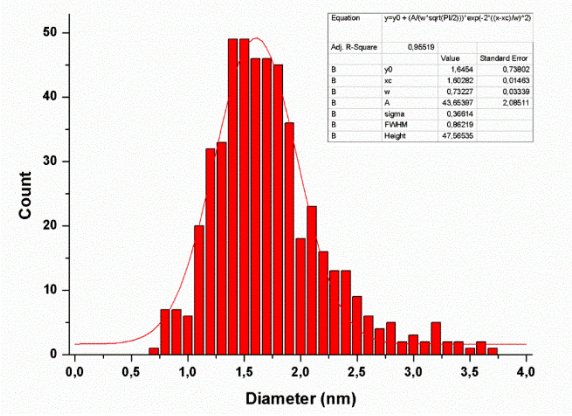

Figure 2.23. Sample TEM images **S1-AuNP** and size distribution: average diameter = 1.6 nm (σ= 0.4 nm).

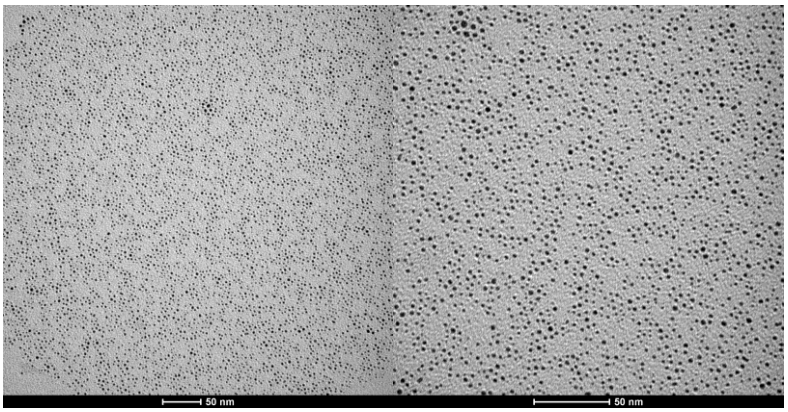

Figure 2.24: TEM of S1-AuNPs**.**

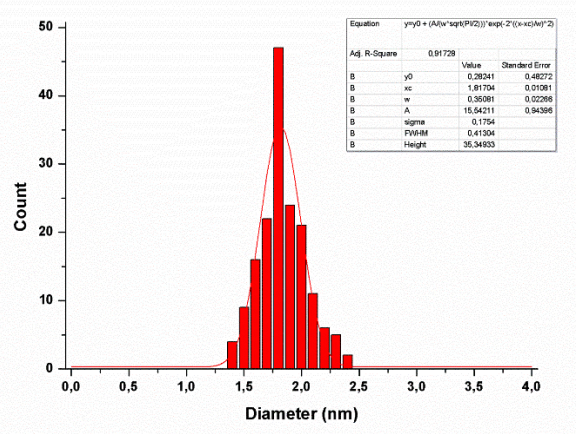

Figure 2.25. Sample TEM images **S2-AuNP** and size distribution: average diameter = 1.8 nm (σ= 0.2 nm).

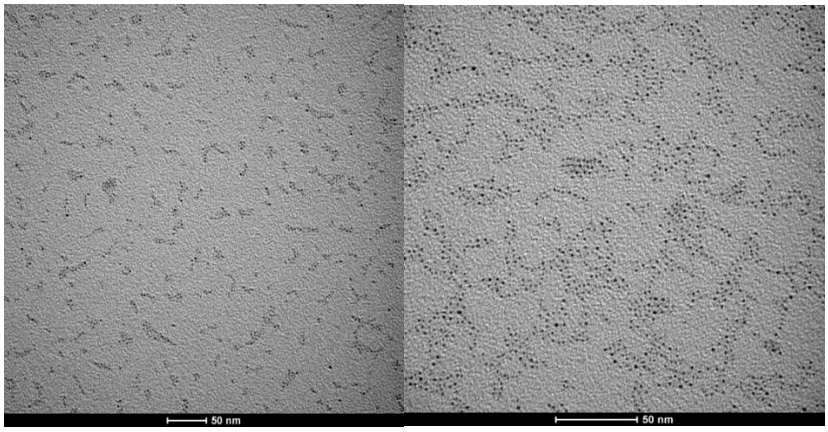

Figure 2.26: TEM of S1-AuNPs.

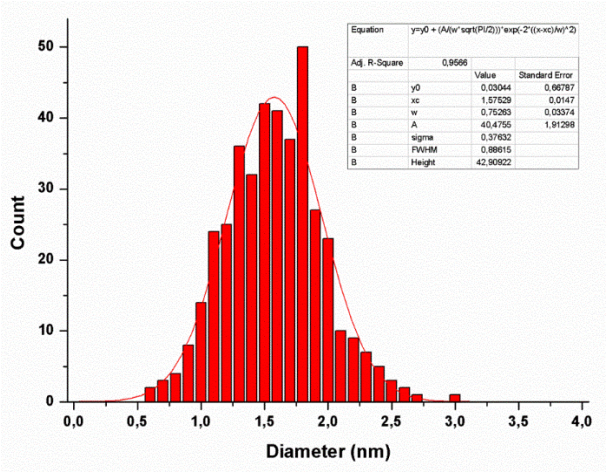

Figure 2.27. Sample TEM images of **S3-AuNP** and size distribution: average diameter = 1.6 nm (σ= 0.4 nm).

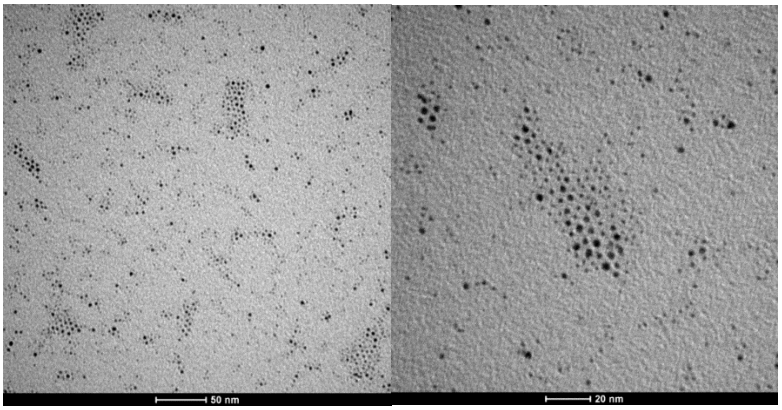

Figure 2.28: TEM of S1-AuNPs.

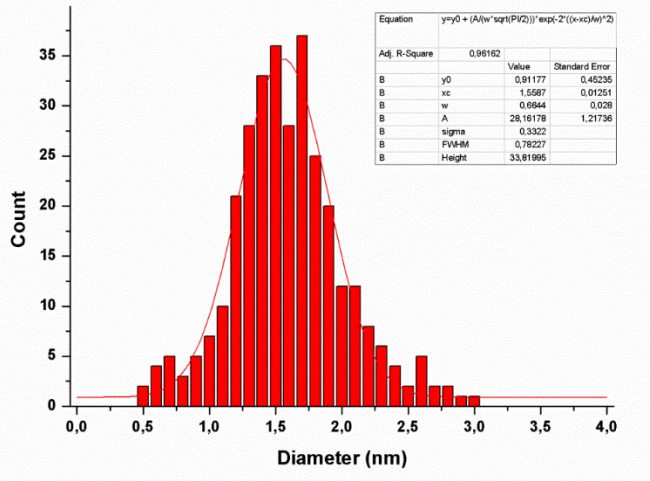

Figure 2.29. Sample TEM images **S4-AuNP** and size distribution: average diameter = 1.6 nm (σ= 0.3nm).

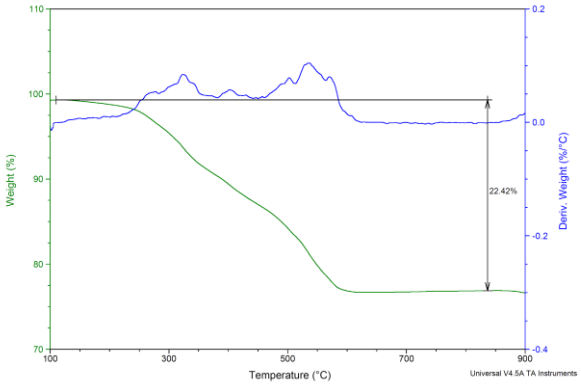

Figure 2.30. TGA analysis of **S1-AuNPs** sample, under air atmosphere.

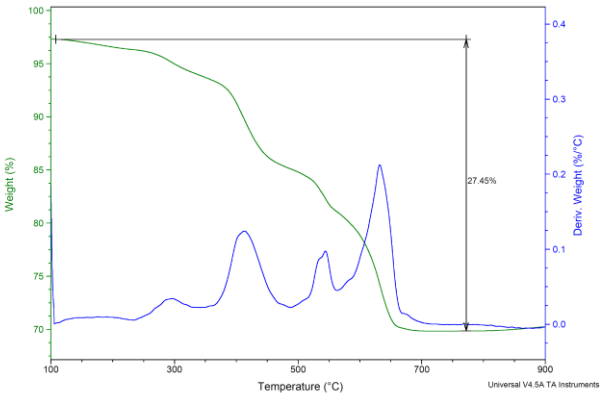

Figure 2.31. TGA analysis of **S2-AuNPs** sample, under air atmosphere.

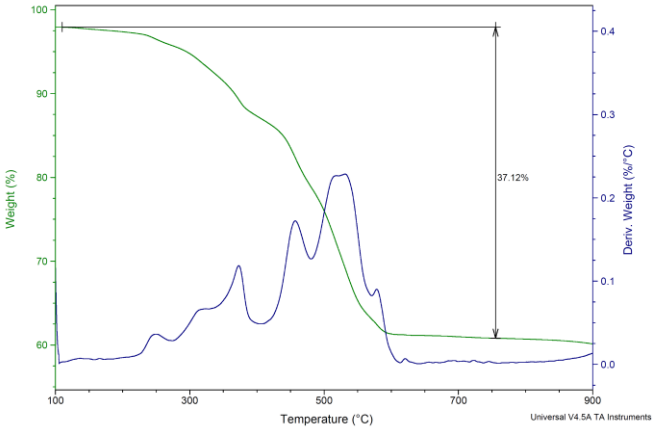

Figure 2.32. TGA analysis of **S3-AuNPs** sample, under air atmosphere.

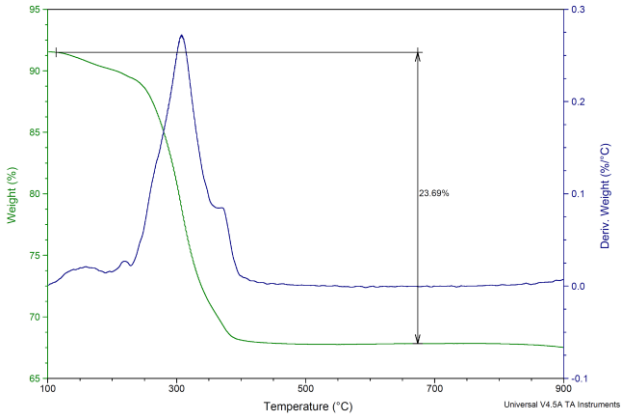

Figure 2.33. TGA analysis of **S4-AuNPs** sample, under air atmosphere.

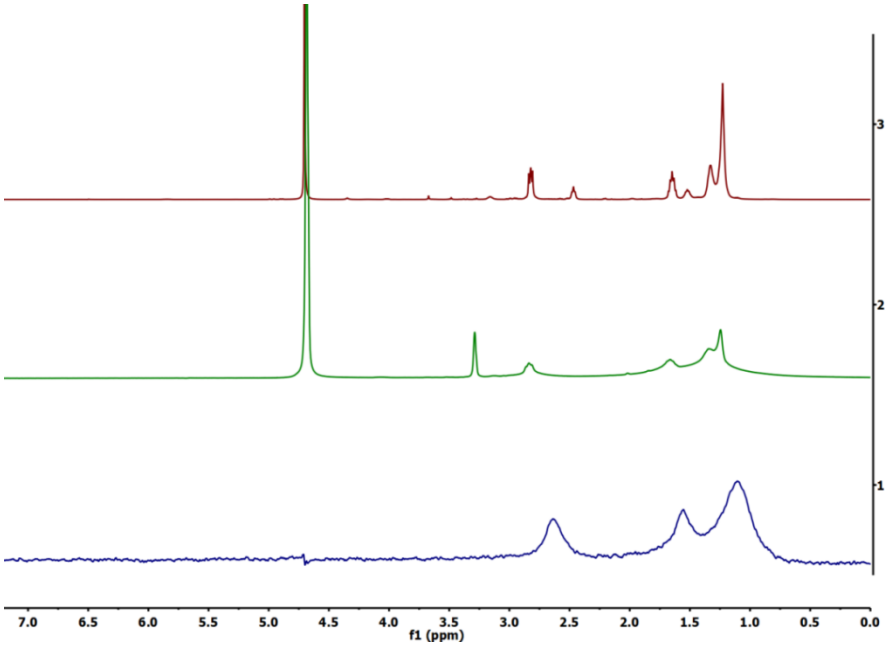

Figure 2.34. ^{1}H-NMR (500 MHz) spectrum in D_2O of: a) deprotected thiol **S1**; b) **S1-AuNPs**; c) diffusion filtered spectrum of **S1-AuNPs**. (* indicates the residual solvents).

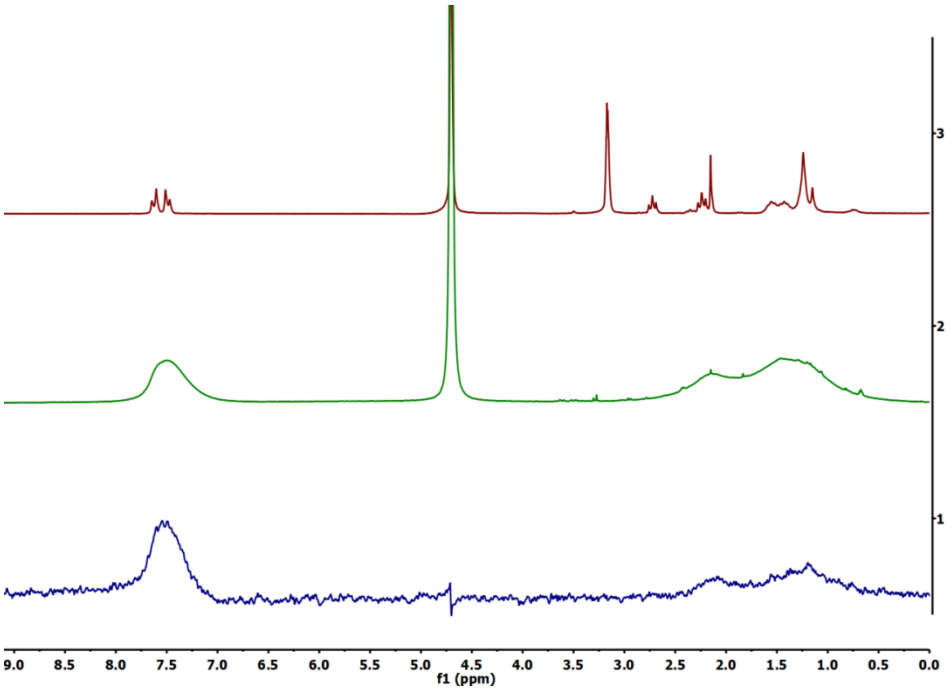

Figure 2.35. ^{1}H-NMR (500 MHz) spectrum of: a) deprotected thiol **S2** in MeOD; b) **S2-AuNPs** in D_2O; c) diffusion filtered spectrum of **S2-AuNPs** in D_2O. (* indicates the residual solvents).

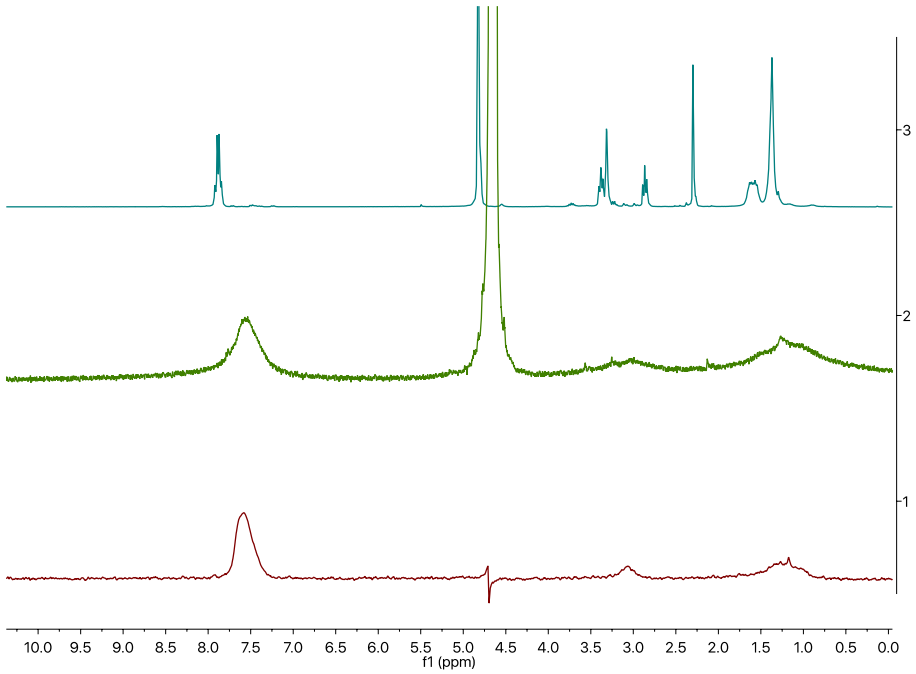

Figure 2.36. ^{1}H-NMR (500 MHz) spectrum of: a) protected thiol **9**; b) Diffusion filter of **S3-AuNPs** and c) ^{1}HNMR of the **S3-AuNPs** (* indicates the residual solvents).

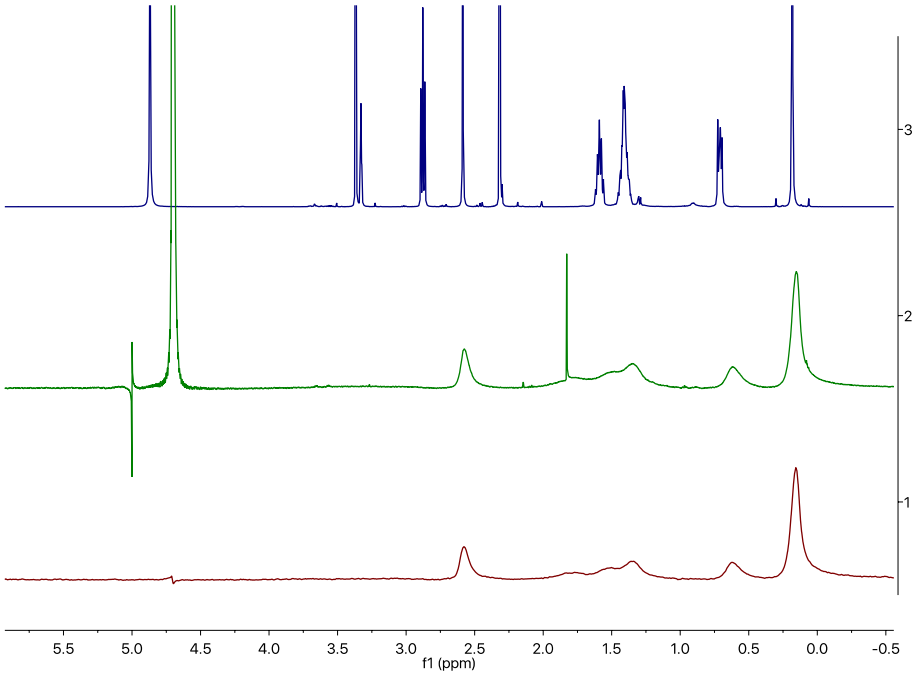

Figure 2.37. ^{1}H-NMR (500 MHz) spectra of: a) Protected thiol (MeOD) **13**; b) ^{1}H-NMR of the **S4-AuNPs** and c) Diffusion filter of **S4-AuNPs** (D_2O) (* indicates the residual solvents).

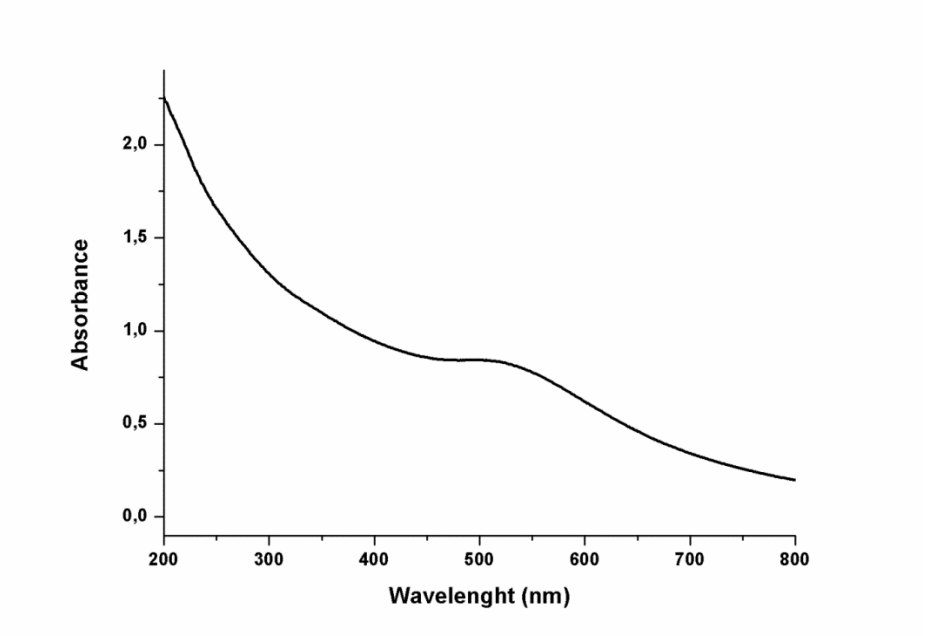

Figure 2.38. UV-Vis spectrum of **S1-AuNPs** (0.1 mg/mL) at 25°C in water.

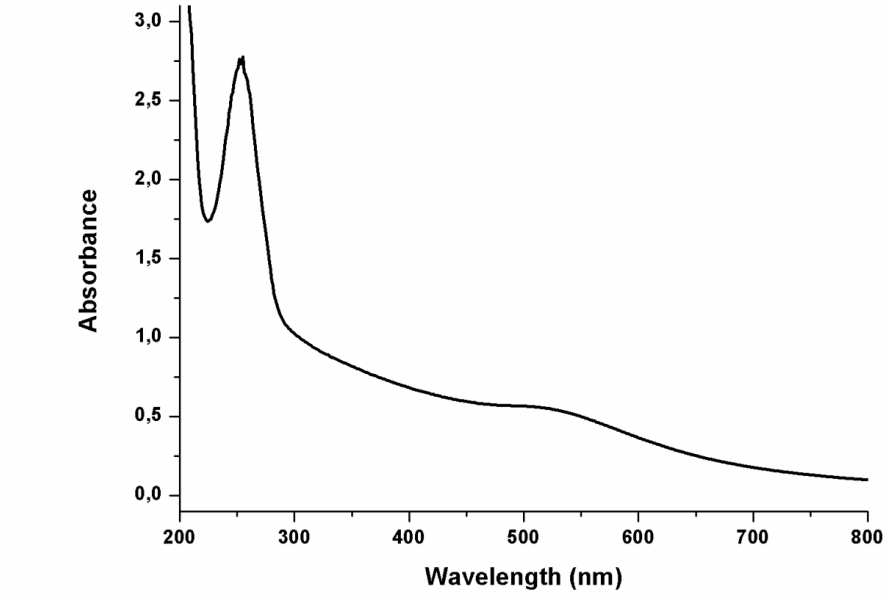

Figure 2.39. UV-Vis spectrum of **S2-AuNPs** (0.1 mg/mL) at 25°C in water. Absorbance peak of thiol aromatic moiety at 270nm.

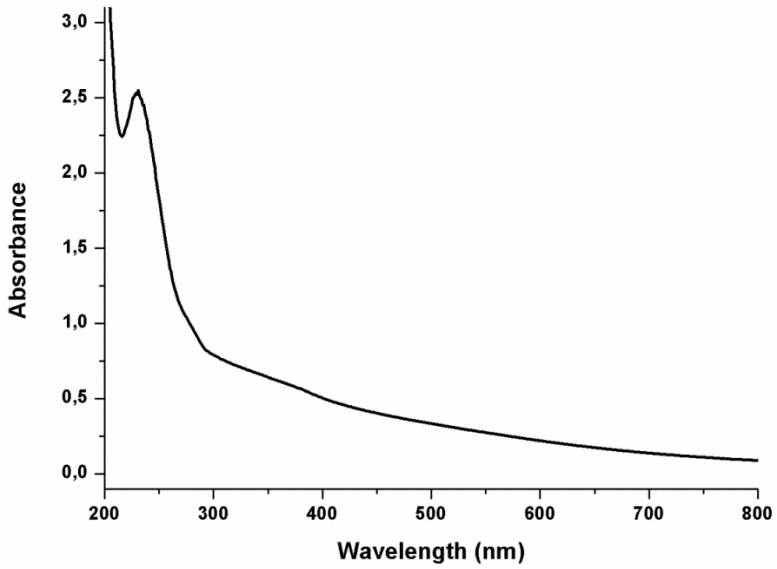

Figure 2.40. UV-Vis spectrum of **S3-AuNPs** (0.1 mg/mL) at 25°C in water. Absorbance peak of thiol aromatic moiety at 270nm.

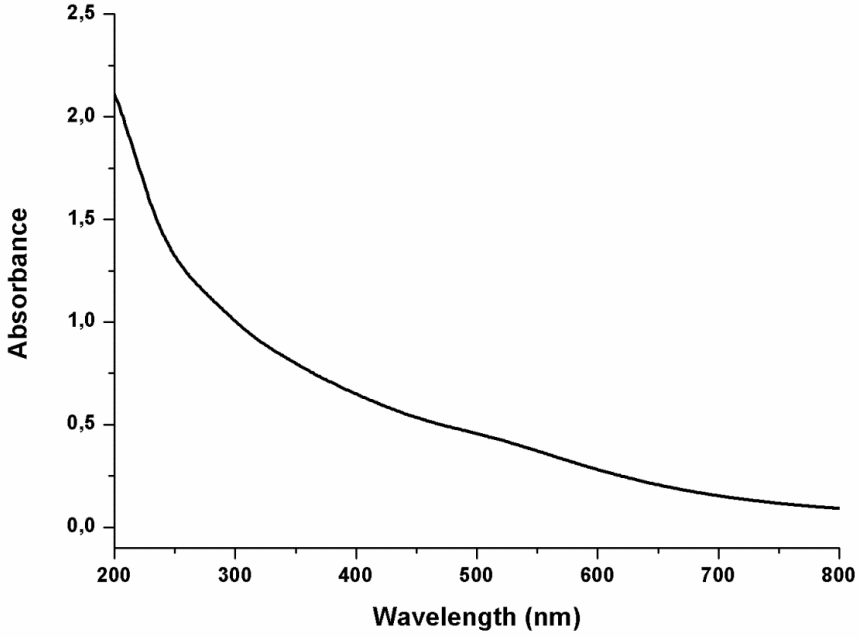

Figure 2.41. UV-Vis spectrum of **S4-AuNPs** (0.1 mg/mL) at 25°C in water.

Bibliography

(1) Znaleziona, J.; Ginterová, P.; Petr, J.; Ondra, P.; Válka, I.; Ševčík, J.; Chrastina, J.; Maier, V. Determination and Identification of Synthetic Cannabinoids and Their Metabolites in Different Matrices by Modern Analytical Techniques - a Review. *Analytica Chimica Acta*. Elsevier May 18, 2015, pp 11–25.

(2) Elkins, K. M.; Weghorst, A. C.; Quinn, A. A.; Acharya, S. Colour Quantitation for Chemical Spot Tests for a Controlled Substances Presumptive Test Database. *Drug Test. Anal.* **2017**, *9* (2), 306–310.

(3) Franz, F.; Angerer, V.; Jechle, H.; Pegoro, M.; Ertl, H.; Weinfurtner, G.; Janele, D.; Schlögl, C.; Friedl, M.; Gerl, S.; et al. Immunoassay Screening in Urine for Synthetic Cannabinoids - An Evaluation of the Diagnostic Efficiency. *Clin. Chem. Lab. Med.* **2017**, *55* (9), 1375–1384.

(4) Gabrielli, L.; Rosa-Gastaldo, D.; Salvia, M. V.; Springhetti, S.; Rastrelli, F.; Mancin, F. Detection and Identification of Designer Drugs by Nanoparticle-Based NMR Chemosensing. *Chem. Sci.* **2018**, *9* (21), 4777–4784.

(5) Jang, Y.; Jang, M.; Kim, H.; Lee, S. J.; Jin, E.; Koo, J. Y.; Hwang, I. C.; Kim, Y.; Ko, Y. H.; Hwang, I.; et al. Point-of-Use Detection of Amphetamine-Type Stimulants with Host-Molecule-Functionalized Organic Transistors. *Chem* **2017**, *3* (4), 641–651.

(6) Masseroni, D.; Biavardi, E.; Genovese, D.; Rampazzo, E.; Prodi, L.; Dalcanale, E. A Fluorescent Probe for Ecstasy. *Chem. Commun.* **2015**, *51* (64), 12799–12802.

(7) Biavardi, E.; Federici, S.; Tudisco, C.; Menozzi, D.; Massera, C.; Sottini, A.; Condorelli, G. G.; Bergese, P.; Dalcanale, E. Cavitand-Grafted Silicon Microcantilevers as a Universal Probe for Illicit and Designer Drugs in Water. *Angew. Chemie - Int. Ed.* **2014**, *53* (35), 9183–9188.

(8) Jana, N. R.; Peng, X. Single-Phase and Gram-Scale Routes toward Nearly Monodisperse Au and Other Noble Metal Nanocrystals. *J. Am. Chem. Soc.* **2003**, *125* (47), 14280–14281.

(9) Manea, F.; Bindoli, C.; Polizzi, S.; Lay, L.; Scrimin, P. Expeditious Synthesis of Water-Soluble, Monolayer-Protected Gold Nanoparticles of Controlled Size and Monolayer Composition. *Langmuir* **2008**, *24* (8), 4120–4124.

(10) Lucarini, M.; Franchi, P.; Pedulli, G. F.; Gentilini, C.; Polizzi, S.; Pengo, P.; Scrimin, P.; Pasquato, L. Effect of Core Size on the Partition of Organic Solutes in the Monolayer of Water-Soluble Nanoparticles: An ESR Investigation. *J. Am. Chem. Soc.* **2005**, *127* (47), 16384–16385.

(11) Lucarini, M.; Franchi, P.; Pedulli, G. F.; Pengo, P.; Scrimin, P.; Pasquato, L. EPR Study of Dialkyl Nitroxides as Probes to Investigate the Exchange of Solutes between the Ligand Shelf of Monolayers of Protected Gold Nanoparticles and Aqueous Solutions. *J. Am. Chem. Soc.* **2004**, *126* (30), 9326–9329.

(12) Boccalon, M.; Bidoggia, S.; Romano, F.; Gualandi, L.; Franchi, P.; Lucarini, M.; Pengo, P.; Pasquato, L. Gold Nanoparticles as Drug Carriers: A Contribution to the Quest for Basic Principles for Monolayer Design. *J. Mater. Chem. B* **2015**, *3* (3), 432–439.

(13) Guarino, G.; Rastrelli, F.; Mancin, F. Mapping the Nanoparticle-Coating Monolayer with NMR Pseudocontact Shifts. *Chem. Commun.* **2012**, *48* (10), 1523–1525.

(14) Riccardi, L.; Gabrielli, L.; Sun, X.; De Biasi, F.; Rastrelli, F.; Mancin, F.; De Vivo, M. Nanoparticle-Based Receptors Mimic Protein-Ligand Recognition. *Chem* **2017**, *3* (1), 92–109.

(15) Sun, X.; Riccardi, L.; De Biasi, F.; Rastrelli, F.; De Vivo, M.; Mancin, F. Molecular-Dynamics-Simulation-Directed Rational Design of Nanoreceptors with Targeted Affinity. *Angew. Chemie - Int. Ed.* **2019**, *58* (23), 7702–7707.

(16) Tucker-Schwartz, A. K.; Farrell, R. A.; Garrell, R. L. Thiol - Ene Click Reaction as a General Route to Functional Trialkoxysilanes for Surface Coating Applications. *J. Am. Chem. Soc.* **2011**, *133* (29), 11026–11029.

(17) Uzun, O.; Hu, Y.; Verma, A.; Chen, S.; Centrone, A.; Stellacci, F. Water-Soluble Amphiphilic Gold Nanoparticles with Structured Ligand Shells. *Chem. Commun.* **2008**, No. 2, 196–198.

(18) McGeary, R. P.; Bennett, A. J.; Tran, Q. B.; Prins, J.; Ross, B. P. An "inside-out" Approach to Suramin Analogues. *Tetrahedron* **2009**, *65* (20), 3990–3997.

(19) Smith, R. J.; Bienz, S. Towards Functionalized Silicon-Containing α-Amino Acids: Asymmetric Syntheses of Sila Analogs of Homoserine and Homomethionine. *Helv. Chim. Acta* **2004**, *87* (7), 1681–1696.

(20) Chen, A.; Shapiro, M. J. NOE Pumping: A Novel NMR Technique for Identification of Compounds with Binding Affinity to Macromolecules. *Journal of the American Chemical Society*. October 7, 1998, pp 10258–10259.

(21) Chen, A.; Shapiro, M. J. NOE Pumping. 2. A High-Throughput Method to Determine Compounds with Binding Affinity to Macromolecules by NMR. *J. Am. Chem. Soc.* **2000**, *122* (2), 414–415.

(22) Salvia, M. V.; Salassa, G.; Rastrelli, F.; Mancin, F. Turning Supramolecular Receptors into Chemosensors by Nanoparticle-Assisted "NMR Chemosensing." *J. Am. Chem. Soc.* **2015**, *137* (35), 11399–11406.

(23) Salvia, M. V.; Ramadori, F.; Springhetti, S.; Diez-Castellnou, M.; Perrone, B.; Rastrelli, F.; Mancin, F. Nanoparticle-Assisted NMR Detection of Organic Anions: From Chemosensing to Chromatography. *J. Am. Chem. Soc.* **2015**, *137* (2), 886–892.

(24) Rastrelli, F.; Jha, S.; Mancin, F. Seeing through Macromolecules: T2-Filtered NMR for the Purity Assay of Functionalized Nanosystems and the Screening of Biofluids. *J. Am. Chem. Soc.* **2009**, *131* (40), 14222–14224.

(25) González-García, T.; Margola, T.; Silvagni, A.; Mancin, F.; Rastrelli, F. Chromatographic NMR Spectroscopy with Hollow Silica Spheres. *Angew. Chemie - Int. Ed.* **2016**, *55* (8), 2733–2737.

(26) Reddy G. N., M.; Ballesteros-Garrido, R.; Lacour, J.; Caldarelli, S. Determination of Labile Chiral Supramolecular Ion Pairs by Chromatographic NMR Spectroscopy. *Angew. Chemie - Int. Ed.* **2013**, *52* (11), 3255–3258.

(27) Pages, G.; Delaurent, C.; Caldarelli, S. Simplified Analysis of Mixtures of Small Molecules by Chromatographic NMR Spectroscopy. *Angew. Chemie - Int. Ed.* **2006**, *45* (36), 5950–5953.

(28) Abraham, T. T.; Barnes, A. J.; Lowe, R. H.; Kolbrich Spargo, E. A.; Milman, G.; Pirnay, S. O.; Gorelick, D. A.; Goodwin, R. S.; Huestis, M. A. Urinary MDMA, MDA, HMMA, and HMA Excretion Following Controlled MDMA Administration to Humans. *J. Anal. Toxicol.* **2009**, *33* (8), 439–446.

3

Structural approach for improved sensitivity [a]

Summary

In this chapter, I explored the possibility to increase the sensitivity of the NOE-chemosensing technique applied to the sensing of designer drugs by acting on the thiol structure. As a matter of fact, lowering the detection limit to 10 μM would allow the use of the technique with biological fluids, i.e. for forensic analysis as well. Hereafter I will show that an already reported nanoparticle, coated with a crown ether moiety, can perform designer drug sensing with improved performance, exploiting different interactions from those at work when dealing with the sulfonate decorated ones. I will then show that a combination of the alkyl sulfonate and crown ether thiols combined on a single nanoparticle further improves the detection limit, lowering it to 200 μM. Eventually, as the crown ether nanoparticle can surprisingly detect phloretic acid due to the interference of potassium ions, I will show how it is

[a]Paragraphs 3.5 to 3.7 of this chapter are an adapted version of a manuscript which I co-authored and that has been already published during my PhD: *^{1}H-NMR Chemosensing of Potassium Ions Enabled by Guest-Induced Selectivity Switch of a Gold Nanoparticle/Crown Ether Nanoreceptor,* X. Sun, D. Rosa-Gastaldo, F. De biasi, F. Rastrelli, F. Mancin, ChemPlusChem **2019**, 84, 1-6.

possible to sense an inorganic specie such as K^+ by using its capability to tune the properties of the crown ether receptor. K^+ detection reaches up to 0.6 mM in 20 minutes with standard instrumentation.

3.1 Effect of the NP monolayer on the sensing

In a recent work from Riccardi et al,[1] computational studies performed on monolayer coated AuNPs have shown that AuNPs can behave in a manner that is reminiscent of the interaction among a protein and a ligand. In the study, they used nanoparticles coated with different thiols characterized by three different portions with different roles: an alkyl chain (hydrophobic) close to the nanoparticle, an oligoethylene glycol chain (hydrophilic) at the solvent-exposed end, and an amide function linking the two (**1** and **2** in *Figure 3.1*).

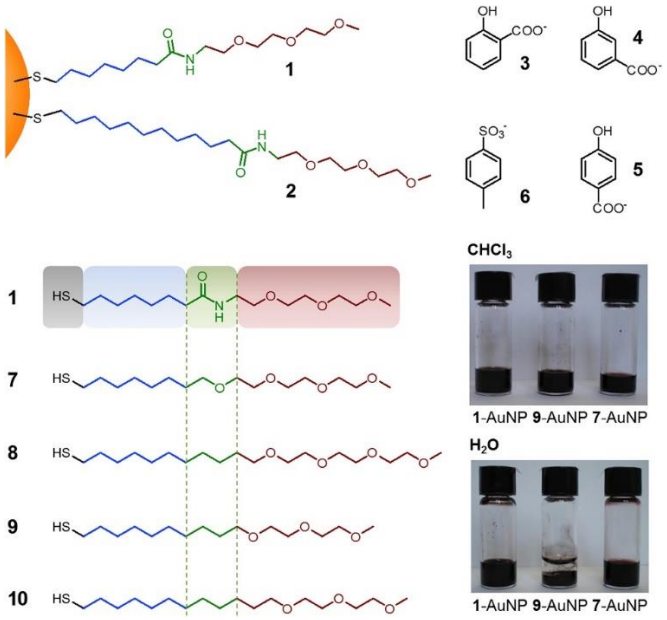

Figure 3.1. Upper: the monolayer-protected nanoparticles (thiols **1** and **2**) and analytes (**3**-**6**) investigated in early studies. Lower: nanoparticle coating thiols (**1** and **7**-**10**) used in this study and the solubility of representative samples in $CHCl_3$ and water. Picture by Riccardi et al.[1]

They also synthesized analogous thiols devoid of the amide function, that was replaced by an ether moiety (thiols **7** and **9** in *Figure 3.1*) or by extra methylene groups (thiols **8**, **9**, **10** in *Figure 3.1*). Other differences introduced regarded the length of the alkyl or oligoethylene glycol chains.

The differences in structure affect first of all the solubility: **1**-AuNP is fully soluble in water, **7**-AuNP and **8** are sparingly soluble, AuNP-**9** and **10** are completely insoluble in water.

1-AuNP binds selectively to the salicylate (**3**), with respect to 3- and 4-hydroxybenzoate and 4-methybenzenesulfonate (molecules **4**, **5**, **6**). **2**-AuNP can bind also **6**, but only marginally **4** and **5**. **7**-AuNp and **8** don't bind salicylate, even if they may seem structurally similar to **1**-AuNP (the signals in the NOE pumping spectra are hardly spotted and have a signal to noise ratio lower than 3). The results of the NOE pumping experiments with some of those NPs are reported in *Figure 3.2*.

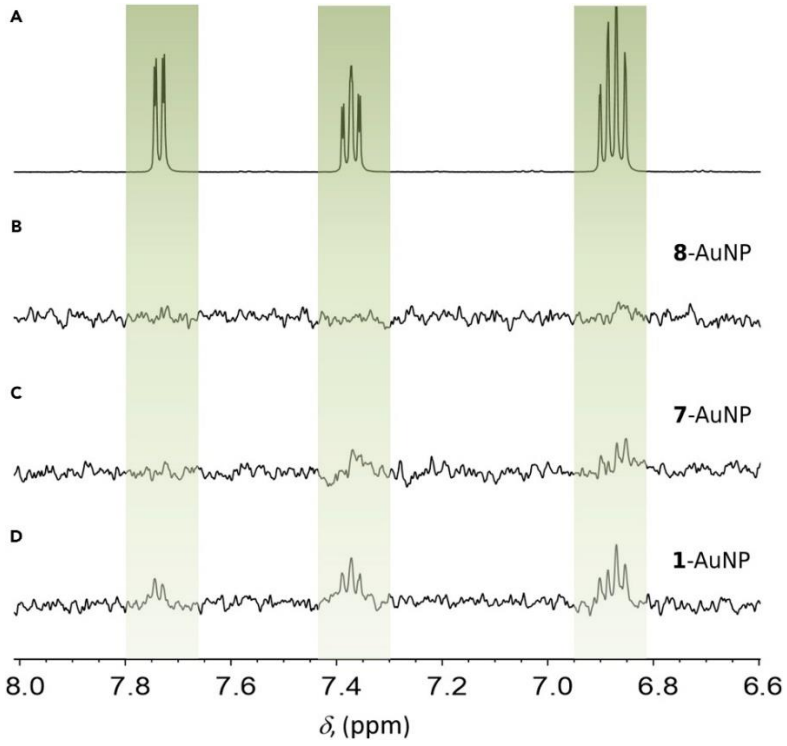

Figure 3.2. sensing experiments from the work cited a) ^{1}H-NMR of the sodium salicylate 5mM in D_2O; b-d) NOE-pumping experiments in presence of AuNP-8, 7, and 1 respectively. (conditions:AuNP 15 μM, carbonate buffer 20mM pD=10, 298 K). Picture by Riccardi et al.[1]

MD simulations explains this phenomenon: all the AuNPs have a spherical conformation in chloroform, but the simulation in water shows a differentiated behavior: **1**-AuNP is spherical, as well as **7-**AuNP, whereas **8**-AuNP and **9** start having a pronounced oval shape, that with **10**-AuNP is almost rugby ball-like. In the latter, the thiols are packed at the two extremities of the nanoparticle, where the chains are aligned and packed and the structure is overall stiffer. This bundling of thiols is visible also, to a lesser extent, in **7**, **8**, and **9**-AuNP. Bundled thiols expose the alkyl chains to water, increasing the hydrophobic attraction forces that lead the nanoparticles to precipitate. In the case of **1**-AuNP, the spherical shape of the nanoparticle exposes the hydrophilic moiety to the solvent while shielding the inner alkyl chains. This way, the thiols are not stacked together and are free to move, so that they can form hydrogen bonds between the chains, but also with the solvent molecules. This grated mobility leads to the formation of small cavities in the monolayer where a small molecule such as salicylate can bind. These cavities are transient, meaning that they change in position and number and they can last from few picoseconds to few tenths of nanoseconds. Their dynamic nature is due to the constant reorganization of the monolayer thiols.

Comparison of MD simulations with experiments showed that better results in salicylate sensing are reached when the contact time of the analyte with the monolayer is longer and the analyte can reach deeper inside the cavity (both things improve magnetisation transfer). In a second paper from Sun et al.,[2] the simulation studies were performed on a different set of nanoparticles, with the length of the oligoethylene glycol and alkyl chain being the same, and different linking moieties with different capabilities of donating or receiving hydrogen bond are introduced (and compared with the original amide in **1**-AuNP). This way, they demonstrated how even small changes in the thiol structure, guided by MD simulation, can lead to 10-fold improved affinity for the target molecule, from 10^2 M^{-1} to 10^3 M^{-1}. Combined with new STD experiments, discussed in the following chapter, this affinity increase led to a 100-fold decrease of the detection limit in the NMR-chemosensing experiment. This means that the sensing system can be used in micromolar concentration

range. Notably, in the previous chapter we discussed how it is possible, using high affinity nanoparticles and STD experiments, to detect phenethylamines in the micromolar range.

Therefore, it is possible to improve the sensitivity of the NMR-chemosensing by acting on the design of the thiol structure to improve the affinity; care must be taken in designing the thiol, considering not only the single molecule, but also the dynamics of the monolayer as a whole.

3.2 Thiol design

Starting from this result I decided to try to improve the nanoparticle affinity for phenethylamines by increasing the number of possible interactions. It is quite difficult to implement several interacting points in a single thiol, for this reason I decided to explore the use of mixed monolayers, where different thiols can provide different interactions simultaneously. The thiols used in this chapter are reported in *Figure 3.3*.

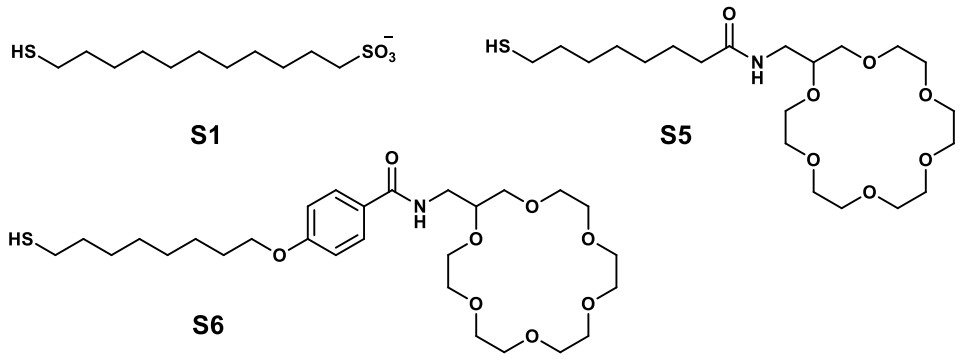

Figure 3.3. Structure of the thiols used in this chapter.

The properties of thiol **S1** have been extensively analysed in the previous chapter: it can sense designer drug analogues taking advantage of both the complementarity of charge between its sulfonate moiety and the positively charged ammonium group part of the phenethylamines backbone, and hy-

drophobic interactions, thus allowing the aromatic moiety of the analyte to fit in the inner part of the monolayer.[3] For these reasons I selected this thiol as the first component of the mixed monolayer, providing both ion pairing and hydrophobic interactions. The structure of phenethylamines allows for the establishment of other two kinds of interaction, namely H-bonds and π-π interaction, which could be provided by the other components of the monolayer.

Thiol **S5** contains a crown ether moiety; when used to coat a nanoparticle, it can provide a double interaction (in water): the formation of three hydrogen bonds between the primary ammonium moiety of the drug and the 18-crown-6 ether residue[4,5] and the hydrophobic interaction between the aromatic ring of the phenethylamine and the inner portion of the monolayer. Note that the crown-ether moiety, as reported, is expected to bind selectively primary ammonium ions over N-alkylated ammoniums. The synthesis is straightforward, following an already reported procedure.[4] It started from 8-bromoctanoic acid, which was reacted with potassium thioacetate to introduce the acetyl-protected thiol moiety. The carboxylic acid was then activated as pentafluorophenol ester and converted in high yield in the desired product by simply coupling it with the commercially available 2-aminomethyl-18-crown-6. The thioacetate deprotection can be conveniently carried out by refluxing the thioacetate in an acid solution.

Finally, thiol **S6** is an improved version of the design of benzenesulfonate thiols **S2** and **S3**, described in the previous chapter. In this case, the negative charge is replaced by the crown-ether; by doing so, the aromatic ring should be placed at the right distance for potential stacking interaction with the drug. Since the benzene moiety contains an electron-donating alkoxy group, the interaction with electron-poor drugs should be favoured over that with electron rich ones. The synthesis, reported at the end of the chapter in the additional information, started from the acetylation of 4-hydroxybenzoic acid. In this way, the carboxylic acid could be activated and coupled to the amino derivative of the crown ether. At this point, the acetate was cleaved with sodium

methoxide in methanol. As a last step, the now free phenol derivative was reacted under basic conditions with a bromoalkyl linker, where the thiol group was previously inserted, in this case, as trityl-protected moiety. I chose the trityl group because it's more resistant under the basic conditions used for the last step, and it's easy to remove using hydrochloric acid in perfluoroisopropanol in the presence of a silane scavenger. The nanoparticles obtained with this thiol had a problem of water solubility, probably because of the aromatic ring. They were readily soluble in methanol, so I made a stock solution in methanol and then diluted it in water. This way I could obtain a stable water solution of **S6-AuNP** (with traces of methanol, less than 5%).

3.3 Mixed monolayer AuNPs

For the NOE pumping experiments described in the next paragraph, I used gold nanoparticles **S1_5-AuNP** with a mixed monolayer, composed of thiol **S1** and **S5**. Nanoparticles with mixed monolayers can be synthesized in two ways, either by direct synthesis or thiol exchange.

For the first option, a solution containing the desired amount of the two thiols is added to the DOA passivated nanoparticles. The composition of the final nanoparticle reflects the composition of the initial mixture to different extents, but other factors enter in play affecting the respective binding efficiency of the thiols. Indeed, the monolayer formed in these conditions may not be the most thermodynamically stable but simply the kinetic product, as rearrangements of the first monolayer formed require slow exchange reactions. In general, an equimolar mixture of thiols rarely gives a nanoparticle with a 50:50 monolayer composition, especially if the two thiols are substantially different (i.e a neutral thiol and a charged one). For this reason, a trial and error procedure is often needed in order to get the desired composition. Secondly, but not less important, the two thiols can produce different popula-

tions of nanoparticles with different coating, or nanoparticles bearing different thiol domains on the surface. If the determination of the average coating composition is as simple as treating a sample with iodine and analyse the NMR of the solution obtained, understanding the disposition of the thiols on the monolayer is not so straightforward.

The second method cited, thiol exchange, can lead to a more even distribution of the thiols with respect to the previous one. In this case, the starting point is a solution of a nanoparticle covered with one of the desired thiols. A defined amount of the second thiol is added to this solution, and then left reacting for a long time, typically overnight. The solvent used has to be a good solvent for the nanoparticle but also for the two thiols. Purification with size-exclusion chromatography is usually necessary at the end. This way, an equilibrium is formed between the entering thiol and the leaving thiol so that, by adjusting the equivalents of the entering thiol, it is possible to get the desired composition. In addition, the exchange condition grants the formation of the most thermodynamically stable coating, provided that the exchange reaction is continued for a sufficiently long time. In this case as well, final composition of the monolayer is not predictable, as it depends not only from the thiols' ratio used, but from several other parameters, hence a trial and error approach is again needed to get the desired composition. **S1_5-AuNP** were, synthesized with a mixture 50:50 of thiols **S1** and **S5**, obtaining a monolayer richer in thiol **S5** (2:1 ratio).

3.4 Sensing experiments

I first investigated the monolayer protected AuNPs discussed above for sensing experiments using the NOE-pumping. NOE-pumping should be the first protocol to be used to explore the sensing capabilities of a new nanoparticle, because there is no possibility of a false positive interaction. A signal from the

analyte in the NOE-pumping experiment means that there is interaction between the analyte and the AuNP. The same is not necessarily true in a STD experiment, where false positive signals due to accidental saturation of the analytes or subtraction artefacts might appear (see infra).

I tested, first of all, **S5-AuNP**. This nanoparticle is already described in literature and it has been extensively used by Salvia et al[4] in methanol, where it was demonstrated that the crown ether receptor grafted on a nanoparticle shows different selectivity than the receptor alone in solution. The authors succeed in the detection and identification of primary amines and also in the discrimination of two biogenic diamines (cadaverine and putrescine) in mixtures where monoamines and α-amino acids were present. The selectivity of the system in water has been only partially explored, but they can successfully detect a large concentration (10 mM) of tyramine and putrescine.

I performed all my experiments in the same conditions of the ones in *Chapter 2:* 15 μM of gold nanoparticles (corresponding to 1mM in coating thiol), different concentrations of the designer drug analogue and HEPES buffer 10 mM. It appears clear from *Figure 3.4* that **S5-AuNP** are different in many ways from **S1-AuNP**.

First of all, they can discriminate primary amines from secondary and tertiary ones, at least at 1 mM concentration. If the concentration is raised at 2 mM, some signals start to appear also from the methylated amines, especially in the case of methoxy substituents that have a sharp singlet at 3.7 ppm that starts to raise from the noise. Secondly, **S5-AuNP** does not show the interaction with phloretic acid that was seen in the case of **S1-AuNP** at 1 mM concentration but, if the concentration of the substrate is raised to 5 mM, surprisingly the signals start to appear.

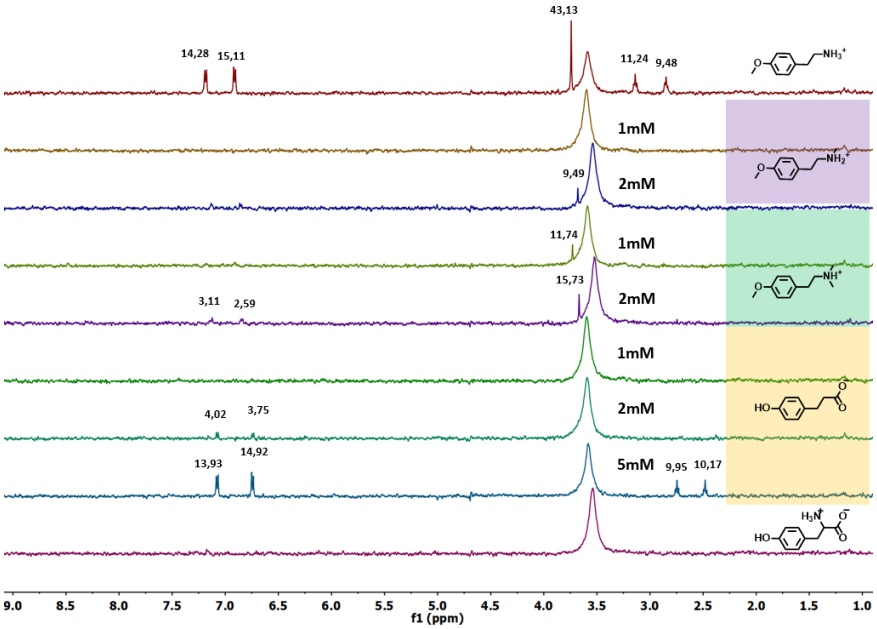

Figure 3.4 spectra obtained from NOE pumping experiments of samples containing **S5-AuNP** 15 μM, the analytes at concentration reported in the figure and HEPES buffer 10 mM pD=7. The numbers on the peaks indicate their S/N ratio.

Interesting enough, in all cases, the signal to noise ratio appears to be higher than in the case of **S1-AuNP**, even at half the concentration of analyte used. Indeed, for **S5-AuNP** reach a S/N around 15 for the aromatic signals, while in the case of **S1-AuNP** S/N it never exceeded the value of 5. This means that these nanoparticles are better than **S1-AuNP** in transferring the magnetisation to the analyte. This phenomenon can be explained by noting that, during the recognition event, the crown ether moiety must somehow wrap around the analyte to grant both H-bonding and hydrophobic interaction.

Any attempt to calculate the binding constant by fluorescence titration as for **S1-AuNP** failed. This means that the constant is at least two orders of magnitude lower than that of **S1-AuNP**.

Indeed, if we compare the effect of changing the analyte concentration with *Figure 2.17* in the previous chapter, and take into account that apparently **S5-AuNP** are better in transferring magnetisation than **S1-AuNP** we can easily conclude that affinity of **S5-AuNP** for phenethylamines is in the range 100-

1000 M^{-1}. Previous studies on the detection of anions by neutral nanoparticles revealed a binding constant around 100 M^{-1} for NPs providing hydrophobic interaction and a single H-bond and around 1000 M^{-1} for NPs providing hydrophobic interaction and two cooperating H-bonds. Results in *Figure 3.2* are in good agreement with these results: primary amines, that can bind to the NPs by hydrophobic interaction and multiple H-Bonds have greater affinity for **S5-AuNP** than secondary and tertiary amines, that can form a smaller number of H-bonds.

Notwithstanding the smaller affinity, **S5-AuNP** can detect primary phenethylamines at lower concentrations than **S1-AuNP**. Hence, the strength of the interaction between analyte and nanoparticle (binding constant) is not the only parameter to take into account when trying to improve a receptor.

In the case of phloretic acid, the sole hydrophobic interaction can't explain the recognition, because neutral molecules as phenylalanine and other not shown are not recognized by **S5-AuNP**. The other possibility, studied in more detail in the next paragraphs, is that some of the crown ether moieties of the nanoparticles are already complexed with some metal cations, such as Na^+ or K^+, from the thiol synthesis step. In this case, the 18-crown-6 is positively charged and capable to interact with the phloretate anion. With no surprise, **S5-AuNP** can't detect an amino acid such as phenylalanine.

I then studied the behaviour of mixed monolayer nanoparticle, **S1_5-AuNP** with both thiol **S1** and **S5**. I expected that the presence of the negative charge should have strengthened the interaction, as that could cooperate with the crown ether in the recognition of the ammonium group. The results are reported in *Figure 3.5*. Once again, the results go in the expected direction, i.e. the mixed nanoparticles detect the analyte at 1 mM concentration maintaining the selectivity for the primary ammoniums, but the signal to noise ratio is only slightly improved with respect than **S1-AuNP** and it is worse than **S5-AuNP**. In this case as well, it has not been possible to measure the binding

constants via fluorescence titrations, suggesting a low affinity of the NP for the analyte.

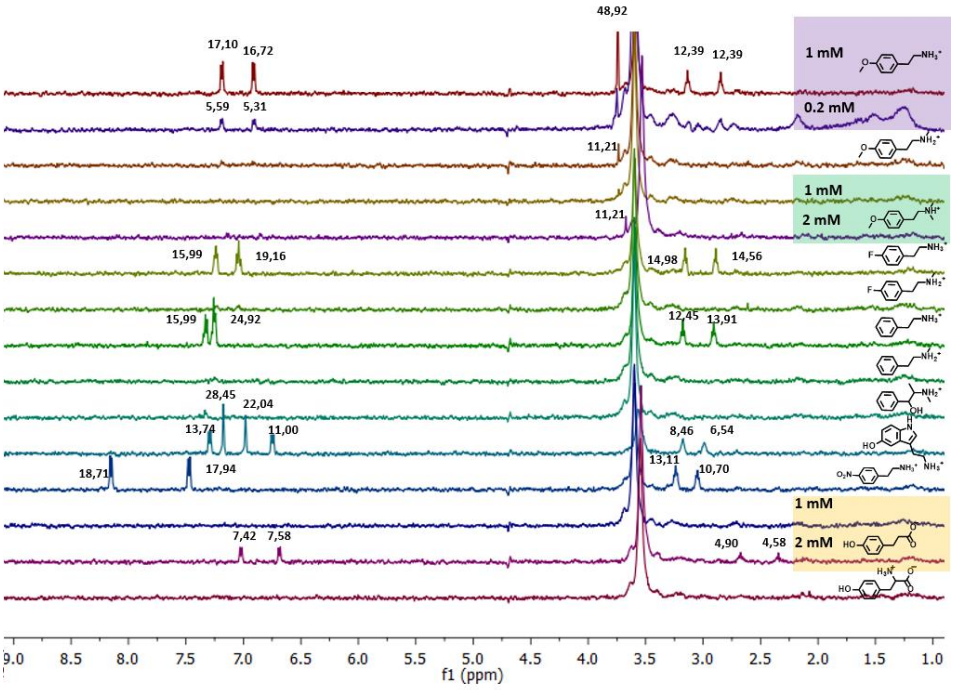

Figure 3.5. spectra obtained from NOE pumping experiments of samples containing **S1_5-AuNP** 15 μM, the analytes at concentration reported in the figure and HEPES buffer 10 mM pD=7. The numbers on the peaks indicate their S/N ratio.

At the end, these mixed nanoparticles behave in a very similar way to **S5-AuNP**. A possible hypothesis to explain this behaviour is that the sulfonate moieties can interact with the metal cations trapped in the crown ether and hence the couple of receptors is "neutralised" and it's not effective for the sensing of new analytes (or, the enhancement is lower than the one that could potentially be reached).

Finally, I tested the effectiveness of **S6-AuNP**. From the ^{1}H-NMR spectrum and from the diffusion filter spectrum it is clear that the monolayer is really stiff. All the signals are very broad and, in some cases barely visible. The affinity constant in this case as well falls in the range where detection is not possible by fluorescence titrations. The sensing experiments reported in *Figure 3.6*,

show a signal to noise ratio lower than the two previous examples. So, again, the insertion of an aromatic ring in the receptor does not seem a convenient way to improve recognition.

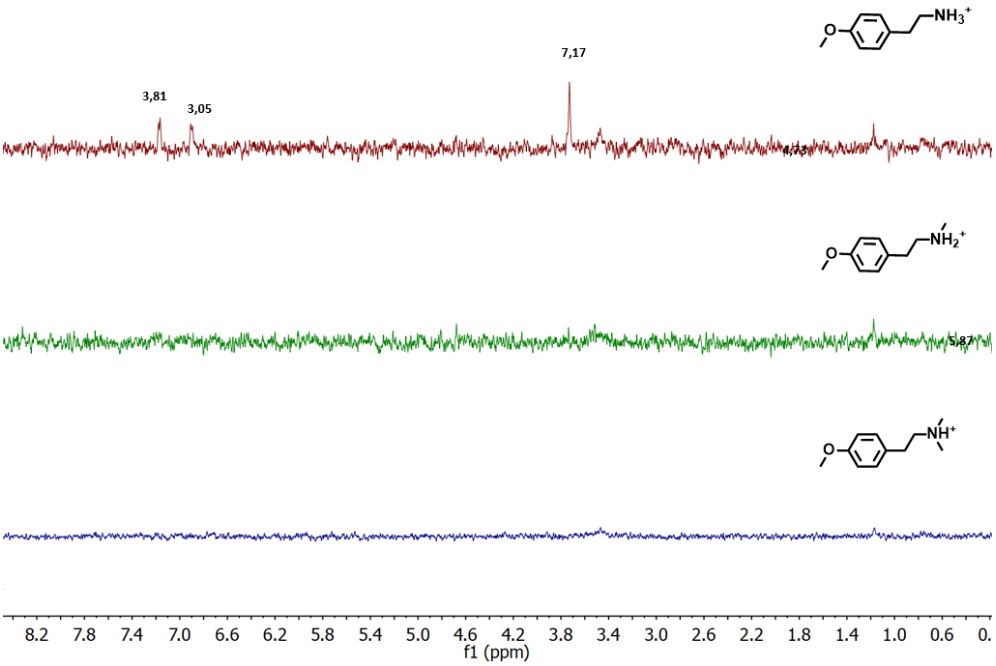

Figure 3.6. spectra obtained from NOE pumping experiments of samples containing **S6-AuNP** 15 μM, the analytes 1 mM and HEPES buffer 10 mM pD=7. The numbers on the peaks indicate their S/N ratio.

3.5 Sensing of K^+

From the preliminary screening of the analytes with **S5-AuNP**, it appears that phloretic acid is detected. If the hypothesis that I made in the previous paragraph is correct, that is, if it's true that the acid is detected because of the complexation of cations complexed to the crown ether, we reasoned that this could be used for the detection of inorganic cations by monitoring the signals of different guest molecules. In particular, potassium ions are the best guests for 18-crown-6. We reasoned that the binding of potassium ions to the crown

ether moieties should prevent the detection of a primary amine, both because the receptor is already occupied by K^+, and because of the consequent charge repulsion. Considering the reasons for the displacement of tyramine by K^+, we noticed that the binding of the cation to the crown ether moiety not only prevents ammonium from binding, but also substantially changes the nature of the nanoparticle. Indeed, the coating thiols are converted from neutral-amphiphiles to cationic-amphiphiles. This modification converts the nanoparticles into receptors for amphiphilic organic anions, as it enables the simultaneous occurrence of ion pairing and hydrophobic partition with this class of substrates (*Figure 3.8b*).[1,3,6]

The potassium dependent appearance and disappearance of the signals of organic molecules in the NOE pumping spectra of the sample could be used for the determination to the presence and concentration of the cation.

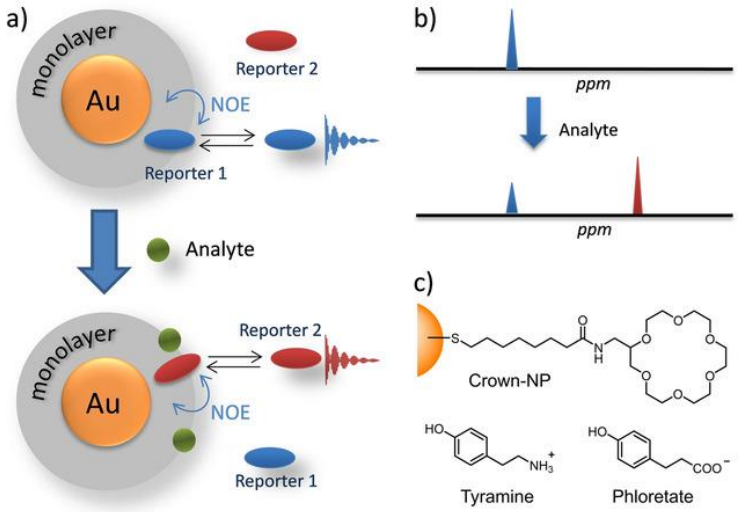

Figure 3.7. a) Guest-induced modulation of the nanoparticle-to-reporter magnetization transfer exploited in this paragraph. b) Schematic representation of the signal produced. c) Nanoparticles and NMR reporters used. Figure from the above mentioned work. [7]

To prove this idea, I used **S5-AuNP** and recorded the NOE-pumping spectra of different solutions in D_2O containing the nanoparticles (15 μM corresponding to 1 mM in thiol), tyramine (5 mM) and increasing amounts of KCl. To

avoid interferences from Na^+, the solutions were buffered with HEPES/Me_4NOH at pD=7. From the spectra reported in *Figure 3.8* I could observe that tyramine signals decrease as the concentration of K^+ increases. When no potassium is present, tyramine can bind the nanoparticle and the resulting NOE signals are observed. On the other hand, increasing amounts of K^+ reduce the affinity of the nanoparticles for the organic reporter and its signals progressively decrease. Remarkably, the standard ^1H NMR spectra of the different solutions were all identical as both the interactions of tyramine and K^+ with **S5-AuNP** do not produce any significant modification of the nanoparticle signals in the second conditions. Hence, when the NOE-pumping experiment is used, tyramine becomes an effective ^1H NMR reporter of the presence of K^+ in the solution, with a mechanism that follows the Indicator Displacement Assay (IDA) protocol.[8–10] However, the on-off sensing mode featured by the **S5-AuNP**/tyramine system may be affected by errors and artefacts, which are usually ameliorated if the sensing modes can be turned into a ratiometric one.[11]

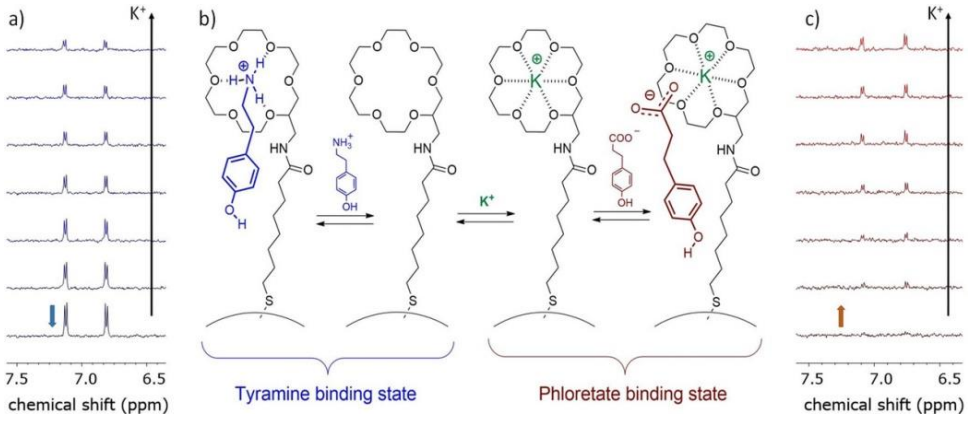

Figure 3.8. a) NOE pumping subspectra of a sample containing tyramine (5 mM) and **S5-AuNP** (20 μM) in HEPES/Me_4NOH buffered D_2O (pD = 7.0) in the presence of increasing amounts of KCl (from the bottom: 0, 2.5, 5, 10, 20, 30 and-50 mM); b) Schematic representation of the K^+ induced affinity switch of **S5-AuNP**; c) NOE pumping subspectra of a sample containing phloretate (5 mM) and **S5-AuNP** (20 μM) in HEPES/Me_4NOH buffered D_2O (pD = 7.0) in the presence of increasing amounts of KCl (from the bottom: 0, 2.5, 5, 10, 20, 30 and-50 mM). Figure from the above mentioned work.[7]

On this premise, I recorded the NOE pumping spectra of a series of solutions of **S5-AuNP** (15 μM) and phloretic acid (5 mM) containing increasing amounts of KCl. As expected, phloretate signals were not present in the spectrum in the absence of K^+, because the neutral nanoparticles have a marginal affinity for organic anions (*Figure 3.8* c). On the other hand, phloretate signals appeared with increasing intensity as the concentration of the metal ion increased (*Figure 3.8* c), since K^+ complexation turns the nanoparticles into a receptor for organic anions. Comforted by these results, I finally repeated the experiment using **S5-AuNP** in combination with both tyramine and phloretic acid, both at 5 mM concentration.

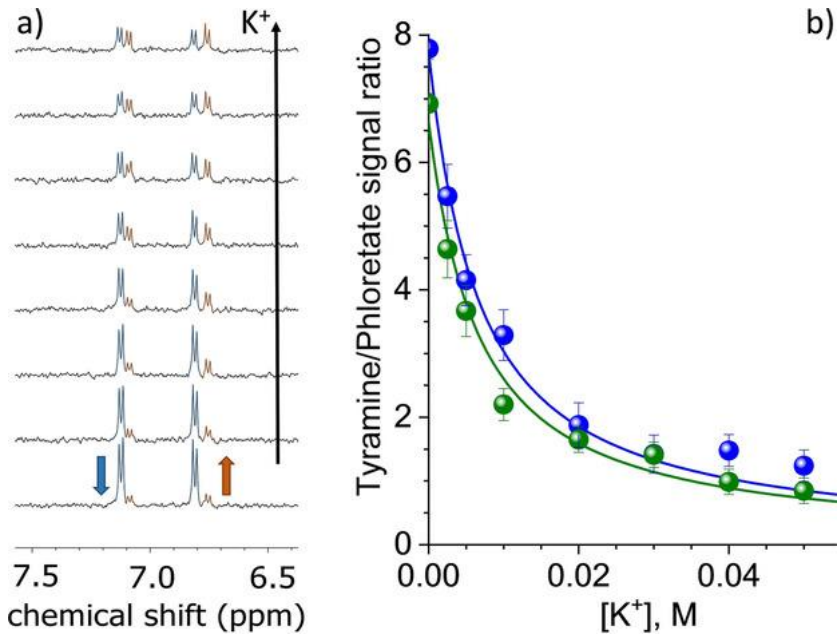

Figure 3.9. a) NOE pumping subspectra of a sample containing tyramine (5 mM), phloretate (5 mM) and **S5-AuNP** (20 μM) in HEPES/Me_4NOH buffered D_2O (pD=7.0) in the presence of increasing amounts of KCl (0–50 mM); b) Plot of the integral ratios vs K^+ concentration for the signals at 7.1 (blue) and 6.8 (green) ppm (the lines represent the best fitting of the data with a 1 : 1 binding model). Figure from the above mentioned work.[7]

In this case, a ratiometric behavior was observed, with the tyramine signals decreasing and the phloretate signals increasing as the potassium concentra-

tion grows (*Figure 3.9*). The ratios of the integrated signal intensities for the two species are plotted in *Figure 3.9 b* as function of the K^+ concentration. The data follow a saturation profile that can be used as calibration curve for the determination of potassium concentration and could be fitted with a 1:1 binding model. The limit of detection (defined as the minimum concentration of analyte producing a signal larger than three times the noise) was 0.6 mM, established on the basis of these data. In addition, when I repeated the experiment using STD (Saturation Transfer Difference)[6,12] in place of NOE pumping, I obtained the same behavior reducing the acquisition time to 20 minutes (see additional information paragraph). The affinity constant obtained by the fitting of the data of *Figure 3.9 b*, which represents the apparent average affinity of the nanoparticle-bound crown ether moieties for K^+ in the presence of tyramine and phloretate (each 5 mM), was 165±12 M^{-1}. This value is close to that of 107 M^{-1} reported[5] for the binding of K^+ to 18-crown-6 in water, suggesting that the two organic reporters produce a small interference to the binding of potassium.

3.6 Possible interferents

In this light, I also investigated the potential interference of other metal cations belonging to the first and second groups, such as Na^+, Mg^{2+}, Ca^{2+}.

Results reported in *Figure 3.10* reveal that the sensing system does not respond to the presence of such cations at 20 mM concentrations. In biological environments, the most relevant interference to K^+ detection is the presence of a large amount of Na^+. For this reason, I investigated the response of the **S5-AuNP** /tyramine/phloretate sensing system to K^+ in the presence of 100 mM NaCl. A ratiometric behavior similar to that obtained in the absence of NaCl was observed, and the fitting of the data provided an apparent binding constant of 83±11 M^{-1}, confirming that the presence of a large excess of sodium ions only marginally affects the sensing performance. This evidence was

further confirmed by the results obtained by analysing a sample of commercial artificial urine (Surine®). The K^+ content in this sample was determined by ICP-MS to be1.8±0.2 mM. An aliquot of 300 µL of Surine was mixed in the NMR tube with 300 µL of a D_2O solution containing **S5-AuNP**, tyramine, phloretate and the buffer, and then the NOE-pumping experiment was performed. Using the calibration curve obtained in the presence of NaCl 100 mM, a concentration of 0.9±0.7 mM could be determined (expected value: 0.9 mM). Such a value, notwithstanding the large errors arising from being close to the limit of detection, is remarkably close to the one determined via ICP-MS. As a final experiment, I turned my attention to investigating whether this method could also be applied to samples containing other organic species or biomolecules. Signal crowding and overlapping typical of mixtures of organic compounds would prevent the use of standard ^{1}H-NMR experiments to monitor the receptor state. I hence performed the NOE pumping experiment on a sample containing, besides KCl (10 mM) and **S5-AuNP** (20µM), also tyramine, phloretate, phenylalanine and arbutin (all 5mM). All these organic compounds have aromatic moieties whose signals have similar chemical shift values.

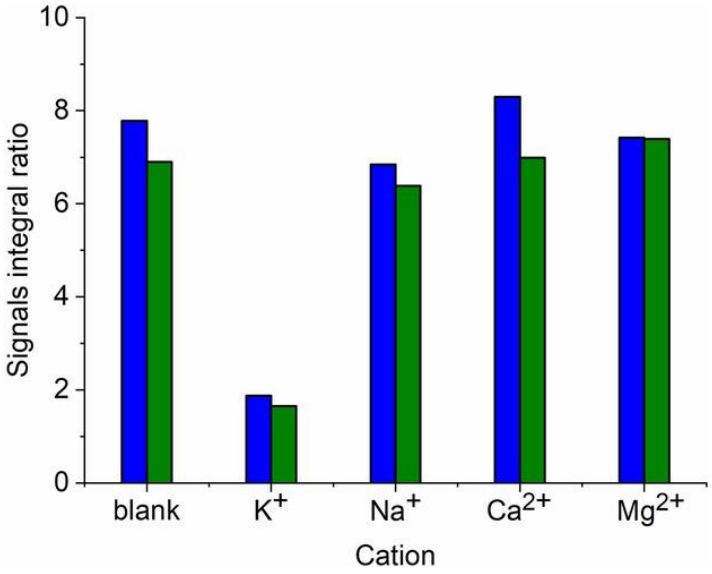

Figure 3.10. NOE pumping sensor response to different monovalent and divalent metal cations each at 20 mM concentration in HEPES/Me_4NOH buffered D_2O (pD=7.0). Figure from the above mentioned work.[7]

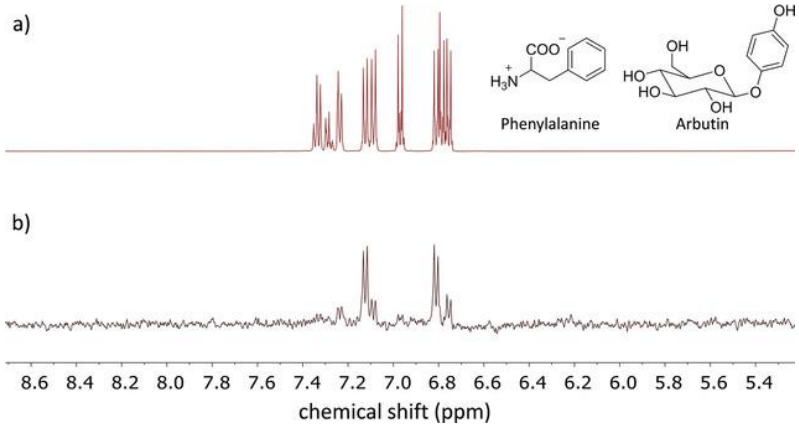

Figure 3.11. a)^{1}H-NMR subspectrum of a sample containing tyramine (5 mM), phloretate (5 mM), phenylalanine (5 mM) and arbutin (5 mM), KCl (10 mM) and **S5-AuNP** (20 µM) in HEPES/Me_4NOH buffered D_2O (pD=7.0); b) NOE-pumping subspectrum of the same mixture.

The ^{1}H-NMR spectrum of this mixture highlights a severe signal crowding in the aromatic region and signals of the K^+ reporters partially overlap with those of the other species present (*Figure 3.11a*). On the other hand, in the NOE pumping spectrum only the signals of tyramine and phloretate are detected (*Figure 3.11b*). The ratio of the integrals of the two reporters is that expected for the presence of 10 mM of the potassium cation, confirming that the interference is produced by the additional organic species added to the sample. proteins interference can be relevant too, as they can interact with the nanoparticles or with the reporters thus affecting the signals produced. To test this possibility, I performed a NOE pumping experiment on a sample containing albumin at the concentration of 3 mg/mL.[13] The results obtained indicate that albumin indeed interacts with phloretate, resulting in a signal with constant intensity in the NOE pumping spectra. The sensing system is however still capable to detect K^+ with a ratiometric behavior and similar sensitivity (the apparent binding constant measured in these conditions was 160±80 M^{-1}).

3.7 Conclusion

In this chapter I introduced the use of 18-crown-6 decorate AuNPs for the sensing of designer drugs. Compared to **S1-AuNP** studied in the previous chapter, **S5-AuNP** show selectivity for primary amines, so all the mono and di-methylated designer drugs are not sensed. This is due to the alkylation of the amine group of the phenethylamine, that both lowers the capability to form hydrogen bonds with the crown ether and introduces steric hindrance. The selectivity shows that all the interactions are crucial and that even the weakening of one single interaction (H-bond) creates a relevant diminution of selectivity. The idea of this project was to combine a higher number of interactions to get nanoparticles with higher affinity and selectivity. I worked towards this goal along two pathways: by adding two interactions in one thiol with **S6-AuNP**, and by putting two thiols on one nanoparticle with a mixed monolayer with **S1_5-AuNP**. As suggested by previous works, inserting all the interactions on one thiol can lead to bad sensitivity mostly because of solubility problems in water.

The behaviour of the mixed nanoparticles was unexpected, in that in terms of sensitivity and selectivity they behave just as the **S5-AuNP**. A possible explanation to this fact could be that the two thiols are unevenly disposed on the nanoparticle surface, so the domain of crown thiols could reproduce the crown nanoparticle behaviour. A similar distribution wold also require regions covered with sulfonate thiol **S1**, and these ones should behave like the well-described nanoparticles with higher affinity and lower selectivity. On the other hand, with an even distribution of the two thiols on the surface, I would have expected that the presence of the negative charge, cooperating with the crown ether recognition, would reinforce the interaction leading to an improved affinity, but still retaining the crown selectivity. The behaviour observed suggests instead that the anionic thiols do not to have any effect on the nanoparticle analyte interaction. This can be possible only if the sulfonate groups are busy making an ionic couple that actually prevents them from interacting with the analyte. This interaction could be favoured by the presence

of the crown ether, that can interact with cations such as sodium or potassium and keep them in close proximity of the sulfonate groups. The residue recognition is due to the crown ether moieties not coupled with the sulfonate. If this is true, it means that it should be possible to modulate the selectivity of the crown ether according to its complexed state - or lack thereof. Hence, I presented a sensing system that can effectively detect potassium ions also in biological media. The system uses a ratiometric response; in addition, the modularity of the system may allow to test different reporters, either to reduce their interaction with possible interferents or to improve the separation and integration of the signals. In conclusion, I have shown that nanoparticle receptors, and in principle other macromolecular receptors, can be used to enable the detection of potassium ions by ^{1}H-NMR, using magnetization transfer experiments. The key point is the ability of the analyte to modulate the interaction between the macromolecular species and the reporter, which is in turn signalled by the occurrence of the magnetization transfer. The method is simple, fast (the duration of the NMR experiment can be reduced down to 20 minutes) and does not require any sample pre-treatment. The detection limit determined with the system studied here is similar to other ^{19}F-based[14] or 18-crown-6[15] chemosensors and is well compatible with the analysis of K^+ in relevant biological samples. In addition, while several other efficient methods are available for potassium detection, the modularity of the system described should easily allow for further improvements, or detection of other analytes.

Supplementary information

General

Solvents were purified by standard methods. All commercially available reagents and substrates were used as received.

TLC analyses were performed using Merck 60 F254 precoated silica gel glass plates. Column chromatography was carried out on Macherey-Nagel silica gel 60 (70-230 mesh).

NMR spectra were recorded using a Bruker AV III 500 spectrometer operating at 500 MHz for ^{1}H, 125.8 MHz for ^{13}C. Chemical shifts are reported relative to internal Me_4Si. Multiplicity is given as follow: s = singlet, d = doublet, t = triplet, q = quartet, qn = quintet, m = multiplet, br = broad peak.

ESI-MS mass spectra were obtained with an Agilent Technologies LC/MSD Trap SL mass spectrometer.

TEM images were recorded on a Jeol 300 PX electron microscope. One drop of sample was placed on the sample grid and the solvent was allowed to evaporate. TEM images were analysed with ImageJ software to measure the diameters distribution and average values.

TGA were run on 1 mg nanoparticle samples using a Q5000 IR model TA instrument from 30 to 1000 °C under a continuous air flow.

NMR sample preparation

Stock solutions of AuNPs and analytes were prepared in D_2O, stock solution of HEPES buffer at pD=7.01 was prepared in D_2O and the pH adjusted either with NaOD or Me_4NOH. Analytes were commercially available or synthesized with standard literature procedures. NMR tubes were prepared adding the correct amount of stock solutions and D_2O to reach the final volume of 600 μl.

Thiol S1

Synthesis of thiol **S1** has been already reported in *Chapter 2.*

Thiol S5

Thiol **S5** has been prepared according to the procedure reported by Salvia et al.[4] Detailed synthesis procedures and characterizations are already published.

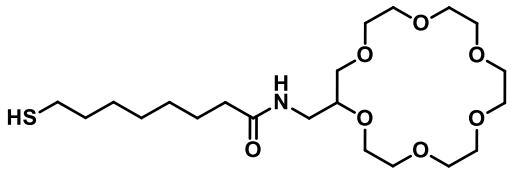

1

Figure 3.12: thiol used as nanoparticle coating for **AuNP-5**.

Thiol S6

Thiol **S6** has been prepared according to the following reaction scheme (*Figure 3.12*).

*4-acetoxybenzoic acid (**1**).*

4-hydroxybenzoic acid (1.005 g, 7.28 mmol) was dissolved in 60 ml of dry DCM. Acetic anhydride (1.4 ml, 14.81 mmol) and pyridine (1.2 ml, 14.87 mmol) were added and the mixture was stirred overnight at room temperature under inert N_2 atmosphere. The solvent was removed and 20 ml of a saturated $NaHCO_3$ solution were added. Upon acidification with HCl 37% the product precipitated as white solid. Filtration with gooch and washing with cold water yielded the desired product **1** with 81%

^{1}H-NMR (500 MHz, CD_3CN) δ (ppm): 8.07 (d, 2 H), 7.24 (d, 2 H), 2.30 (s, 3 H)

^{13}C-NMR (125.8 MHz, CD_3CN) δ (ppm): 169.1, 166.1, 154.7, 131.2, 127.6 , 122.1, 20.3

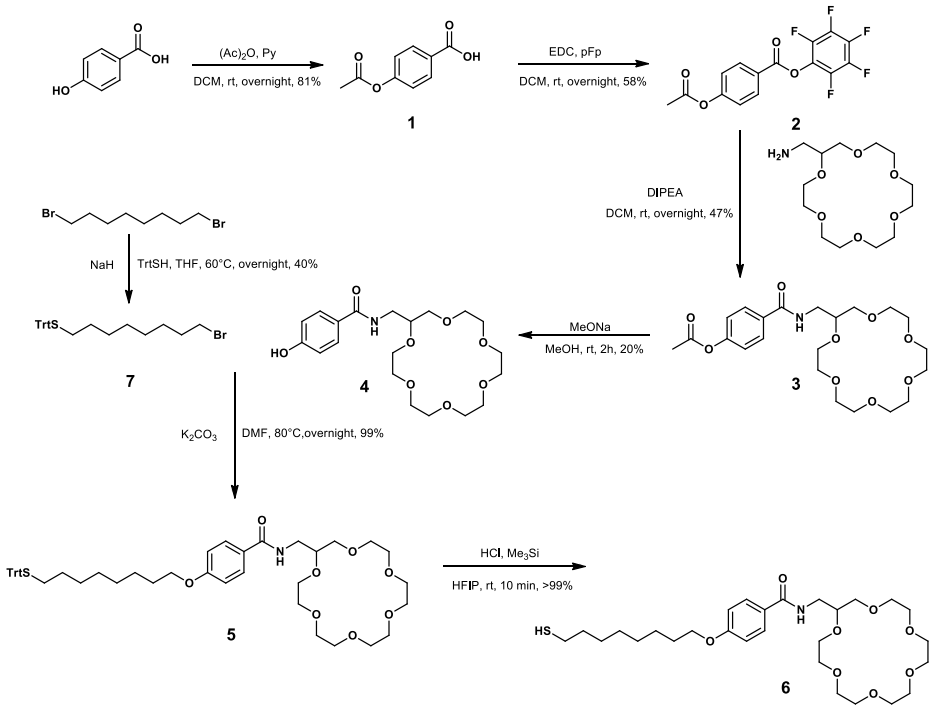

Figure 3.12: pathway followed for the synthesis of thiol **S6**

*Pentafluorophenyl-4-acetoxybenzoate (**2**).*

4-acetoxybenzoic acid **1** (200 mg, 1.11 mmol) was dissolved in 5 ml of dry DCM. EDC (255 mg, 2.24 mmol) and pentafluorophenol (412 mg, 2.24 mmol) were added. After overnight stirring at room temperature under inert N_2 atmosphere, the solvent was removed and the product purified by column chromatography (petroleum ether/EtOAc 9:1) yielding **2** as a sticky oil with 58% yield.

^{1}H-NMR (500 MHz, $CDCl_3$) δ (ppm): 8.26 (d, 2 H), 7.32 (d, 2 H), 2.38 (s, 3 H)

*N-(18-crown-6)methyl-4-acetophenylamide (**3**).*

Pentafluorophenyl-4-acetoxybenzoate **2** (142 mg, 0.41 mmol) was dissolved in 4ml of DCM. DIPEA (0.118 ml, 0.68 mmol) and 2-aminomethyl-18-crown-6 (100 mg, 0.34 mmol) were added and the reaction left overnight stirring at

room temperature under inert N_2 atmosphere. The product was purified by column chromatography (DCM/MeOH 95:5 to 9:1) yielding **3** as a sticky oil with 47% yield.

^{1}H-NMR (500 MHz, $CDCl_3$) δ (ppm): 7.90 (d, 2 H), 7.16 (d, 2 H), 3.65 (m, 25 H), 2.31 (s, 3 H)

^{13}C-NMR (125.8 MHz, $CDCl_3$) δ (ppm): 169.0, 166.7, 152.9, 132.9, 128.6, 121.6, 71.1, 70.9-70.5, 41.7, 21.2

*N-(18-crown-6)methyl-4-hydroxyphenylamide (**4**).*

N-(18-crown-6)methyl-4-acetophenylamide 3 (85 mg, 0.18 mmol) was dissolved in 5ml of dry MeOH. $NaOCH_3$ (41 mg, 0.76 mmol) was added, and the suspension was let stirring at room temperature for 3h. The solvent was removed and the product was purified by column chromatography (DCM/MeOH 9:1) yielding **4** as a sticky oil with 20% yield.

^{1}H-NMR (500 MHz, $CDCl_3$) δ (ppm): 7.90 (d, 2 H), 7.16 (d, 2 H), 3.65 (m, 25 H),

^{13}C-NMR (125.8 MHz, $CDCl_3$) δ (ppm): 169.0, 166.7, 152.9, 132.9, 128.6, 121.6, 71.1, 70.9-70.5, 41.7, 21.2

*N-(18-crown-6)methyl-4-(8-(trytylthio)-octyloxy) phenylamidehydroxyphenylamide (**5**).*

4 (15 mg, 0.036 mmol) was dissolved in 2ml of dry DMF. **7** (24 mg, 0.056 mmol) and K_2CO_3 (22 mg, 0.16 mmol) were added, and the suspension was let stirring overnight at 80°C. The solvent was removed and the product was purified by column chromatography (DCM/MeOH 9:1) yielding **5** as a sticky oil with 99% yield.

^{1}H-NMR (500 MHz, CD_2Cl_2) δ (ppm): 8.07 (d, 2 H), 7.45 (d, 6 H), 7.32 (t, 6 H), 7.25 (t, 3 H), 6.95 (d, 2 H), 4.01 (t, 2 H), 3.68 (m, 25 H), 2.17 (t, 2 H), 1.78 (qn, 2 H), 1.42 (qn, 2 H), 1.30 (qn, 8 H)

^{13}C-NMR (125.8 MHz, CD_2Cl_2) δ (ppm): 161.6, 154.2, 145.1, 130.8, 129.6, 127.8, 126.5, 113.9, 70.3, 68.1, 67.5, 40.4, 31.8, 29.1, 28.5, 25.9,

*N-(18-crown-6)methyl-4-(8-(mercaptoctyloxy)phenylamide (**6**).*

5 (27 mg, 0.036 mmol) was dissolved in 1 ml perfluoroisopropanol. 5μl of triethylsilane were added together with 5 μl of concentrated. The solution was stirred for then minutes and the solvent removed in vacuo. The product was used as it is for the synthesys of AuNP-**5.**

^{1}H-NMR (500 MHz, CD_2Cl_2) δ (ppm): 8.07 (d, 2 H), 7.45 (d, 6 H), 7.32 (t, 6 H), 7.25 (t, 3 H), 6.95 (d, 2 H), 4.01 (t, 2 H), 3.68 (m, 25 H), 2.17 (t, 2 H), 1.78 (qn, 2 H), 1.42 (qn, 2 H), 1.30 (qn, 8 H)

^{13}C-NMR (125.8 MHz, CD_2Cl_2) δ (ppm): 161.6, 154.2, 145.1, 130.8, 129.6, 127.8, 126.5, 113.9, 70.3, 68.1, 67.5, 40.4, 31.8, 29.1, 28.5, 25.9.

7 was synthesized as reported in literature. The obtained product had matching NMR characterization with the one there reported

Synthesis and characterizations of AuNPs

Monolayer protected gold nanoparticles (AuNP) were prepared following a previously reported two-step procedure and as described in the previous chapter.[16]

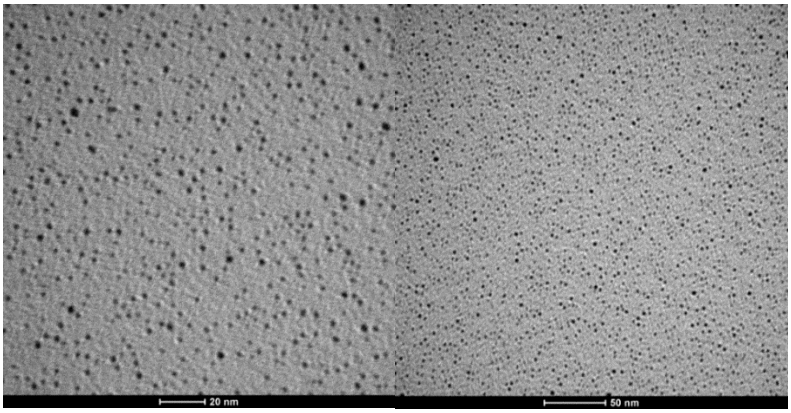

Figure 3.13: TEM images of **AuNP-5**.

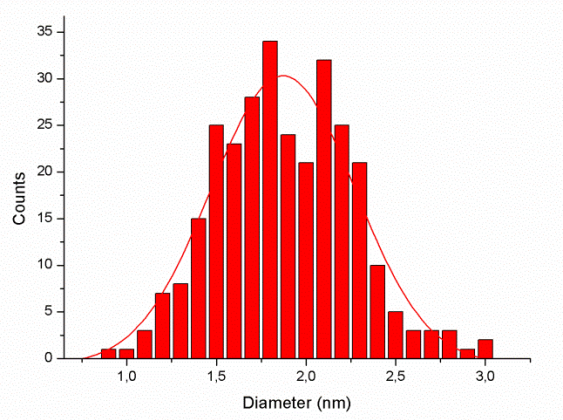

Figure 3.14. size distribution of **AuNP-5** and fitting curve parameters: average diameter d=1.9 nm (σ=0.4nm).

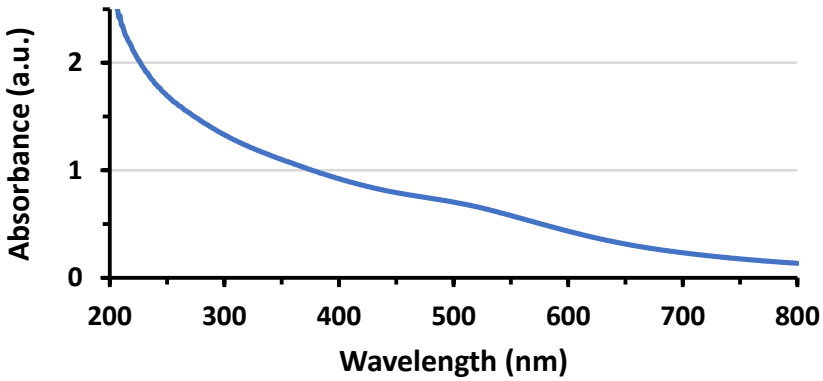

Figure 3.15. UV-Vis spectrum of a solution of **AuNP-5** (H_2O, 0.1 mg/ml).

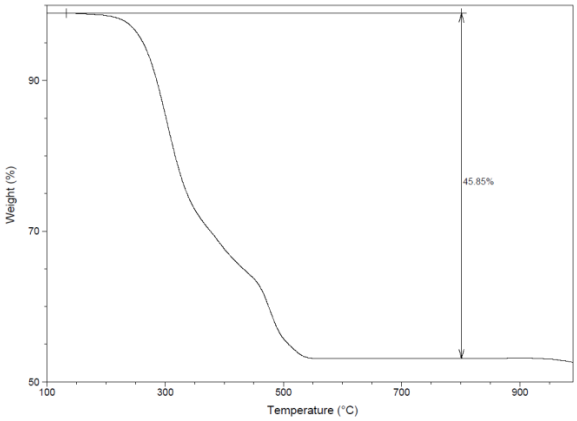

Figure 3.16. TGA analysis of **AuNP-5** (1mg, 100°C to 1000°C, ramp 10°C/min, air atmosphere). Weight loss 45.85%.

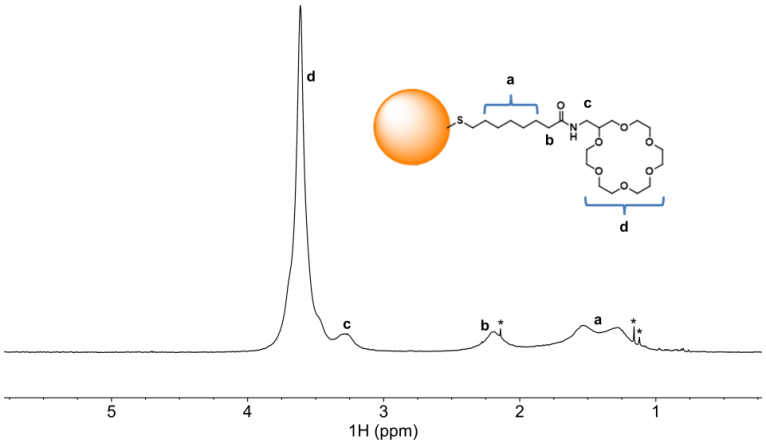

Figure 3.17. ^{1}H NMR (500 MHz, D_2O) spectrum of **AuNP-5**. * indicates minor organic impurities.

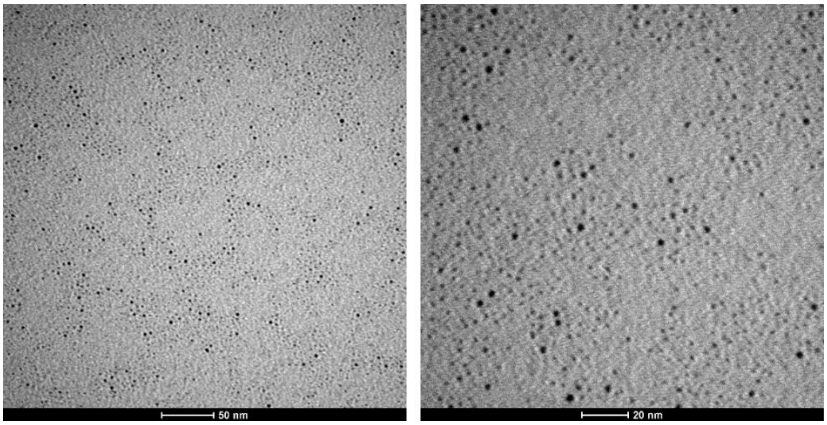

Figure 3.18: TEM images of **AuNP-1_5**.

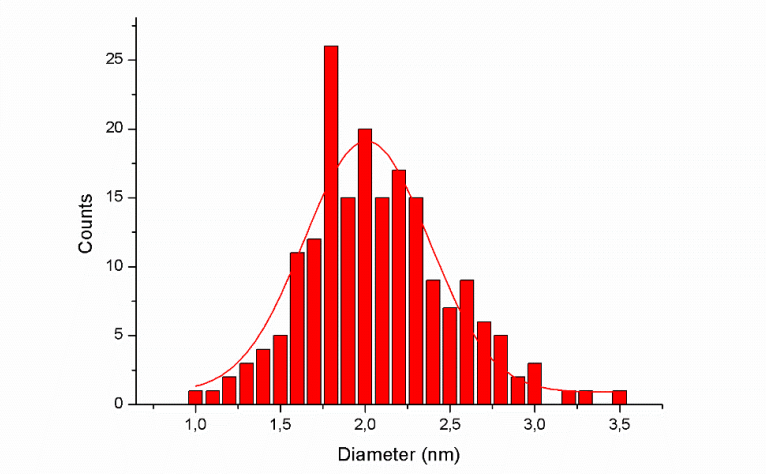

Figure 3.19. size distribution of **AuNP-1_5** and fitting curve parameters: average diameter d=2.0 nm (σ=0.4nm).

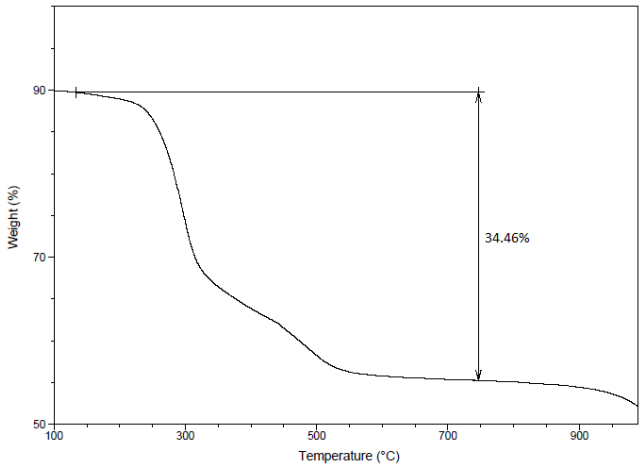

Figure 3.20. TGA analysis of **AuNP-5** (1mg, 100°C to 1000°C, ramp 10°C/min, air atmosphere). Weight loss 34.46%.

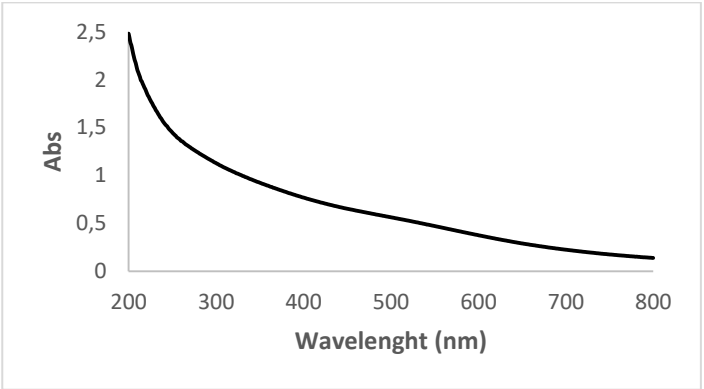

Figure 3.21. UV-Vis spectrum of a solution of **AuNP-1_5** (H_2O, 0.1 mg/ml).

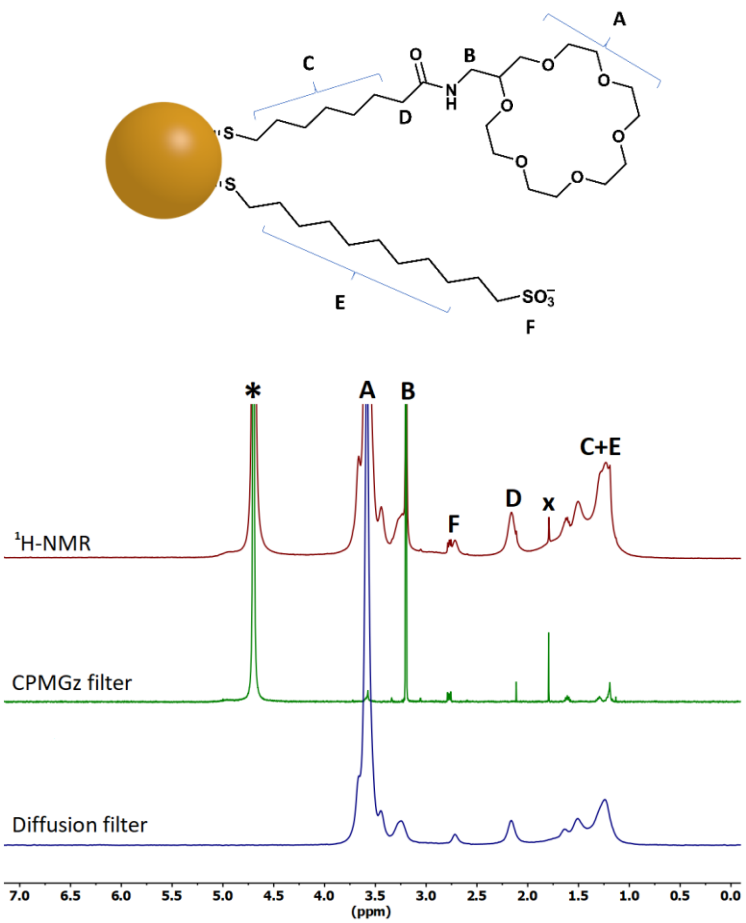

Figure 3.22. ^{1}H NMR (500 MHz, D_2O) spectrum of **AuNP-1_5** with assignation of the signals. * indicates water residual signal, x indicates minor organic impurity.

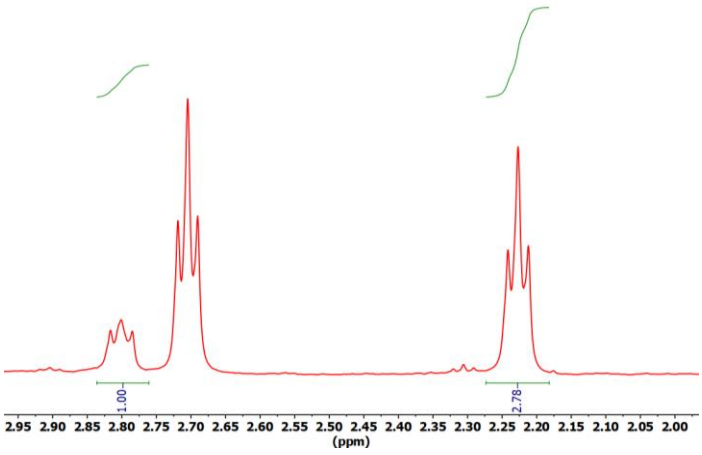

Figure 3.23. detail of ^{1}H NMR (500 MHz, D_2O) spectrum of **AuNP-1_5** after I_2 treatment. The integration shows the ratio if thiol **S1** and **S5** on the NPS.

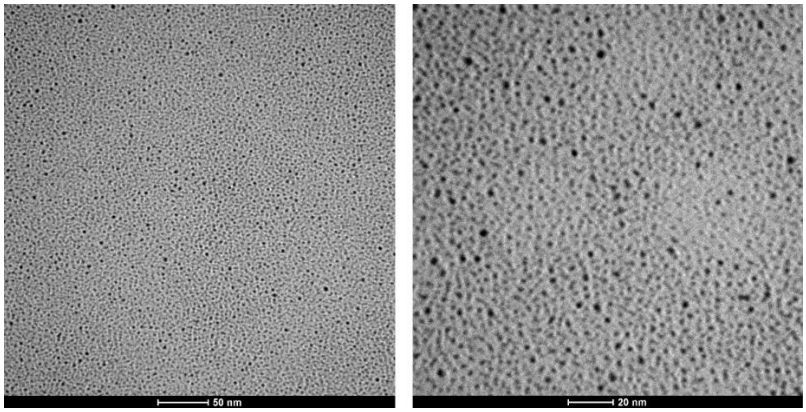

Figure 3.24: TEM images of **AuNP-6**.

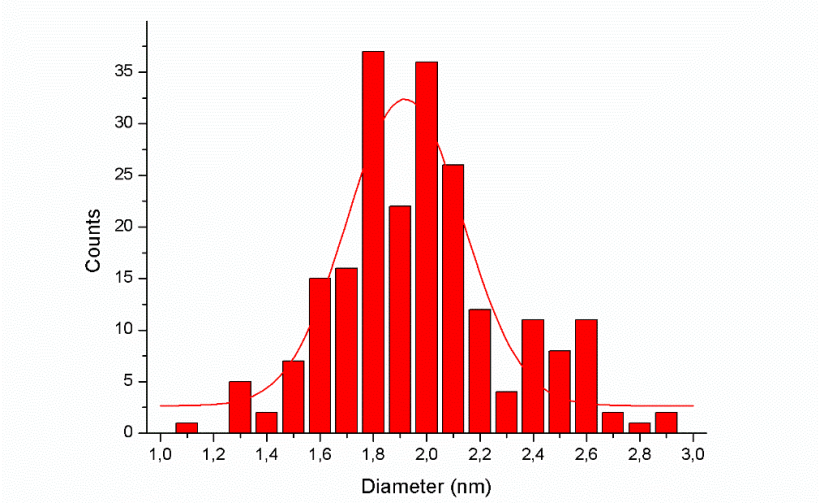

Figure 3.25. size distribution of **AuNP-6** and fitting curve parameters: average diameter d=2.0 nm (σ=0.4nm).

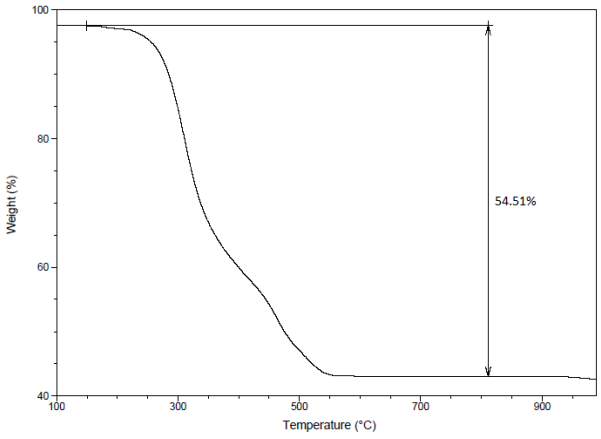

Figure 3.26. TGA analysis of **AuNP-5** (1mg, 100°C to 1000°C, ramp 10°C/min, air atmosphere). Weight loss 34.46%.

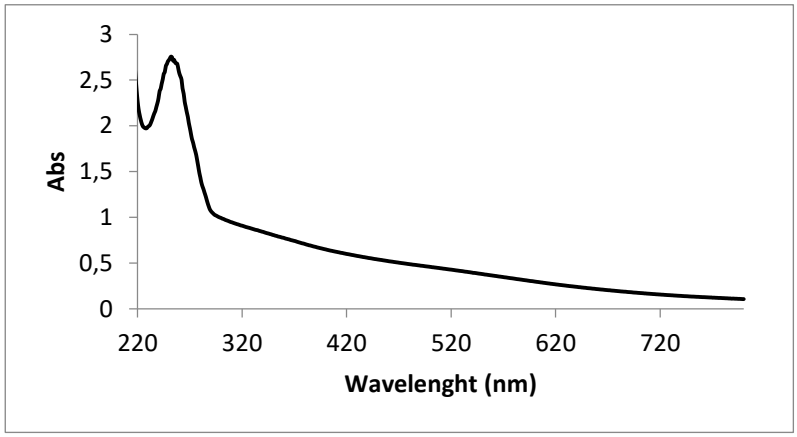

Figure 3.27. UV-Vis spectrum of a solution of **AuNP-6** (H_2O, 0.1 mg/ml).

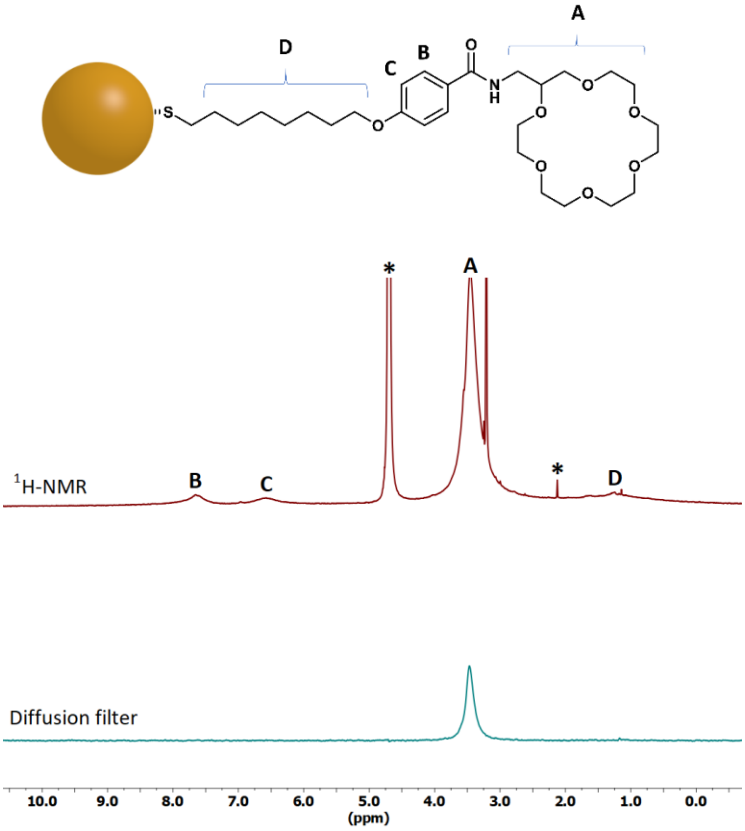

Figure 3.28. ^{1}H NMR (500 MHz, D_2O) spectrum of **AuNP-1_5** with assignation of the signals. * indicates water residual signal, x indicates minor organic impurity.

AuNP-1 were available from a previous work.[3] Detailed synthesis procedures and full characterization are reported in *Chapter 2*.

Bibliography

(1) Riccardi, L.; Gabrielli, L.; Sun, X.; De Biasi, F.; Rastrelli, F.; Mancin, F.; De Vivo, M. Nanoparticle-Based Receptors Mimic Protein-Ligand Recognition. *Chem* **2017**, *3* (1), 92–109.

(2) Sun, X.; Riccardi, L.; De Biasi, F.; Rastrelli, F.; De Vivo, M.; Mancin, F. Molecular-Dynamics-Simulation-Directed Rational Design of Nanoreceptors with Targeted Affinity. *Angew. Chemie - Int. Ed.* **2019**, *58* (23), 7702–7707.

(3) Gabrielli, L.; Rosa-Gastaldo, D.; Salvia, M. V.; Springhetti, S.; Rastrelli, F.; Mancin, F. Detection and Identification of Designer Drugs by Nanoparticle-Based NMR Chemosensing. *Chem. Sci.* **2018**, *9* (21), 4777–4784.

(4) Salvia, M. V.; Salassa, G.; Rastrelli, F.; Mancin, F. Turning Supramolecular Receptors into Chemosensors by Nanoparticle-Assisted "NMR Chemosensing." *J. Am. Chem. Soc.* **2015**, *137* (35), 11399–11406.

(5) Atwood, J. L.; Gokel, G. W.; Barbour, L. J. *Comprehensive Supramolecular Chemistry II*.

(6) De Biasi, F.; Rosa-Gastaldo, D.; Sun, X.; Mancin, F.; Rastrelli, F. Nanoparticle-Assisted NMR Spectroscopy: Enhanced Detection of Analytes by Water-Mediated Saturation Transfer. *J. Am. Chem. Soc.* **2019**, *141* (12), 4870–4877.

(7) Sun, X.; Rosa-Gastaldo, D.; De Biasi, F.; Rastrelli, F.; Mancin, F. 1 H NMR Chemosensing of Potassium Ions Enabled by Guest-Induced Selectivity Switch of a Gold Nanoparticle/Crown Ether Nanoreceptor. *Chempluschem* **2019**.

(8) Ghale, G.; Nau, W. M. Dynamically Analyte-Responsive Macrocyclic Host-Fluorophore Systems. *Acc. Chem. Res.* **2014**, *47* (7), 2150–2159.

(9) Nguyen, B. T.; Anslyn, E. V. Indicator-Displacement Assays. *Coordination Chemistry Reviews*. December 2006, pp 3118–3127.

(10) Wiskur, S. L.; Ait-Haddou, H.; Lavigne, J. J.; Anslyn, E. V. Teaching Old Indicators New Tricks. *Acc. Chem. Res.* **2001**, *34* (12), 963–972.

(11) *Fluorescent Chemosensors for Ion and Molecule Recognition*; Czarnik, A. W., Ed.; ACS Symposium Series; American Chemical Society: Washington, DC, 1993; Vol. 538.

(12) Salvia, M. V.; Ramadori, F.; Springhetti, S.; Diez-Castellnou, M.; Perrone, B.; Rastrelli, F.; Mancin, F. Nanoparticle-Assisted NMR Detection of Organic Anions: From Chemosensing to Chromatography. *J. Am. Chem. Soc.* **2015**, *137* (2), 886–892.

(13) Cain, L. D.; Nie, L.; Hughes, M. G.; Johnson, K.; Echetebu, C.; Xu, G. Y.; Hulsebosch, C. E.; McAdoo, D. J. Serum Albumin Improves Recovery from Spinal Cord Injury. *J. Neurosci. Res.* **2007**, *85* (7), 1558–1567.

(14) Sakamoto, T.; Hayakawa, H.; Fujimoto, K. Development of a Potassium Ion Sensor for 19F Magnetic Resonance Chemical Shift Imaging Based on Fluorine-Labeled Thrombin Aptamer. *Chem. Lett.* **2011**, *40* (7), 720–721.

(15) Pérez-Mitta, G.; Albesa, A. G.; Knoll, W.; Trautmann, C.; Toimil-Molares, M. E.; Azzaroni, O. Host-Guest Supramolecular Chemistry in Solid-State Nanopores: Potassium-Driven Modulation of Ionic Transport in Nanofluidic Diodes. *Nanoscale* **2015**, *7* (38), 15594–15598.

(16) Manea, F.; Bindoli, C.; Polizzi, S.; Lay, L.; Scrimin, P. Expeditious Synthesis of Water-Soluble, Monolayer-Protected Gold Nanoparticles of Controlled Size and Monolayer Composition. *Langmuir* **2008**, *24* (8), 4120–4124.

4

Enhanced detection of analytes by water-STD [a]

Summary

Properly designed monolayer-protected nanoparticles (2 nm core diameter) can be used as nanoreceptors for selective detection and identification of organic molecules in complex mixtures. As we saw in the previous chapters, the molecular recognition mechanism is driven by the combination of electrostatic and hydrophobic interactions within the coating monolayer. Detection of psychoactive drugs (such as amphetamines and methamphetamines) and metabolites is performed by using magnetization (NOE) or saturation (STD) transfer NMR experiments.[1–4] The technique used, called nanoparticle-assisted "NMR chemosensing", is an experimental protocol that exploits the selective recognition abilities of nanoparticle receptors to isolate the NMR spectrum of the analyte from that of the mixture, allowing broad-class multianalyte detection and even univocal identification of unknowns. While the intrinsic sensitivity of the first reported

[a]Paragraphs 4.1 to 4.4 of this chapter are an adapted version of a manuscript which I co-authored and that has been already published during my PhD: *Nanoparticle-Assisted NMR Spectroscopy: Enhanced Detection of Analytes by Water-Mediated Saturation Transfer*, F. De Biasi‡, D. Rosa-Gastaldo‡, X. Sun, F. Mancin, and F. Rastrelli* *J. Am. Chem. Soc* .2019,141, 12,

protocols[2] was modest, we have found that water spins in long-lived association with the nanoparticle monolayer constitute an alternative source of magnetization that can deliver a remarkable boost of sensitivity, especially when combined with saturation transfer experiments.[3] Moreover, we have discovered that a non-covalent coupling of the gold nanoparticles to bigger (20 nm) colloidal silica nanoparticles favors the saturation transfer, leading to a detection limit of 5 μM with standard instruments. The approach is general and can be applied to analyte-nanoreceptor systems of different compositions.

4.1 Water LOGSY and proteins

We saw in the previous chapters how gold nanoparticles can work with NMR-chemosensing techniques in water, and the election techniques are NOE-pumping and STD experiments. They both take advantage of the fact that the nanoparticle is a relatively big entity in solution, where transient binding pockets can form, and the recognition can occur. This recalls the behaviour of some proteins. Such an analogy is supported when considering that the nano-particles used in this work have an average formula of $Au_{180}SR_{70}$, that leads to an average molecular weight of 60000, and average hydrodynamic radius of 5-8 nm. Albumin, taken as representative globular protein, has a molecular weight of about 50000 and a hydrodynamic size of about 5 nm.

On the basis of these considerations, in collaboration with the group of prof. Rastrelli, we reasoned that a third experiment traditionally used for proteins could suit the NMR chemosensing technique as well. This experiment is called water-LOGSY (water Ligand Observed via Gradient SpectroscopY). Tradition-ally used to screen a set of molecules that could bind a protein and find the actual ligands[5], it relies on the fact that the compounds in solution can get saturation either from the protein, in case they bind it, or from the solvent.

For this reason, the source of magnetisation are not the spins of the receptor (as in the case of NOE pumping or STD) but the spins or the solvent, usually water. The sample contains two different kinds of water molecules: most are free in solution but a few of them are trapped in the protein (or in the monolayer). When water is irradiated it can transfer magnetization to the analyte with to different signs. Bulk water molecules will transfer magnetization with negative sign and protein (nanoparticle)-bound water molecule will transfer magnetization with positive sign, as they have the same correlation time as the protein. Non-binding sample molecules will get straight magnetization from the bulk water molecules, whereas binding molecules, that have to be in fast exchange with the nanoparticle, will receive their magnetization from the protein bound molecules and also from the protein, which received it from water itself. As consequence, signals of interacting molecules will have a positive sing in the difference spectra, and signals from non-interacting molecules negative signs.

Molecular dynamics calculations made by Riccardi et al.[6] and Sun et al.[7] clearly show that some water molecules in long lived association with the nanoparticle are present and could be a source of magnetization that could be transferred to the interacting analytes. Nicely, the water-LOGSY experiment is claimed to have lower limits of detection than the STD experiment.

To see if this idea could work, we chose the best candidate to the detection of designer drugs: **S5-AuNP**. Since the idea behind optimization is to reach concentrations relevant for body fluids, in this case I used a phenethylamine that is not a drug: serotonin. The interest in this molecule is due to its involvement in cancer cell migration, metastatic processes and angiogenesis, and above a certain limit - in urine, for example - it could be a tumour marker.[8]

For the first experiment we prepared a sample of 6.3 μM **S5-AuNP** (corresponding to 0.5 mM thiol **S5**) with 0.5 mM serotonin (**4**) as the binding candidate, complemented with 0.5 mM N-methyl-phenethylamine (**5**) and 0.5 mM phloretic acid (**6**) as the non-interacting species. In this case, unlike NOE

pumping, non -deuterated water is needed, so the sample was prepared in H_2O:D_2O = 90:10 buffered with 10 mM phosphate at pH = 7.0.

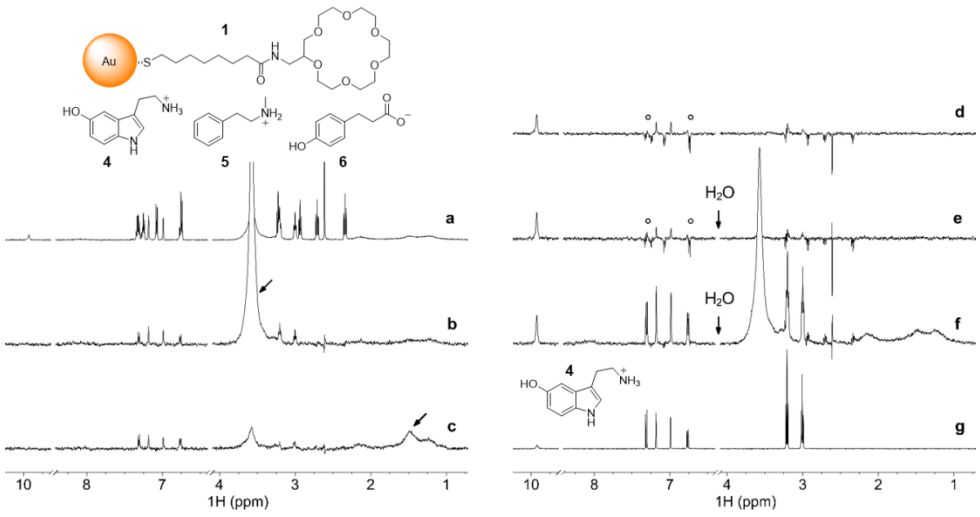

Figure 4.1. ^{1}H NMR spectra of 0.5 mM serotonin (4), 0.5 mM N-methyl-phenethylamine (5), 0.5 mM phloretic acid (6) and 0.5 mM **S5-AuNP**. a) Plain ^{1}H NMR spectrum with DPFG-PE (W5) solvent suppression. b) and c): standard STD spectra with 2 s saturation at the frequencies highlighted by the arrows. d) water LOGSY with 2 s mixing time. The conventional phase of the signals has been reversed to facilitate the comparison with STD spectra. e) water-STD featuring 180° Gaussian pulses and 2 s saturation at the frequency of H_2O. f) Same as e, but with 5560° high-power Gaussian pulses. g) 1H NMR reference spectrum of serotonin. Spectra b) – f) were acquired with 64 total scans, corresponding to a duration of about 10 min each. Circles denote the accidental superposition of resonances belonging to interacting and non-interacting analytes (see text). Figure from the above mentioned work.[9]

The resulting water-LOGSY spectrum is reported in *Figure 4.1d*, along with the plain ^{1}H spectrum for reference (*Figure 4.1a*) and two STD spectra (*Figures 4.1b* and 4.*1c*) obtained saturating two different signals of the nanoparticle. In this case as well, as with proteins, the resonances of binding and non-binding analytes in the water-LOGSY spectrum appear with opposite signs depending on the interaction of the analytes with bulk water[10,11] or with water in long lived association with the NP monolayer. That's the reason why the signals of serotonin **4** are positive (confirming its interaction with the monolayer) and those of **5** and **6** are negative (they were inserted as negative controls, so they were not expected to interact with AuNP).

It is visible from *Figure 4.1* that, contrary to our expectations, in the water-LOGSY experiment the signal to noise ratio of the serotonin signals is not increased with respect to the standard STD experiments. Moreover, the fact that in the case of water LOGSY the non-interacting analytes are not disappearing from the spectrum, but they are still present with opposite phase, leads to signal overlap. In the (common) occurrence of two interacting and non-interacting signals at the same frequency, this can lead to the disappearing of the signal from the spectrum, or in any case to a more difficult spectrum interpretation. This is something that should be avoided if the goal is detecting something.

It's important to note that from the two STD spectra reported in *Figure 4.1* it is possible to understand how serotonin is binding **S5-AuNP**. While saturating the crown ether moiety, all the signals of serotonin appear with an intensity close to the one of the ^{1}H spectrum, whereas if the alkyl signals of the nanoparticle are saturated, only the signals of the indole appear, and the two methylene groups are barely visible. This show that the 18-crown-6 plays a dominant role in the recognition and that the indole of the serotonin is buried in the monolayer, in contact with the alkyl chains of the monolayer. The binding constant of serotonin with **S5-AuNP** from a ^{1}H-NMR titration was estimated to be $K_a \approx 100\ M^{-1}$. The method of calculation is reported in the supplementary information paragraph.

4.2 Water STD and high saturation

With the water LOGSY experiment, we confirmed that serotonin can bind **S5-AuNP** and that water can be used as an effective source of magnetization in the system under analysis as well, with results comparable in terms of sensitivity to a standard STD experiment on the nanoparticle. However, the presence of both the interacting and the non-interacting analytes in the spectrum

is something that has to be improved, so we focused our attention on improving these aspects. We started by saturating the water signal instead of the ones of AuNP. A similar strategy had been suggested also by Dalvit et al. in the context of water-LOGSY as an alternative to the transient NOE.[12] A pulse sequence furtherly described in the additional information paragraph was set and called "water-STD" (water-Saturation Transfer Difference)

The resulting spectra are shown in *Figure 4.1e*: again, both the techniques show the signals of serotonin with a similar intensity. The difference between the two experiment is that in the case of STD, working on steady state saturation, all the binding events should be effective in the same way, while in the case of Water LOGSY, with the same problem of NOE-pumping , the magnetization transfer is at maximum efficiency just after the inversion of the magnetization and the efficiency of each binding event drops significantly for late binding events. Water STD also shows the same limitation of water LOGSY when extended to unknown mixtures, that is, signal cancellation due to partial or total superimposition of signals of interacting and non-interacting species that have different sign. This can be seen in *Figures 4.1d* and *4.1e* (circles).

Since the false negative is a really annoying drawback in NMR-chemosensing, we tried to overcome this problem by increasing the power of the Gaussian pulses in the STD experiment. This way, the pulse loses selectivity, generating a "leak" of the rf field at larger offsets. Eventually, such a leaked RF field can reach the signals of the analytes and allow their partial saturation. The partial saturation affects in two different ways the signals of the interacting analytes (generated by NOEs from bound water) and the signals of the non-interacting analytes (generated by NOEs from bulk water). The first ones are weakened to a lesser extent than the second ones. Moreover, the leaked radiofrequency can also saturate the AuNP spins, adding a second source of magnetization that can be transferred to the interacting analytes. Notably, since the spins of the monolayer and those of bound water molecules share the same slow tum-

bling regime, the two sources provide concurrent effects in the final STD spectrum.

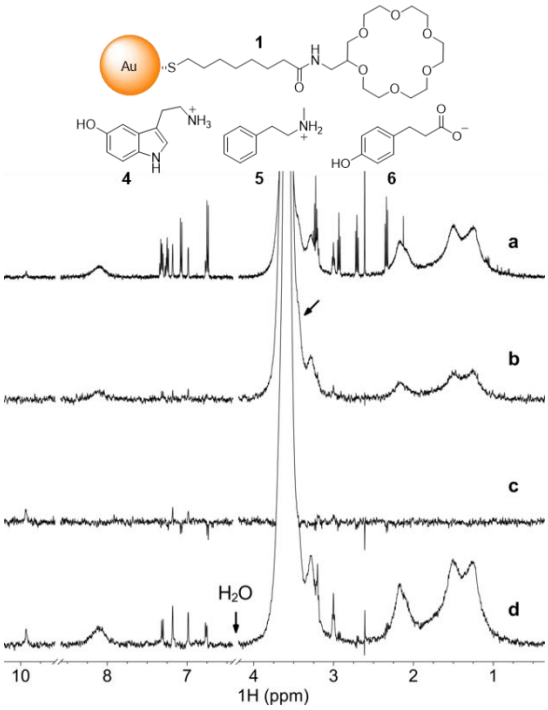

Figure 4.2. ^{1}H-NMR spectra of 50 μM serotonin (**4**), 50 μM N-methyl-phenethylamine (**5**), 50 μM phloretic acid (**6**) and 0.5 mM **AuNP-5**. a) Plain ^{1}H-NMR spectrum with DPFG-PE (W5) solvent suppression. b) standard STD spectrum with 2 s saturation at the frequency highlighted by the arrow. c) water-LOGSY with 2 s mixing time. d) HP water-STD with 2 s saturation at the frequency of H_2O. The total acquisition time for spectra b) – d) is the same (60 min). Figure from the above mentioned work.[9]

To test the efficacy of high-power (HP) saturation, the acquisition protocol has been optimized on the 0.5 mM sample of serotonin and interferents in phosphate buffer, reducing the signals of all the analytes as much as possible. With the same set of parameters, we performed the same experiment in presence of the **S5-AuNP**. The resulted spectrum is reported in *Figure 4.1f*. In this case, compared to water-LOGSY and water-STD, the HP water-STD experiment delivers an impressing 300% enhancement on the signals of serotonin in only 10 minutes, and no interfering resonances from non-interacting species, just as expected. We then lowered the concentration of all the analytes

down to 50 μM, keeping the concentration of **S5-AuNP** unchanged, and we repeated the HP water-STD experiment with a predetermined acquisition time of about 60 minutes. The resulting spectrum is reported in *Figure 4.2d*, together with the ^{1}H spectrum (*4.2a*), the standard STD (*4.2b*) and the water-LOGSY (*4.2c*) for comparison. Once again, the resonances of serotonin are clearly visible with an average S/N ratio of 9.49 in the spectral region 6.5–7.5 ppm. The signals are only barely visible in the spectra obtained with the other two techniques

4.3 Affinity tuning

The same water-LOGSY, STD, and HP water-STD experiments were repeated using **S4-AuNP** (already discussed in *Chapter 1*). Interesting enough, when going from a HEPES buffered system to a phosphate buffered system these nanoparticles see their affinity fall to Kb ≈ 6000 M^{-1}, still higher than the one shown by **S5-AuNP** in the same conditions. In this case a sample with serotonin and phenethylamine 50 μM and **S4-AuNP** 0.5 mM was prepared, only serotonin is recognized with an impressive enhancement of the signals in the HP water-STD spectrum (*Figure 4.3d*). Looking at these results, it seems possible to improve the sensitivity of water-STD just by raising the saturation. However, this would lead to an excessive saturation of the analytes, that can in turn cause false positives.

If the association constant between AuNP and analyte is too big, the apparent lineshape of the interacting analyte can be broadened. Even though a broadened signal does not necessarily affect the STD efficiency, a broadened signal can be undetectable in the final spectrum, leading to a what can be described as a false negative.[13] When this is the case, it is possible to modify the populations of the free and bound analytes by playing with the relative concentrations of the analytes and the NPs, based on the fact that decreasing the nanoparticle concentration will increase the fraction of unbound analyte.

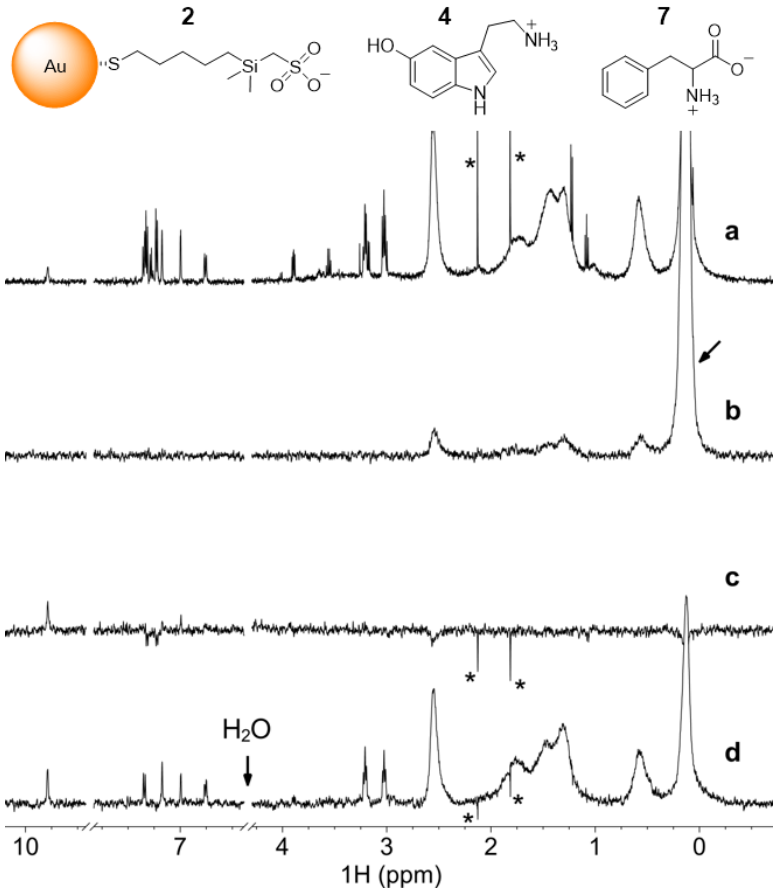

Figure 4.3. ^{1}H NMR spectra of 50 μM serotonin (**4**), 50 μM phenylalanine (**7**) and 0.5 mM **S4-AuNP**. a) Plain ^{1}H NMR spectrum with DPFG-PE (W5) solvent suppression. b) standard STD spectrum with 2 s saturation at the frequency highlighted by the arrow. c) water-LOGSY with 2 s mixing time. d) HP water-STD with 2 s saturation at the frequency of H_2O. The total acquisition time for spectra b)–d) is the same (60 min). Asterisks denote impurities. Figure from the above mentioned work.[9]

In *Figure 4.4* it is reported the effect of nanoparticles concentration in HP water-STD spectra when serotonin interacts with **S5-AuNP** (weak binding, $K_a \approx$ 100 M-1) and **S4-AuNP** (stronger binding to a rigid monolayer, see *Chapter 1* $K_a \approx$ 1000 M-1). In the case of weak binding, a low concentration of **S5-AuNP** results in no signal (*Figure 4.4b,* c), which suggests that the fraction of bound species is too low to provide a significant saturation transfer during the experiment. The signal is however recovered when the NPs concentration in-

creases (*Figure 4.4a*). On the other hand, in the case of strong binding, a lower concentration of **S4-AuNP** corresponds to a narrowing of the signals in water-STD spectra (*Figure 4.4d-f*). In this case the fraction of bound species, while low enough not to broaden the analytes signals, is still enough to provide an effective saturation transfer.

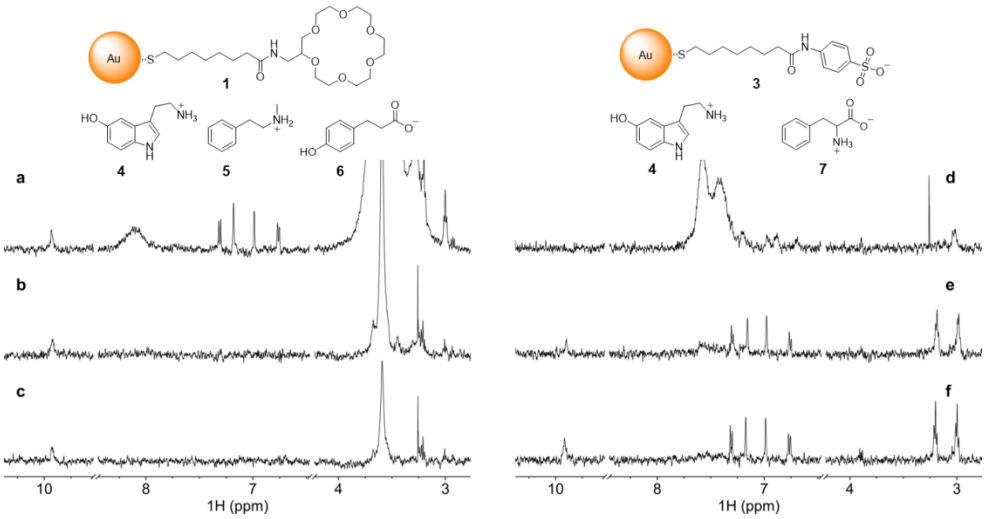

Figure 4.4. Left: HP water-STD spectra of 50 μM serotonin (**4**), 50 μM N-methyl-phenethylamine (**5**), 50 μM phloretic acid (**6**) with a) 500 μM **S5-AuNP** b) 50 μM **S5-AuNP**, (c) 25 μM **S5-AuNP**. Right: HP water-STD spectra of 50 μM M serotonin (**4**) and 50 μM M phenylalanine (**7**) with d) 500 μM **S4-AuNP** e) 50 μM **S4-AuNP**, f) 25 μM **S4-AuNP**. In all the samples the solvent medium is H_2O : D_2O = 90:10 with 10 mM phosphate buffer. Figure from the above mentioned work.[9]

In summary, the experimental conditions can be optimized to provide meaningful results both in the case of weak and in the case of strong binding between nanoparticles and analytes. Indeed, the proper nanoparticle concentration can be quite easily estimated on the basis of its affinity for the specific analyte under investigation.

4.4 Biselective saturation

Since in all the nanoparticles presented up to now there is an alkyl spacer, whose protons resonate between 1 and 2 ppm, we thought that the simultaneous saturation of water and of the AuNP monolayer could give a boost of signal. This is feasible if the saturating pulse is split into two sidebands, e.g. by cosine modulation of the parent selective pulse, thus a direct saturation of the NP monolayer can be obtained by placing one of the two sidebands close to the alkyl resonances.

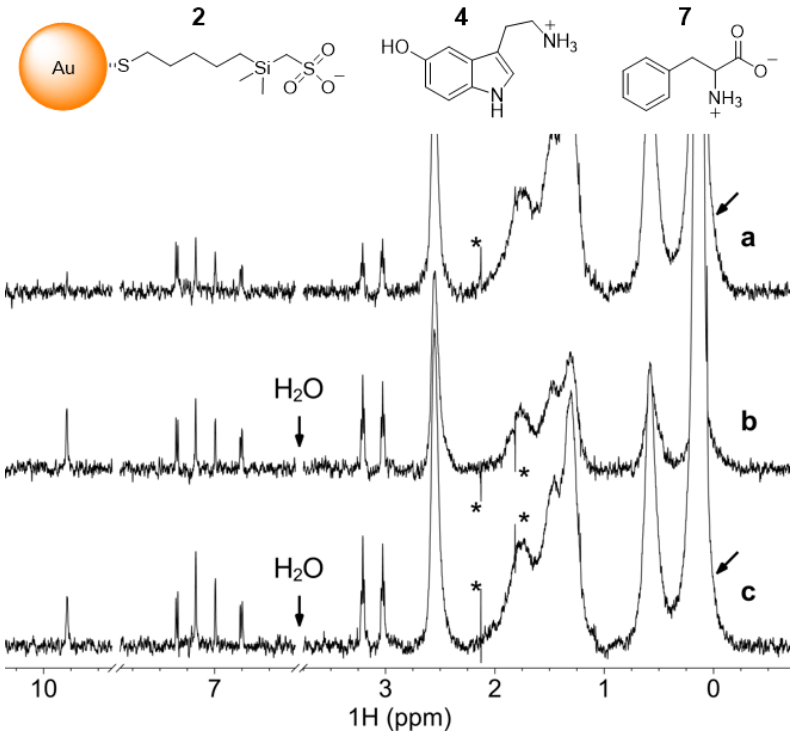

Figure 4.5. ^{1}H-NMR spectra of 50 μM serotonin (**4**), 50 μM phenylalanine (**7**) and 0.5 mM **S4-AuNP**. a) and b): high power saturation at the frequencies indicated by the arrows. c) simultaneous biselective saturation of water and alkyl resonances achieved by cosine modulation at 1144 Hz. Asterisks denote impurities. Figure from the above mentioned work.[9]

The advantages of such biselective water-monolayer saturation are presented in *Figure 4.5*: trace a) reports a high-power STD spectrum of 50 μM serotonin

(**4**), 50 μM phenylalanine (**7**) and 0.5 mM **S4-AuNP** obtained upon saturation of the dimethylsilyl resonances, while trace b) reports the same high-power STD spectrum obtained by saturating water (note that this is the same spectrum of *Figure 4.3d*). In both cases, the saturating rf field has the same power and leads to an appreciable enhancement on serotonin, whose resonances in the region 6.5– 7.5 ppm reach an average S/N ratio of 5.10 for trace 5a and 6.94 for trace 5b. Nonetheless, the simultaneous biselective saturation of water and dimethylsilyl resonances returns a spectrum with even more intense signals, with an average S/N ratio of 8.64 in the same 6.5−7.5 ppm region.

4.5 Towards lower detection limits

From the HP water-STD experiments shown in the previous paragraphs we reached a successful detection of a concentration of 50 μM of serotonin reducing the acquisition compared to the earlier NMR-chemosensing experiments reported in *Chapter 2* and *3*. Moreover, the combination of the just explained technique with higher field magnets and cryoprobes should give the opportunity to further decrease the detection limit.

A different approach to the same aim is currently under investigation in our lab: we reasoned that it should be possible to improve the magnetization transfer from the nanoparticle to the analyte, increasing the rotational correlation time of the receptor. Theoretically this could be done increasing slightly the diameter of the AuNP, but this requires the optimization of a new synthetic protocol. Moreover, it has been shown[14] that increasing the dimension of the AuNP affects also the biding constant. So, we tested the possibility bind electrostatically **S1-AuNP** (see *Chapter 2*) to commercially available colloidal silica (LUDOX® CL, alumina coated, positively charged) to increase the rotational correlation time without affecting the characteristics of the sensor.

The relative quantity of AuNPs and silica NPs has been determined by NMR titration: LUDOX were added to the sample until the peaks of AuNP completely disappear from the spectrum. Some poliethyleneglycol (PEG2000) is necessary to improve the stability of the system against aggregation. In *Figure 4.6* are reported the spectra obtained for a sample containing serotonin 10 μM, **S1-AuNP** 15 μM and 1% PEG2000 in H_2O : D_2O 90:10 in phosphate buffer 1 mM pH=7. From top to bottom a) is the ^1H spectrum; b) HP water-STD c) HP water-STD of the sample without AuNP in presence of LUDOX; d) HP water-STD of the sample with the self-assembled AuNP-LUDOX complex. With this system it's possible to successfully detect a concentration of 10 μM of serotonin in 4 h of acquisition. Moreover, the system is adaptable to other AuNPs and other substrates (e.g. positively charged AuNPs and LUDOX® HS, to detect

carboxylic acids). The possibility to use this system in biologically relevant conditions, as for sensing of metabolites in urine is currently under investigation.

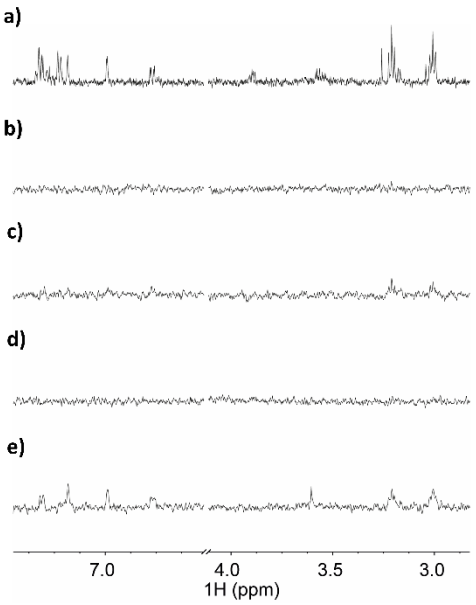

Figure 4.6. a) plain ^{1}H-NMR with solvent suppression; b) HP water-STD of a sample containing serotonin 10 μM and phenylalanine 10 μM c) HP water-STD of a sample containing serotonin 10 μM, phenylalanine 10 uM, and **S1-AuNP** 15 μM (concentration expressed as thiol concentration); d) HP water-STD of a sample containing serotonin 10 μM, phenylalanine 10 μM, and LUDOX-CL; d) HP water-STD of a sample containing serotonin 10 μM, phenylalanine 10 μM, **S1-AuNP** 15 μM (concentration expressed as thiol concentration) and LUDOX-CL. In the experiments with LUDOX and **S1-AuNP** 1% of PEG2000 is added to improve the stability of the system.

4.6 Conclusions

In conclusion, we have demonstrated that, with respect to the NOE pumping experiments proposed in early NMR chemosensing protocols, water spins bound to NPs monolayers can deliver a remarkable boost of sensitivity in con-

junction with STD experiments. Furthermore, by carefully raising the power of the saturation pulses, a bonus sensitivity gain can be appreciated because of the concurrent partial saturation of the monolayer spins. More generally, thanks to the peculiar chemistry of AuNPs, water saturation can be complemented with the saturation of alkyl resonances, leading to a new class of biselective "water-monolayer" STD experiments.

Thanks to this novel approach, the determination of analytes in the micromolar range becomes possible in reasonable acquisition times, even with standard instruments (a 500 MHz NMR spectrometer in our case) and with relatively simple nanoreceptors.

Moreover, the water-STD can be applied successfully to a self-assembled AuNP-LUDOX receptor, lowering the detection limit to 10 μM in 4 h. In this context, the major obstacles that still need to be addressed mainly concern the quantitation of the target analytes in matrices with interfering/competitive species.

Supplementary information

Solvents were purified by standard methods. All commercially available reagents and substrates were used as received. Thiols **S2**, **S4**, **S5** and corresponding monolayer protected gold nanoparticles (AuNP) were prepared as detailed in *Chapter 2* and *Chapter 3* of this thesis.

NMR sample preparation: stock solutions of AuNPs and analytes **4**-**7** were prepared in D_2O, stock solution of phosphate buffer at pH=7.01 was prepared in Milli-Q® water adding the appropriate amount of Na_2HPO_4, NaH_2PO_4 and adjusting the pH with NaOH 1M. Compounds **4**, **6** and **7** are commercially available, compound **2** hydrochloride was prepared from the corresponding amine with a procedure already reported[1]. NMR tubes were prepared adding the correct amount of stock solutions, D_2O and Milli-Q® water to reach the final volume of 600 μl with a H_2O:D_2O ratio of 90:10.

Binding constants estimation

As it was not possible to measure the binding constants of the systems used through fluorescence titrations in phosphate buffer (suggesting that K_{ass}< $5{\cdot}10^{\wedge 4}$, as previously determined[15]), the binding constants AuNPs-serotonin (**4**) were measured through ^{1}H-NMR using a NOE-pumping titration for **S5-AuNP**, and a chemical shift titration for **S4-AuNP** and **S2-AuNP**. Data obtained were fitted with DynaFit® using the following 1:1 binding models. Considering the nature of the AuNPs, and the assumption that binding occurs following a 1:1 binding model involving multiple, independent and equivalent binding sites on the nanoparticle monolayer, the binding constants obtained through the NMR titrations must be considered as an average estimation.

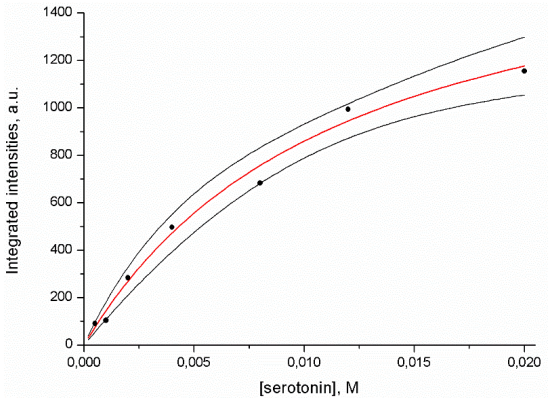

Figure 4.7: Plot of integrated intensities arising from all the aromatic signals of serotonin in NOE-pumping experiments with **S5-AuNP** as a function of serotonin concentration (black dots). Alkyl signals of the nanoparticle were used as reference. The best fit of the data obtained from DynaFit® is shown (red line) with 95% confidence intervals (black lines). Conditions: [**S5-AuNP**] corresponding to 1mM of thiol **1** and serotonin 0.5, 1, 2, 4, 8, 12, 20 mM in phosphate buffer 20mM, pD=7.01. The association constant Ka is 93±22 M^{-1}. The error is estimated from the fitting.

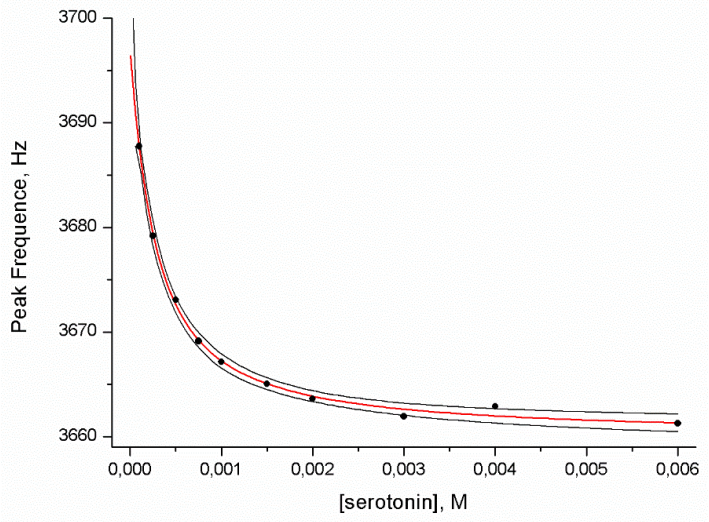

Figure 4.8: Plot of the frequency of an aromatic signal of serotonin as a function of serotonin concentration (black dots). Up-field shift is observed during titration. The best fit of the data obtained from DynaFit® is shown (red line) with 95% confidence intervals (black lines). Conditions: [**S4-AuNP**] corresponding to 1mM of thiol **2** and serotonin 0.1, 0.25, 0.5, 0.75, 1, 1.5, 2, 3, 4, 6 mM in phosphate buffer 20mM, pD=7.01. The association constant Ka is 6600±4400 M^{-1}. The error is estimated from the fitting.

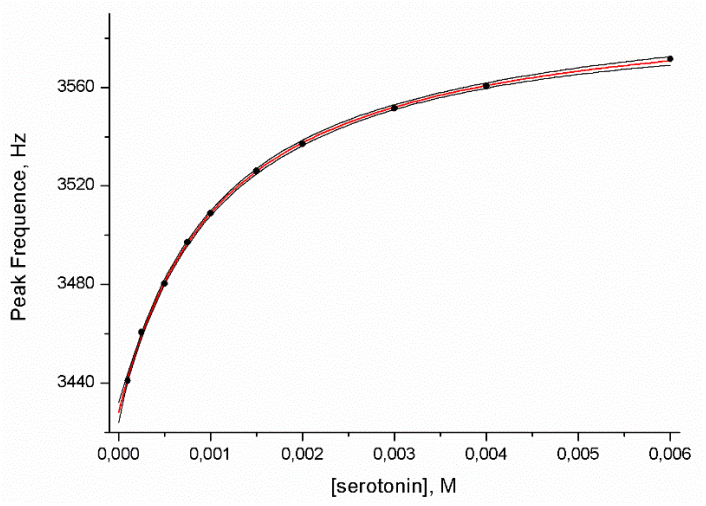

Figure 4.9: Plot of the frequency of one of the aromatic signals of serotonin as a function of serotonin concentration (black dots). Downfield shift is observed during the titration. The best fit of the data obtained from DynaFit® is shown (red line) with 95% confidence intervals (black lines). Conditions: [**S2-AuNP**] corresponding to 1mM of thiol **3** and serotonin 0.1, 0.25, 0.5, 0.75, 1, 1.5, 2, 3, 4, 6 mM in phosphate buffer 20mM, pD=7.01. The association constant Ka is 1000±230 M^{-1}. The error is estimated from the fitting.

Additional NMR experiments

All the NMR spectra were recorded on a Bruker AVANCE III spectrometer operating at 500.13 MHz ^{1}H Larmor frequency and equipped with a 5 mm *z*-gradient broadband inverse (BBI) non-cryogenic probe. All the samples were dissolved in a mixture of H_2O:D_2O = 90:10, unless otherwise specified, and the nanoparticles' concentrations in the following spectra are referred to the coating thiols. Solvent suppression was achieved with a DPFG-"perfect echo" (PE) with W5 clusters as the refocusing element (figure S10).[16,17]

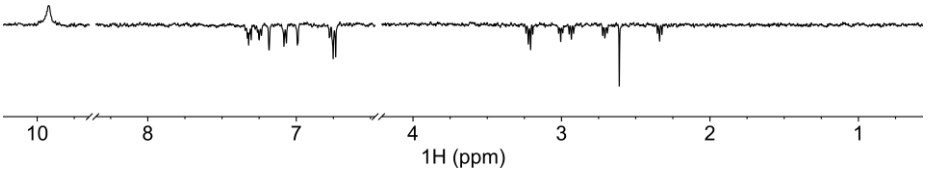

Figure 4.11: Water LOGSY spectrum of a mixture containing **4**, **5**, and **6** 0.5 mM each and 10 mM phosphate buffer (pH = 7). All the signals appear with a negative phase except for the one at 9.8 ppm, which belongs to the serotonin NH proton in slow exchange with water protons.[18] The mixing time for the transient-NOE magnetization transfer was optimized and set to 2 s. The conventional phase of the signals in water-LOGSY spectra has been reversed to facilitate the comparison with STD spectra.

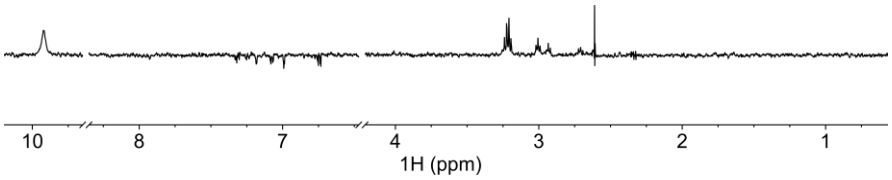

Figure 4.12: High power water-STD spectrum of a mixture containing **4**, **5**, and **6** 0.5 mM each and 10 mM phosphate buffer (pH = 7). Saturation was achieved by means of a train of 40 Gaussian pulses of 50 ms each. The strength of the pulses was adjusted to minimize the signals in the difference spectrum.

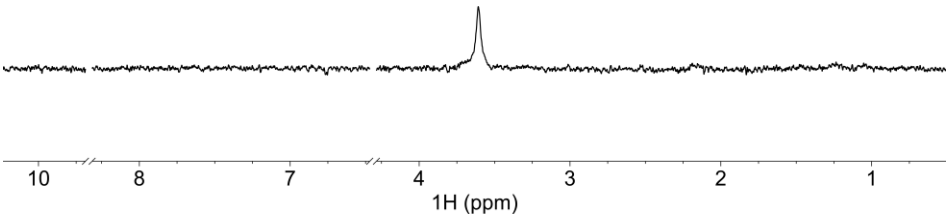

Figure 4.13: NOE-pumping spectrum of a mixture containing **4**, **5**, and **6** 0.5 mM each, **S5-AuNP** 0.5 mM and 10 mM phosphate buffer in D_2O (pD = 7). No analyte is detected. The phase of the spectrum has been reversed for uniformity with all the other spectra.

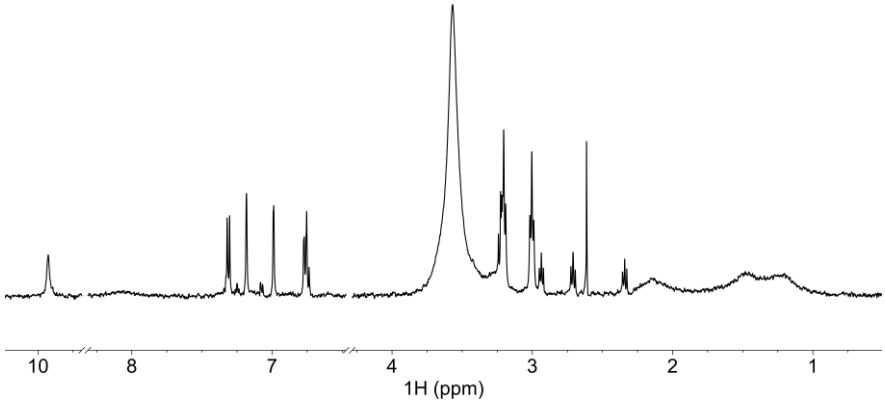

Figure 4.14: High power water-STD spectrum of a mixture containing **4**, **5**, and **6** 0.5 mM each, **S5-AuNP** 0.5 mM and 10 mM phosphate buffer (pH = 7). Saturation was achieved by means of a train of 40 Gaussian pulses of 50 ms each. False positives clearly appear due to the large power of the saturating RF field.

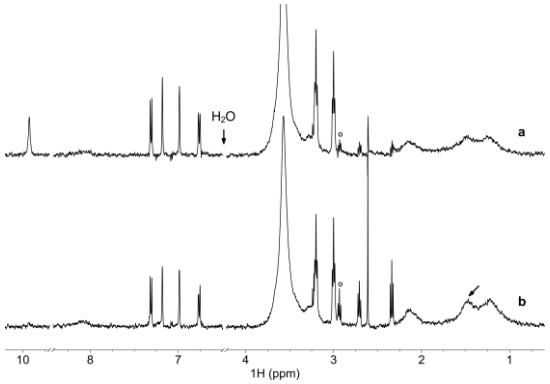

Figure 4.15: **a** High power water-STD spectrum of a mixture containing **4**, **5**, and **6** 0.5 mM each, **S5-AuNP** 0.5 mM and 10 mM phosphate buffer (pH = 7). **b** High power STD spectrum of the same sample at frequency indicated by the arrow. In both spectra, saturation was achieved by the same train of 40 Gaussian pulses. The peak highlighted by the circle, appearing as a false positive, is located about halfway between the frequencies of the saturating field used in **a** and **b,** but its intensity is much larger in the spectrum where the alkyl resonances are saturated.

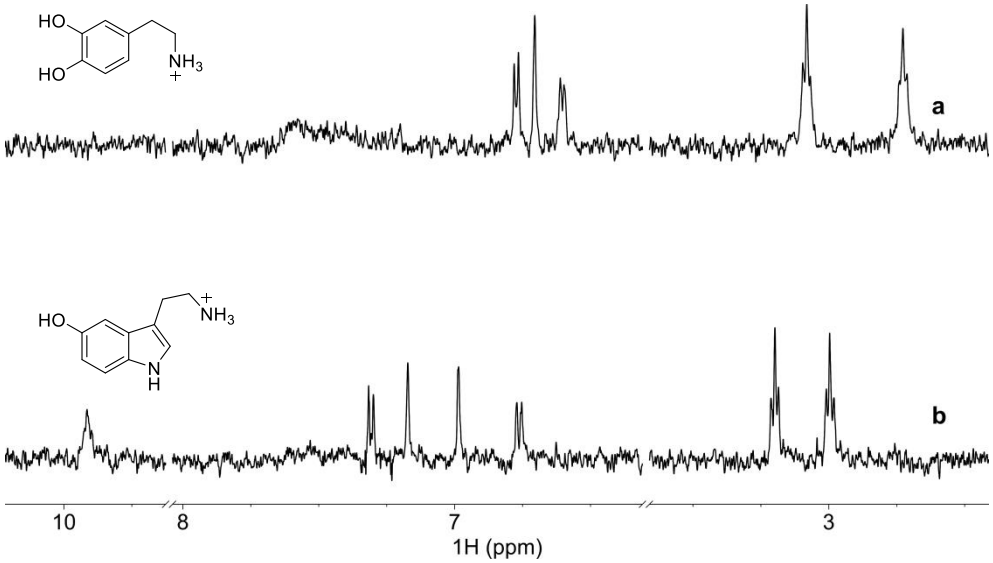

Figure 4.16: **a** High power water-STD spectrum of a mixture containing 50 μM dopamine, **S4-AuNP** 50 μM and 0.5 mM phosphate buffer (pH = 7). **b** High power water-STD spectrum of a mixture containing **4** (serotonin) and **7** 50 μM each, **3**-AuNP 25 μM and 10 mM phosphate buffer (pH = 7). Spectrum **b** is the same as in *Figure 4.4f*, and is shown here for comparison purposes. In both **a** and **b** saturation was achieved by means of a train of 40 Gaussian pulses of 50 ms each.

Bibliography

(1) Salvia, M. V.; Salassa, G.; Rastrelli, F.; Mancin, F. Turning Supramolecular Receptors into Chemosensors by Nanoparticle-Assisted "NMR Chemosensing." *J. Am. Chem. Soc.* **2015**, *137* (35), 11399–11406.

(2) Gabrielli, L.; Rosa-Gastaldo, D.; Salvia, M. V.; Springhetti, S.; Rastrelli, F.; Mancin, F. Detection and Identification of Designer Drugs by Nanoparticle-Based NMR Chemosensing. *Chem. Sci.* **2018**, *9* (21), 4777–4784.

(3) Diez-Castellnou, M.; Salvia, M. V.; Springhetti, S.; Rastrelli, F.; Mancin, F. Nanoparticle-Assisted Affinity NMR Spectroscopy: High Sensitivity Detection and Identification of Organic Molecules. *Chem. - A Eur. J.* **2016**, *22* (47), 16957–16963.

(4) Salvia, M. V.; Ramadori, F.; Springhetti, S.; Diez-Castellnou, M.; Perrone, B.; Rastrelli, F.; Mancin, F. Nanoparticle-Assisted NMR Detection of Organic Anions: From Chemosensing to Chromatography. *J. Am. Chem. Soc.* **2015**, *137* (2), 886–892.

(5) Huang, R.; Bonnichon, A.; Claridge, T. D. W.; Leung, I. K. H. Protein-Ligand Binding Affinity Determination by the WaterLOGSY Method: An Optimised Approach Considering Ligand Rebinding. *Sci. Rep.* **2017**, *7*.

(6) Riccardi, L.; Gabrielli, L.; Sun, X.; De Biasi, F.; Rastrelli, F.; Mancin, F.; De Vivo, M. Nanoparticle-Based Receptors Mimic Protein-Ligand Recognition. *Chem* **2017**, *3* (1), 92–109.

(7) Sun, X.; Riccardi, L.; De Biasi, F.; Rastrelli, F.; De Vivo, M.; Mancin, F. Molecular-Dynamics-Simulation-Directed Rational Design of Nanoreceptors with Targeted Affinity. *Angew. Chemie* **2019**, *131* (23), 7784–7789.

(8) Sarrouilhe, D.; Clarhaut, J.; Defamie, N.; Mesnil, M. Serotonin and Cancer: What Is the Link? *Curr. Mol. Med.* **2015**, *15* (1), 62–77.

(9) De Biasi, F.; Rosa-Gastaldo, D.; Sun, X.; Mancin, F.; Rastrelli, F. Nanoparticle-Assisted NMR Spectroscopy: Enhanced Detection of Analytes by Water-Mediated Saturation Transfer. *J. Am. Chem. Soc.* **2019**, *141* (12), 4870–4877.

(10) Halle, B. Cross-Relaxation between Macromolecular and Solvent Spins: The Role of Long-Range Dipole Couplings. *J. Chem. Phys.* **2003**, *119* (23), 12372–12385.

(11) Frezzato, D.; Rastrelli, F.; Bagno, A. Nuclear Spin Relaxation Driven by Intermolecular Dipolar Interactions: The Role of Solute-Solvent Pair Correlations in the Modeling of Spectral Density Functions. *J. Phys. Chem. B* **2006**, *110* (11), 5676–5689.

(12) Dalvit, C.; Fogliatto, G. P.; Stewart, A.; Veronesi, M.; Stockman, B. WaterLOGSY as a Method for Primary NMR Screening: Practical Aspects and Range of Applicability. *J. Biomol. NMR* **2001**, *21* (4), 349–359.

(13) Neuhaus, D.; Williamson, M. P. *The Nuclear Overhauser Effect in Structural and Conformational Analysis*; Wiley, 2000.

(14) Lucarini, M.; Franchi, P.; Pedulli, G. F.; Gentilini, C.; Polizzi, S.; Pengo, P.; Scrimin, P.; Pasquato, L. Effect of Core Size on the Partition of Organic Solutes in the Monolayer of Water-Soluble Nanoparticles: An ESR Investigation. *J. Am. Chem. Soc.* **2005**, *127* (47), 16384–16385.

(15) Gabrielli, L.; Rosa-Gastaldo, D.; Salvia, M. V.; Springhetti, S.; Rastrelli, F.; Mancin, F. Detection and Identification of Designer Drugs by Nanoparticle-Based NMR Chemosensing. *Chem. Sci.* **2018**, *9* (21), 4777–4784.

(16) Liu, M.; Mao, X. A.; Ye, C.; Huang, H.; Nicholson, J. K.; Lindon, J. C. Improved Watergate Pulse Sequences for Solvent Suppression in NMR Spectroscopy. *J. Magn. Reson.* **1998**, *132* (1), 125–129.

(17) Aguilar, J. A.; Kenwright, S. J. Robust NMR Water Signal Suppression for Demanding Analytical Applications. *Analyst* **2016**, *141* (1), 236–242.

(18) Dalvit, C.; Fogliatto, G. P.; Stewart, A.; Veronesi, M.; Stockman, B. WaterLOGSY as a Method for Primary NMR Screening: Practical Aspects and Range of Applicability. *J. Biomol. NMR* **2001**, *21* (4), 349–359.

5

Colorimetric supramolecular sensor for quick detection of N-BOMes

Summary

Quick and low-cost qualitative detection of new designer drugs is crucial for their immediate on-site identification. In this chapter I am going to show two supramolecular colorimetric chemosensors, based on a complex of cucurbit[8]uril and different tricyclic dyes: thionine and oxonin. The first one responds selectively to NBOMes from street samples with no pre-treatment. The system can be immobilized on paper giving a point-of-care test such as an indicator strip capable to discriminate illegal drugs from other substances.

5.1 Naked eye detection of drugs of abuse

We already examined in *Chapters 1* and *2* the most used routine methods for the analysis of illicit drugs. Most of them need pre-treatment of the sample, trained personal to perform the analysis and the instruments needed are often expensive and require costly maintenance. These problems affect in part also the NMR chemosensing technique previously described.[1] These techniques are reliable and can often give the exact structure of the molecule, their differences being in handling the sample and processing time. In particular analytical cases though, knowing the exact concentration or structure of the drug is not needed in order to identify it. If we think about a police control at a concert or at the airport, it is acceptable to spend only a certain amount of time for an analytical response, to understand if a suspicious white powder is a drug or not. In these cases, even the proof of absence of a drug in the sample is an important information, so that useless seizures of powders such as flour, powdered milk, painkillers are avoided and are not forwarded to further costly analysis. Moreover, people in possession of these powders don't have to be detained as well. The sensor that better fulfills the needs for a quick on-site detection is a colorimetric sensor: chromogenic and fluorogenic probes are characterized by a response -a change of colour-, that is real-time and easy to interpret. In the next sections I will present some relevant examples to better understand the state of the art in colorimetric probes for drug detection.

The first example is the detection of lysergic acid diethylamide, better known as LSD. LSD is a hallucinogenic drug capable to alter the perception of the environment, feelings and behaviour. The LSD molecule shows a fluorescence emission that can vary in the range 400-530nm, according to the pH and nature of the medium used. Baudot and Andre,[2] taking inspiration from a commercially available quick-test for cocaine with problems of false positives, exploited the intrinsic fluorescence of LSD to develop a naked-eye detection method. More in detail, they saw that excitation of a solution of LSD in neutral water shows blue fluorescence, but if a solution 1 M of sodium hydroxide is used as a medium, the emission shifts to green. Using a standard solution of LSD as a reference, the fluorescence of the cell containing the unknown substance is compared. After building calibration curve, an attenuator is used to lower the intensity of the light provided to the sample cell

until the two cells have matching fluorescence. This way, it is possible to estimate the concentration of LSD in the original sample. Fluorescence in basic medium is needed if one wants to discriminate LSD from some possible interferents. Indeed, while it is certain that if blue fluorescence is not observed the sample does not contain the drug, the presence of blue fluorescence might be due to other interferents such as mescaline, 2,5-dimethoxy-4-methyl amphetamine (DOM) and so on. In basic solution though, only the emission of LSD shifts to green, and this way, it can be discriminated.

Precipitation of metal complexes containing drugs of abuse can also be used to build colorimetric sensors. For example, Morris,[3] again taking inspiration from cocaine, reported a presumptive test for ketamine (an anesthetic) using cobalt thiocyanate. Potassium thiocyanate was added to a solution of a basified sample of ketamine. If ketamine is present, a purple precipitate is formed. If the test is negative, a matt blue-green precipitate appears. The source of the colour is a coordination complex of cobalt involving the thiocyanate ion, hydroxide, chloride and, of course, ketamine. Many interferents have been tested and only hydrocodone and few others gave false positive response. The lower detection limit is 10 mg/ml, compared to a concentration of 50-100 mg/ml typically present in commercial samples.

The same principle was applied by Herràez-Hernàndez and co-workers,[4] but in this case the cobalt thiocyanate was immobilized onto a matrix of polydimethylsiloxane. In this case, a strip test is obtained with the polymer turning pink because of the diffusion of the purple precipitate inside the polymer matrix. The limit of detection in this case is of 100 μg/μl and amphetamine and methamphetamine related substances, cocaine, but also normal drugs such as ibuprofen, acetylsalicylic acid, caffeine and other excipients such as starch, s and glucose are not interfering.

As a last example, I report a system that recalls the most common presumptive drug test available on the market (Mandelin, Marquis, Meke): in this case, the authors take advantage of the chemical reactivity of the drug molecule. In this work Yamada and co-workers[5] report a method for detection of MDMA (3,4-methylenedioxymethanpfhetamine) and related compounds, also from seized street tablets, that involves a reaction of the drug with sulfuric acid and chromotropic acid (CTA).

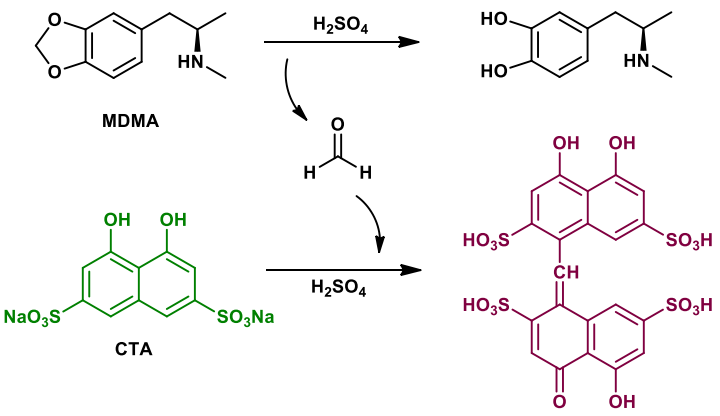

Figure 5.1. Coloured adduct produced by the reaction of formaldehyde with CTA in acid in sulfuric acid. Formaldehyde is produced only when MDMA is present in the sample.

The mechanism (*Figure 5.1*) is quite simple: when the MDMA is left in sulfuric acid, formaldehyde is formed. Formaldehyde reacts then with CTA producing 3,4,5,6-dibenzoxanthilium, a coloured specie that acts as reporter, giving to the solution a red-violet colour (absorbance peak at 570 nm). The colour change in this case is clearly seen by naked eye with a concentration as low as 50 μM. The colour of the tablets, in this case, was not interfering with the test.

5.2 Supramolecular colorimetric tests

Supramolecular chemistry has been used as well for colorimetric sensing. A nice example from Dalcanale and co-workers,[6] for MDMA sensing, is based on a tetra-phosphonate cavitand , with two pyrene moieties inserted in silica nanoparticles coated with a polyethylene glycol shell.

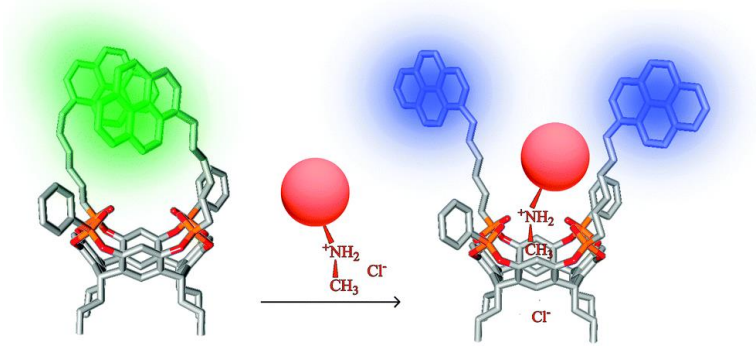

Figure 5.2. Proposed mechanism for the MDMA sensor by Dalcanale and co-workers. Image by Masseroni et al.[6]

As one can see in *Figure 5.2*, when the cavitand is trapped in the hydrophobic cavity of the silica nanoparticles the two pyrene moieties are close to each other, this way the spectrum of pyrene has both the monomer and excimer bands at 395 and 475 nm. When the MDMA is added to the system, it goes inside the cavitand, and its presence pushes apart the two pyrene moieties. This way, there is a strong quenching of the of the excimer emission band. Other methamphetamines are known interferents for this system, as the recognition capability of the cavitand used are based on the presence of the N-methylammonium group. Glycine, sarcosine, glucose and even amphetamine don't produce any variation of the emission.

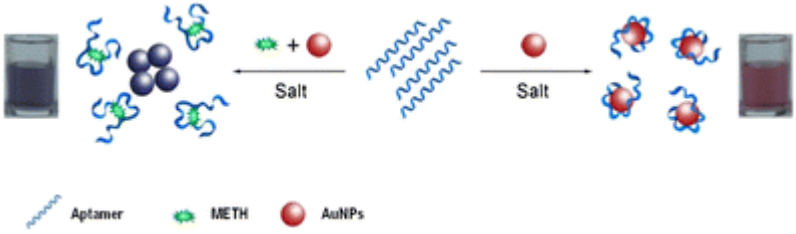

Figure 5.3. Sensor for methamphetamine proposed by Yi and co-workers. A specific methamphetamine aptamer, in presence of salt, coats the gold nanoparticles keeping them in solution (red solution, absorption peak at 525 nm). When methamphetamine is added, the aptamer makes a complex with it, leaving the naked nanoparticles in solution that undergo precipitation (blue solution, absorption at 660 nm). Image by Shi et al.[8]

With a different mechanism, aptamers are also widely used.[7] Aptamers are oligonucleotides that have high selectivity for binding a given molecule. In this case, Yi and co-workers[8] use gold nanoparticle coated with a specific aptamer for methamphetamine recognition (*Figure 5.3*). Since the nanoparticles have an average diame-

ter of 13 nm, they show the characteristic absorption band at 525 nm due to the surface plasmon resonance. The presence of a large amount of $CaCl_2$ in solution does not affect the stability of the gold nanoparticles, as they are protected by the presence of the aptamer. As the affinity of the aptamer is higher for the methamphetamine than for the gold nanoparticles, when the former is added to the solution, the aptamer starts to migrate from the nanoparticle surface, to the solution where it can complex the methamphetamine. The uncoated nanoparticles, exposed to the high salt concentration, are unstable in solution and start to aggregate. The absorption bad shifts from 525 nm to 660 nm producing a colour change visible also by naked eye. The detection limit is around 1 μM and many alkaloids such as morphine or barbital have been tried as interferents, giving negative response.

5.3 Cucurbiturils

Cucurbiturils are a class of cyclic compounds, obtained by reacting glycoluril with formaldehyde. If some evidences of the product go back to 1905 from Behrend and co-workers,[9] the crystal structure of CB[6] was successfully solved only in 1981.[10] The family consists in five main cyclic members, CB[5], CB[6], CB[7], CB[8], and CB[10]. Looking at the 3D structure reported in *Figure 5.4*, it's clear why this molecule is called cucurbituril: it recalls a pumpkin, the most representative member of the botanical *Cucurbitaceae* family.[11]

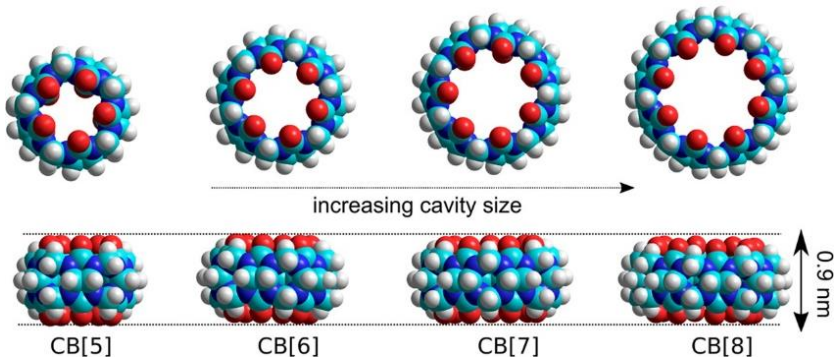

Figure 5.4: 3D structure and size comparison of the most used homologues of cucurbituril.

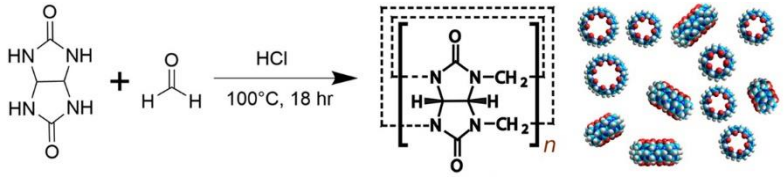

Figure 5.5. Scheme of the synthesis process used to obtain the cucurbiturils. Picture adapted from Barrow et al.[12]

The synthesis of this macrocycles is straightforward: the standard procedures reported requires a mixture of the two reactants in concentrated strong acid at high temperature (typically 100°C) under stirring for 1-24h (*Figure 5.5*). The result is a distribution in all the cucurbituril species, with different percentage for each member. By varying the reaction conditions such as time, temperature, and type of acid, it is possible to direct the reaction towards the formation of the desired ring homologue.[13] Also, the use of templating agents, such as alkali metal cations, has been successfully explored. The purification process to obtain a single cucurbituril homologue as a pure product is quite tricky and different strategies have been reported. Most of them exploit the difference in solubility that different homologues show in different solvents, or column chromatography with extremely polar eluents (e.g. methanol, formic acid). A different approach is complexing in the desired cucurbituril a size specific guest that changes the properties of the desired CB[n] enough to allow its separation.[11]

All the CB[n] can form host-guest complexes with small organic molecules, and they have been successfully used in catalysis,[14] drug delivery,[15] or as part of smart nanomaterials.[16] The main interest is in their hydrophobic cavity that contains high energy water, and is capable to bind guests with high binding constants: this characteristic can positively contribute in self-assembled devices or materials. Since in the rest of the chapter we will use CB[8] as part of a molecular sensor, I'll give a brief overview on the properties of all the members of the family, so that it will be clear why CB[8], and not a different cucurbituril, was chosen.

The smallest homologue is CB[5,] that has a portal diameter of 2.4 Å and an equatorial diameter of 4.4 Å. The cavity volume of 82 $Å^3$ does not allow organic molecules to be hosted inside. CB[5] can form supramolecular complexes with small cations (e.g. ammonium) using the carbonyls of the glycoluril subunits that point out of the

cavity. It can host small gas molecules as well, like N_2, O_2 and others, in aqueous solution and in solid form. The second member is CB[6], the preferential product of most synthesis procedures. In this case, the portal diameter is 3.9 Å, the equatorial 5.8 Å and with a cavity volume of 164 $Å^3$ it forms strong complexes with charged aliphatic amines. *Log* K_a of these complexes range from 2 to 10, according to the structure. The driving force of complexation is the interaction of the ammonium with the carbonyl moieties of the portal, as it was the case for CB[5], but for CB[6] the hydrophobic portion of the molecule fits inside the cavity, displacing the high energy water molecules trapped inside and giving extra stabilization to the complex. In the same fashion, CB[7]can bind aliphatic amines, but the lager portal size 5.4 Å (cavity of 7.3 Å) with a cage volume of 279 $Å^3$, allows the complexation of aromatic compounds as well as bulkier molecules like cobaltocene or adamantylammonium derivatives. The better the molecule fills the cage, the higher the reported binding constants, that, in the case of adamantylammonium, show a *log* K_a higher than 12. The last important homologue is CB[8] with a portal and equatorial diameter of 6.9 Å and 8.8 Å respectively. The cavity volume of 479 $Å^3$ gives the possibility to CB[8] to host inside two molecules to form homo an eteroternary complexes. in this case as well, *log* K_a can be up to 15 for a single inclusion.[12,17] The election method to measure these constants it's ITC, but fluorescence and UV-Vis titrations are also used.

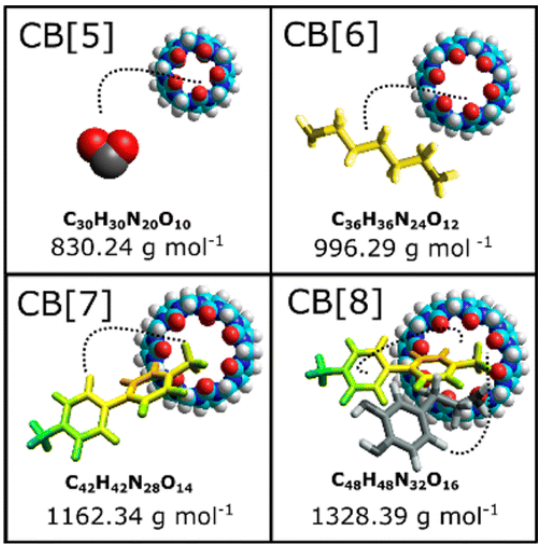

Figure 5.6. Structure of CB[5], CB[6], CB[7], CB[8], molecular formula and molecular weight. Each homologue is reported with a characteristic guest. Picture adapted from Barrow et al.[12]

5.4 Cucurbituril-based drug sensing

Cucurbituril receptors are ideal for supramolecular drug sensing, as they usually bind to amphiphilic or bolaform organic cations. In this area, one can find in literature a few chemosensors that use cucurbituril-dye complexes for the colorimetric sensing of drugs of abuse. I report here an example from Garcia and co-workers[18] that explains the use of a supramolecular sensor array for the detection of γ-hydroxybutirric acid (GHB) in solution. This particular drug is called date-rape drug because, since its main effects are euphoria and loss of inhibition, many cases are reported of prowlers using it in nightclubs to take advantage of other people. Besides the medical and psychological implications of a rape, GHB has important side effects that are strongly dose dependent. Moreover, the range from effective and lethal dose is very narrow, so there is a real risk of accidental overdose, that can lead to situations of coma or even death.

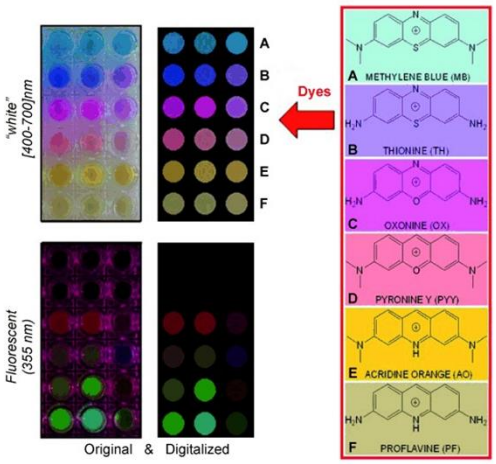

Figure 5.6. original (left) and digitalized (right) images of the dyes used in the work cited, as free molecules and as complexes with cucurbit[7]uril and cucurbit[8]uril. Picture by Baumes et al.[18]

The sensor reported for the detection of GHB in water consists in a series of different complexes of tricyclic dyes with CB[7] and CB[8] (*Figure 5.6*).When GHB is added to a solution of these complexes in a multiwall plate, the complexes show a change of colour as well as a change of emission intensity. These changes are characteristic of every different complex and every different analyte that is added shows a different response. This way, it is possible to discriminate GHB from other

substances. Moreover, the pictures of the plates can easily be digitalized (a good camera is enough) and analysed with a software that can extract the red green and blue (RGB) components for software-based analysis. Adding a cosolvent perturbs the complexation equilibria and improves the detection capability of the system, allowing also a quantification of the GHB present in the sample. However, the ingredients of common soft drinks, such as Coca-Cola®, can interfere with the measurements, and this is a severe inconvenient as GHB is often dissolved in drinks.

5.5 The idea

Reassured by the results reported by Garcia and co-workers, we explored the possibility to design a selective sensor for the detection of N-benzyl-substituted phenethylamines (NBOMes) based on a displacement essay that involves a complex of a tricyclic dye and CB[8]. NBOMes belong to the 5-HT2A receptor agonists category of designer drugs.[19] They have emerged in recent years for recreational purposes as drug of abuse and they can be easily purchased online at cheap prices. Unlike other drugs that have a similar function (e.g. LSD), several side effects and even fatal cases are reported after use.[20,21] The typical dose ranges from 50 to 800 μg and they are commonly sold absorbed on blotter paper, as powder, or as a solution in dropper bottles.[22] From the point of view of the chemical structure, NBOMes are N-(2-methoxybenzil) derivatives of a phenethylamine, with two methoxy groups in position 2 and 5 of the phenethylamine ring and a substituent in position 4 that can be a halogen, a proton or a methyl group. This substituent gives their retail name as 25C (chlorine), 25B (bromine), 25H-NBOMe or others.

With no surprise, the election methods for the routine sensing of these drugs are chromatographical. Quantitative determination of NBOMes have been already reported during the last years using GC-MS, LC-MS, electrochemical methods, ^{1}H-NMR. In some cases, the NBOMes were analysed directly from blotter paper using ATR-FTIR spectroscopy and identified through database screening[23] or using paper spray ionization mass spectrometry (PSI-MS). Analysis of NBOMes is reported also

in biological samples like hair, urine, blood and serum.[24] All these techniques require the structural knowledge of the illicit drugs prior to the analysis, the instrumentation is expensive, and the analysis require trained people. Moreover, the instrumentation is not portable, and the on-site identification is often not possible.

If we look at the structure of the molecule in a "supramolecular way", it consists of two hydrophobic aromatic rings kept together by a flexible phenethylamine linker. The secondary amine, that is protonated in biological conditions, is capable to donate hydrogen bonding. We saw in the previous section that the best guests for CB[8] are aromatic amines, and that, in this case, 1:2 complexes are more likely to form than 1:1 complexes. NBOMe has the possibility to adopt a sandwich like configuration. This way, in a potential cucurbituril complex, the ammonium group could interact with the carbonyl moieties of the portal, leaving the two partially stacked rings inside the cavity. If we think about the most diffused drugs of abuse, this possibility is exclusive of the NBOMes, because potential interferents either have a single ring (amphetamines, methamphetamines, common painkillers) or have a bulky structure with rigid conformation (opioids and other alkaloids).

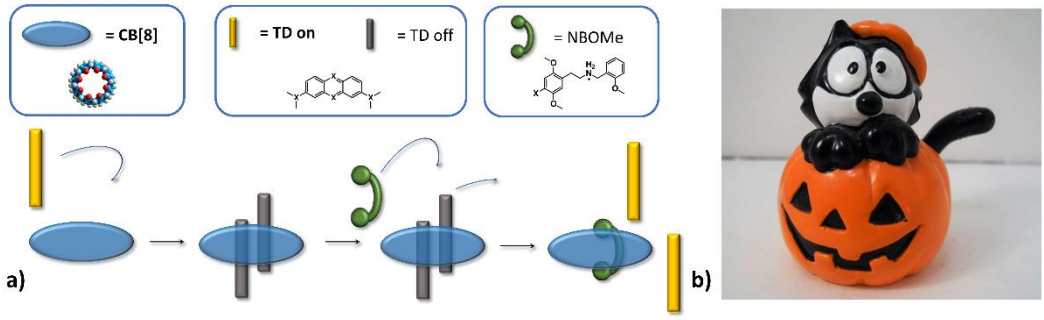

Figure 5.7. a) Felix the cat, one of the most popular characters printed on the blotter paper used to sell NBOMes, representing the drug complexed inside an Halloween pumpkin, the CB[8]; b) schematic representation of the idea of the project.

I therefore thought that, to this aim, the ideal cucurbituril could be CB[8], which is capable of complexing two aromatic molecules at the same time, hence allowing discrimination. The choice of the tricyclic dyes was not straightforward. After comparing different literature sources, I decided to use thionine acetate (TH), a blue dye, because is reported to have the most visible shift between the free and complexed form. Moreover, it's cheap, not harmful and commercially available. I also

wanted to test the emission properties of the system. In this case, TH is not the ideal candidate, because it has a really poor fluorescence quantum yield, that could be detected using a fluorimeter, but not by naked eye. So, I chose oxonine (OX) that has a unitary quantum yield when free in solution, that falls to 0.3, when paired inside the CB[8]. Such a difference can be seen by naked eye. Moreover, the association constants reported for the formation of the complex have a difference of two orders of magnitude compared to the TH. This could allow a different affinity between the two complexes that could, in principle, reflect in a different sensing capability.

5.6 Complexation of tricyclic dyes

The family of tricyclic dies encompasses many molecules formed by three condensed heterocycles, in which the positions 1 and/or 4 of the middle ring are substituted with a heteroatom (some examples are reported in *Figure 5.8*). On the side rings, two amino substituents are present. Depending on which heteroatom is present, and whether the amine is methylated or not, the absorption and the emission properties are different. In addition, since all tricyclic dyes are involved in protonation equilibria, a crucial parameter to control is the pH.

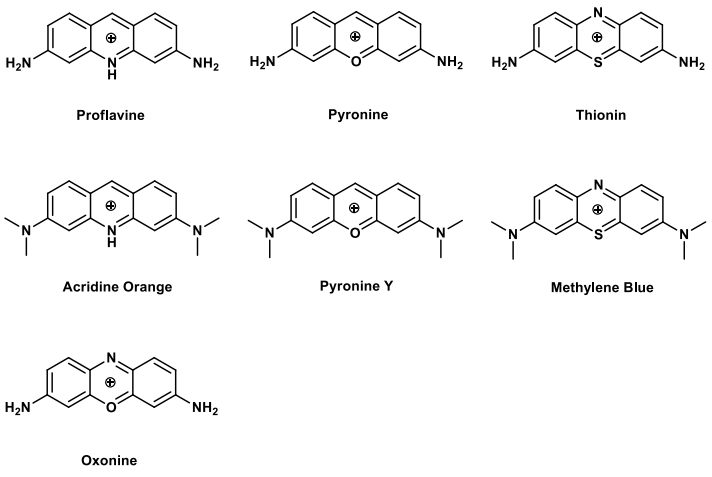

Figure 5.8. Structures of different tricyclic dyes. With simple substitutions on the base structure it is possible to have colours ranging from yellow to blue, to purple.

Since these molecules are positively charged, totally conjugated and therefore planar, they represent the perfect guest for complexation by the bigger homologues of the cucurbituril family. When free in solution, these molecules show an absorption spectrum with the main band in the visible (log ε > 4) always accompanied by a shoulder on the blue side (other characteristic bands are present in the UV region, but they are not useful for the purpose of this sensor). It has been already shown that, by increasing the concentration of the dye in water, the shape and the relative intensity of the bands are affected. Although this fact is not completely understood, the phenomenon is generally attributed to the formation of dimers of the dyes.[25] The correct work concentration to avoid the presence of dimeric species in solution is in the low micromolar. In this range of concentration, any change in the absorption (or emission) spectrum can be ascribed to the sole complexation. Interestingly enough, all the other parameters being the same, the complexation of the dyes inside CB[7] and CB[8] have opposite effect. In the first case, the absorption spectrum corresponds in shape to the one of the free dye, even if it may undergo a modest shift upon complexation. In the second case, upon complexation the spectrum of the dye turns into the spectrum of the dimeric specie. This confirms that CB[8] can bind two dye molecules at the same time, which, being forced in the cavity, must form the dimer.

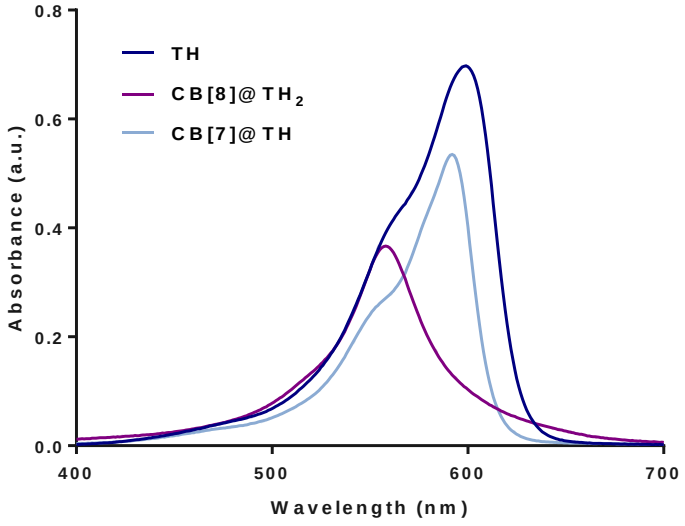

Figure 5.9 Spectra of TH (left): a) the free dye; b) the dye complexed in CB[7]; c) the dye complexed in CB[8].

Complexation affects emission as well: complexation in CB[7] results in a two to three fold enhancement of the fluorescence intensity, explained as a solvent effect, as the cavity of the cucurbituril is more hydrophobic than the solution. However, limited interaction with solvent molecules inside the cage can also explain this fact as it prevents solvent-mediated non radiative decay mechanisms. In the case of CB[8], the emission is partially or totally quenched (it depends on the specific dye). In this case, the quenching comes from the formation of the dimer inside the cavity, putting the dyes in close proximity and letting π-π interactions quench the emission. The log K values range from 6-7 for CB[7] to 13-16 for the dimers in the CB[8].

5.7 The purity of cucurbiturils

It's well known that cucurbiturils are isolated from the reaction mixture as white solids, containing various amounts of water, hydrogen chloride as well as ammonium, sodium or potassium salts that are encapsulated in the cavity. Even commercial samples are sold as "pure", but with non-defined amounts of water or hydrochloric acid of crystallization. Moreover, they are hygroscopic, hence they can easily absorb moisture from air - moisture that, with time leads to an increase of the apparent molecular weight. In a few weeks, the apparent molecular weight of a cucurbituril solid sample can nearly double the one of the actual molecule.[26] As water and other impurities are not organic, in the majority of the cases they are not affecting the binding capabilities of the cucurbituril. Hence, a second purification step is not necessary, but, when an exact concentration is needed, weighting the samples is not enough and the solution needs to be standardized. Moreover, all cucurbiturils are sparingly soluble in water, and after the preparation of a solution, filtration is needed to remove any solid left, and standardization is needed anyways.

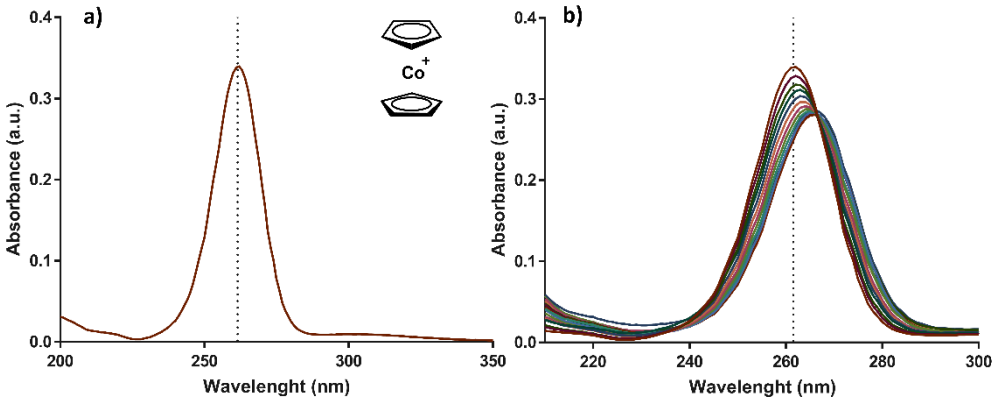

Figure 5.10. a) structure of Cob^+ cation and absorption spectrum. The dotted line indicates the maximum at 261 nm; b) plot of the absorption spectra obtained from a solution of Cob^+ with different amounts of CB[8] added.

Many methods may be used to this aim (NMR, TGA, ITC) but the more convenient seemed the one proposed Yi and Kaifer.[26] Cobaltocenium (Cob^+) is a primary standard, sold as hexafluorophosphate salt. It's a Co(III) ion coordinating two cyclopentadienyl anions. It has been reported that it forms 1:1 complexes with CB[8] (confirmed by MALDI-TOF, UV analysis and NMR titrations) with a high binding constant in acetate buffer at pH=5.5.[27] The absorption spectrum of Cob^+ has a maximum at 261 nm. Upon complexation with CB[8], the absorbance at the maximum decreases and experiences a red shift. Reporting the value of the absorbance at 261 nm versus the concentration of CB[8] added during a titration experiment, the resulting graph is formed by two linear portions, one with a bigger slope obtained for substoichiometric amounts of cucurbituril added, the other one with quasi-zero slope for the points above one equivalent. Extrapolation of the intersection of the two linear parts allows to calculate the actual concentration of the CB[8] solution

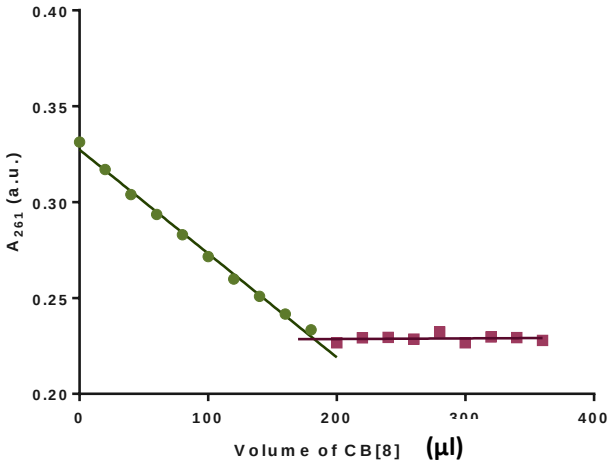

Figure 5.11. Plot of the absorbance at 261 nm vs the volume of CB[8] solution added

In practice, the theoretical amount of CB[8] needed for a 100 µM solution was weighted (as if it would be 100% pure) and dispersed in the correct amount of ultrapure water and sonicated for 30 min. The solid residues were filtered off with a 200 µm cellulose syringe filter. The solution of Cob^+ was prepared weighting a precise amount of solid and dissolving it in ultrapure water (100 µM). An UV-vis spectrum of the solution has been recorded and, knowing that the molar absorptivity coefficient is 34200 M^{-1} cm^{-1} at 261 nm, the exact concentration of the Cob^+ solution was determined (96.5 µM). Then, a 5 µM solution of Cob^+ was titrated with the solution of CB[8] containing the same concentration of Cob^+ (to avoid dilution effects). The actual concentration, extrapolated from the equivalent point of the graph reported in *Figure 5.5*, resulted to be 65 µM.

5.8 Standardization of thionine solution

As I could not find in literature an unambiguous value for the extinction molar coefficient ε of thionine acetate in a buffered aqueous solution (acetate buffer pH 5.5), the 10 mM solution obtained by weighting the exact amount of TH and dissolved in water has been standardized using the solution of [CB]8 obtained from the previous step. It has been already reported that TH forms an heterodimeric complex

with the cucurbituril CB[8]@TH_2 with cumulative formation constant of K=2.5 10^{16} M^{-2}. This value of the formation constant allows to consider the formation of the complex quantitative.

To choose the concentration working range, it has been checked that the absorption peak at 599 nm respects the Lambert-Beer law, so the absorption spectra of different solutions have been recorded in the range 0-35 μM. As the plot of the absorption maxima is linear with the concentration (*Figure 5.12*), the convenient value of 5 μM has been chosen to perform all the other experiments.

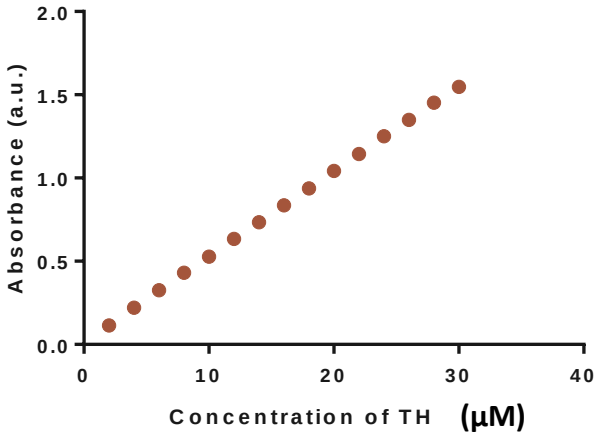

Figure 5.12. Absorbance of TH at 599 nm varies linearly with concentration in the interval 0-35 μM used in this work.

The standardization has been carried out just as the previous one: to a measured amount of TH solution, subsequent increasing amounts of CB[8] were added. After plotting the absorbance against the concentration of cucurbituril added, as for the previous case, the title for the thionine solution has been obtained by extrapolation of the plotted data.

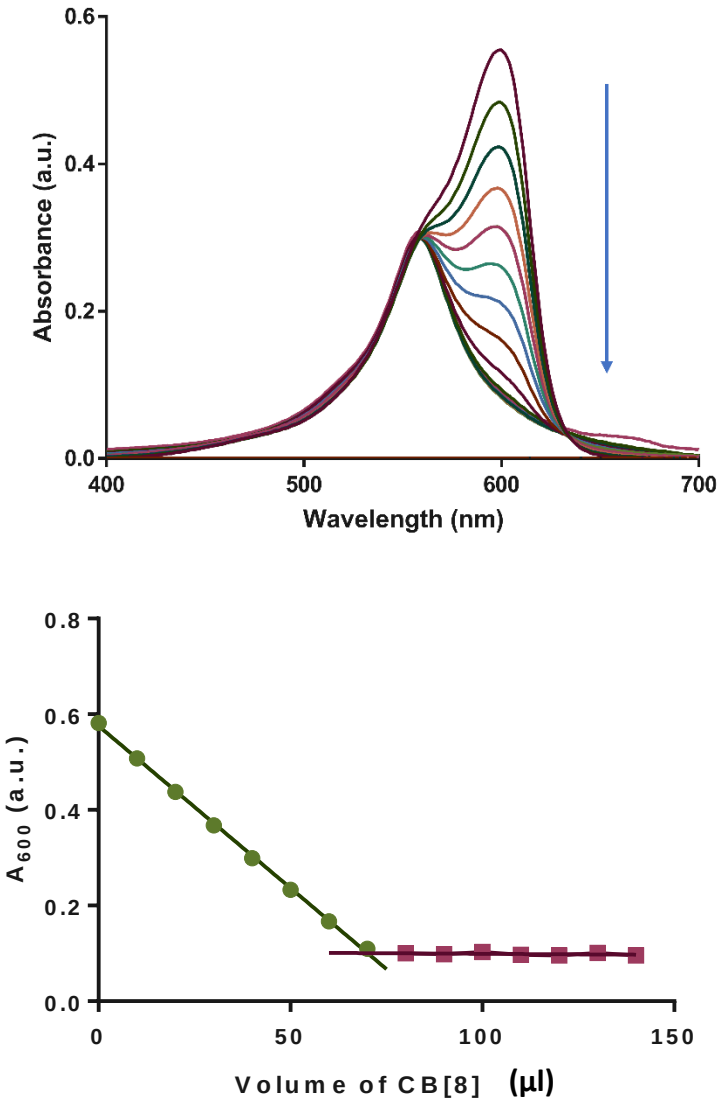

Figure 5.13. top: plot of the absorption spectra obtained during the titration of TH with the standardized solution of CB[8]; b) bottom of the absorbance at 599 nm vs the volume of CB[8] solution added.

5.9 The displacement of the dye

To understand if the idea presented in the *Paragraph 5.5* is valid, we synthesized a not active and already reported structural analogue of NBOMe, (from now on called F-NBOMe (**1**)), using the procedure reported in the additional information chapter. Since F-NBOMe·HCl was not completely soluble in water, I used a mixture of water: methanol 50:50 to dissolve it. The titration, as reported in *Figure 5.14*, was per-

formed by adding increasing amounts of the just prepared F-BOMe solution to a solution of CB[8]·TH_2 in buffered water pH 5.5. I followed the increase of the absorption at 599 nm until the plateau was reached. After reaching a concentration of 0.5 mM of drug, no appreciable changes are seen. As the sensing system works for a drug model, in the next section I report the results obtained with real drugs and some potential interferents.

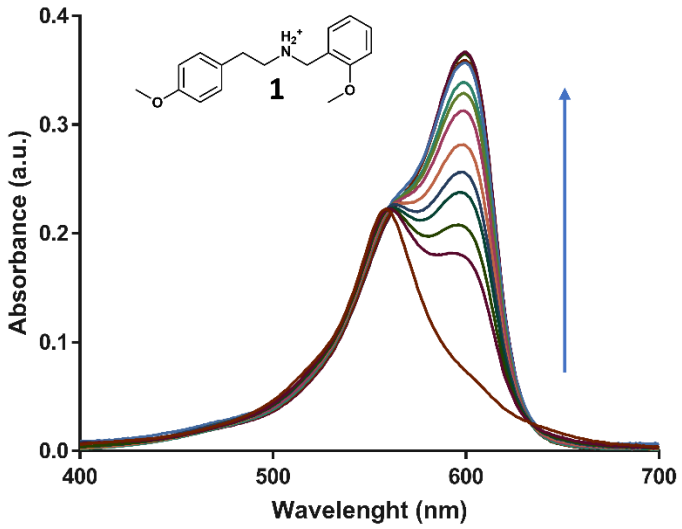

Figure 5.14. Chemical structure of **1** at the pH used for the titration and plot of the displacement titration of a solution of CB[8]@TH_2 complex with **1**.

5.10 Analysis of drugs and interferents

To check if there could be a selectivity among different analytes, the experiments were performed on a series of molecules, reported in *Figure 5.15*. The first one is a 25C-BOMe (**2**), a real representative of the NBOMes: since it has the methoxy groups in different positions than **1**, it's bulkier and the response of the sensor could in principle be different. The other molecules are LSD (**3**), a potential interferent that is often sold absorbed on blotter paper, just as NBOMes; cocaine (**4**), a widely diffused drug, and 3,4-methylenedioxyphenethylamine (**5**) a non-regulated analogue of MDMA. I also chose some non-drug interferents, common substances

that any person, stopped for a random control, could likely have with them: acetyl-salicylic acid (**6**, Aspirin®), naproxen (**7**), and lactose (**8**), a sugar that is often used as an excipient to make any kind of pills, so it's important that it does not give false positives. As last, I tried nicotinamide (**9**). The displacement titrations have been performed as described in the previous paragraph. The complete titration curves are reported in the additional information paragraph at the end of the chapter (*Figure 5.26*).

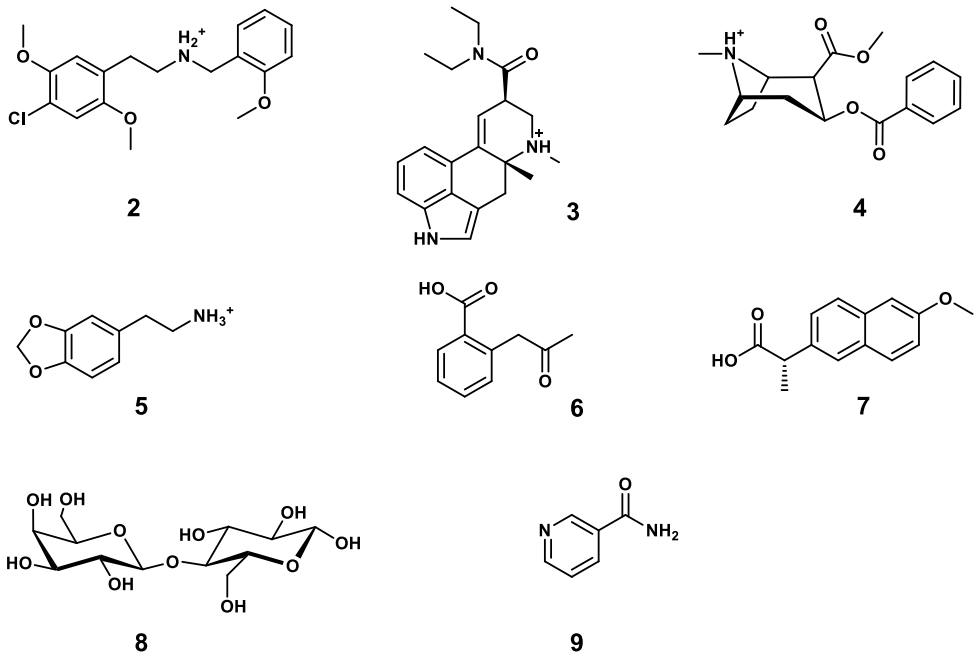

Figure 5.15: analytes used to test the colorimetric sensor.

To understand if the system really is selective, I defined a "response factor", R_{599}^{100}, defined as the difference between the absorbance value at 599 nm when the concentration of analyte reached 100 μM (A_{599}^{100}), and the absorbance at the beginning of the titration (A_{599}^{0}). The value obtained is multiplied by a factor 10 to get R_{599}^{100}. The response factor obtained for each drug is plotted in the histogram in *Figure 5.16*. The value of 100 μM is not arbitrary, but it's the value where the difference between the target analyte **2** and all the other molecules is at its maximum.

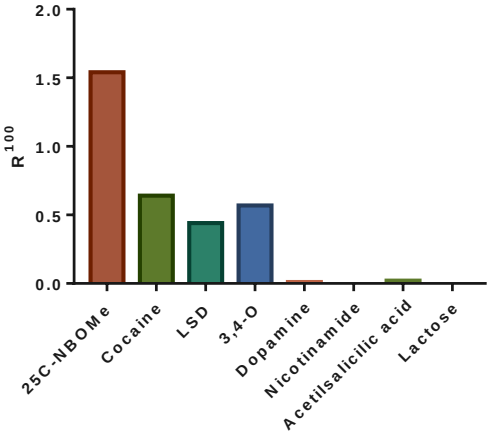

Figure 5.16. Plot of the response factor R_{599}^{100} for the analytes used.

From the histogram it clearly appears that the **2** is the only molecule having a value of R_{599}^{100}, higher than 1 (1.54) and the closer interferents are **4** (0.64), **5** (0.57) and **3** (0.44), with a value of R_{599}^{100} that is over two times smaller than the one of the target drug. All the other interferents considered have a value close to 0. Setting a decisional limit for the response factor, it is possible to discriminate, once set the concentration, the 25C-NBOMe from the other drugs.

5.11 The fluorescent alternative

A system analogue to the one just discussed, but working on fluorescence instead of absorption, would have two main advantages: first of all, the range of explored concentrations could be larger, thus reaching a lower detection limit; secondly, an on-off signal in fluorescence could be clearly visible also by naked-eye with the aid of an UV lamp. The variation must be of course clear, so from on (all emissive) to off (all quenched), otherwise discriminating two slightly different fluorescence intensities by naked eye could be challenging. Therefore, I characterized a second system, analogue to the one just described, but with a different dye: oxonine (OX). Oxonine is not commercial, but the two-step synthesis needed to obtain it is straightforward. I synthesized it with small modifications to an already reported

synthesis, starting from commercial oxazine, performing a double nitration with sodium nitrite in acetic acid and a subsequent reduction with iron in hydrochloric acid. I chose oxonine among all the possible tricyclic dyes because it has a unitary fluorescence yield when free in solution, that falls to 0.3 when complexed as a dimer inside CB[8]. The preliminary steps for the characterization of the sensor are the same as for the TH. The emission spectrum of OX consists in a band with maximum at 602 nm that upon complexation with CB[8] decreases and undergoes a red shift (*Figure 5.17*). The displacement titrations have been performed with analytes selected from the ones used before (molecules **2**-**9**). The response factor R_{602}^{5} in this case is defined as the difference between the emission value at 602 nm when the concentration of analyte reached 5 μM and the emission at the beginning of the titration, and it is reported in *Figure 5.18*. In this case, the selectivity for 25C-NBOMe is less evident (the response is just double than the one of cocaine), but the difference in reactivity between drugs (positive response) and interferents (no response) is retained. The difference between the two systems may be due to the fact that the cumulative complexation constant for OX with CB[8] is two orders of magnitude lower than the one of TH. This makes the complex less stable and the displacement of the dye easier.

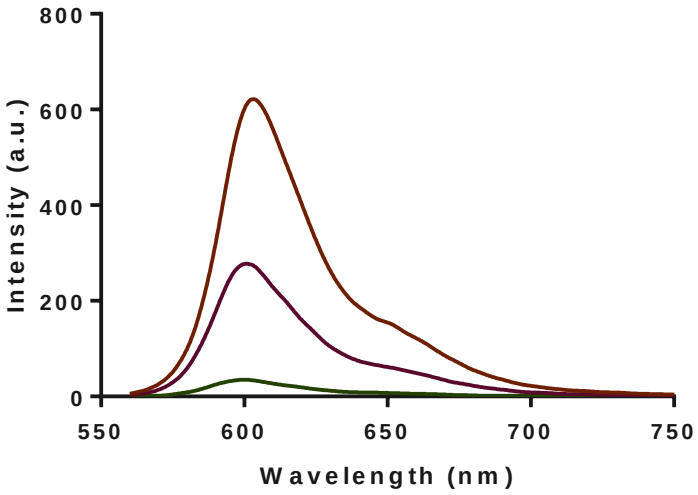

Figure 5.17 plot of the fluorescence emission spectra of OX obtained for increasing amounts of CB[8] added.

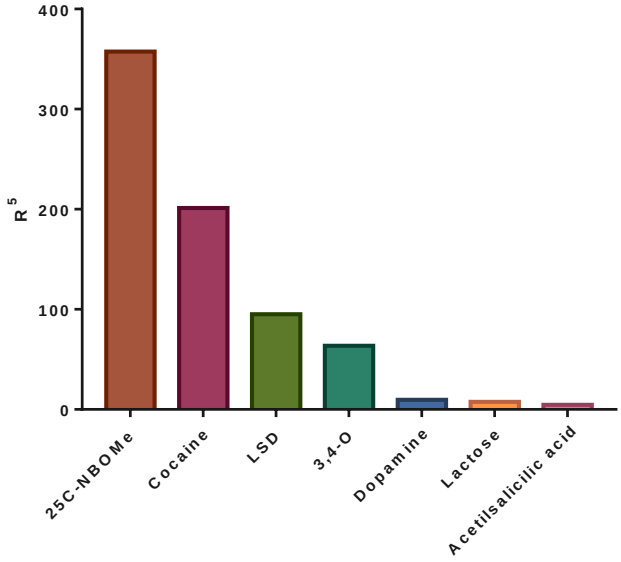

Figure 5.18. Plot of the response factor R^5_{602} for the analytes used

5.12 NMR and ESI-Mass analysis

To confirm the mechanism of displacement of the tricyclic dyes from the CB[8] cavity, I performed some ^{1}H-NMR and ESI mass analysis. For TH, the results are reported in *Figure 5.19*. Spectrum a) is the spectrum of TH in solution, characterized by three signals (two doublets and one singlet); when CB[8] is added to the solution (spectra b to d) a new set of signals is appears, where all the signals are doubled and up-field shifted.

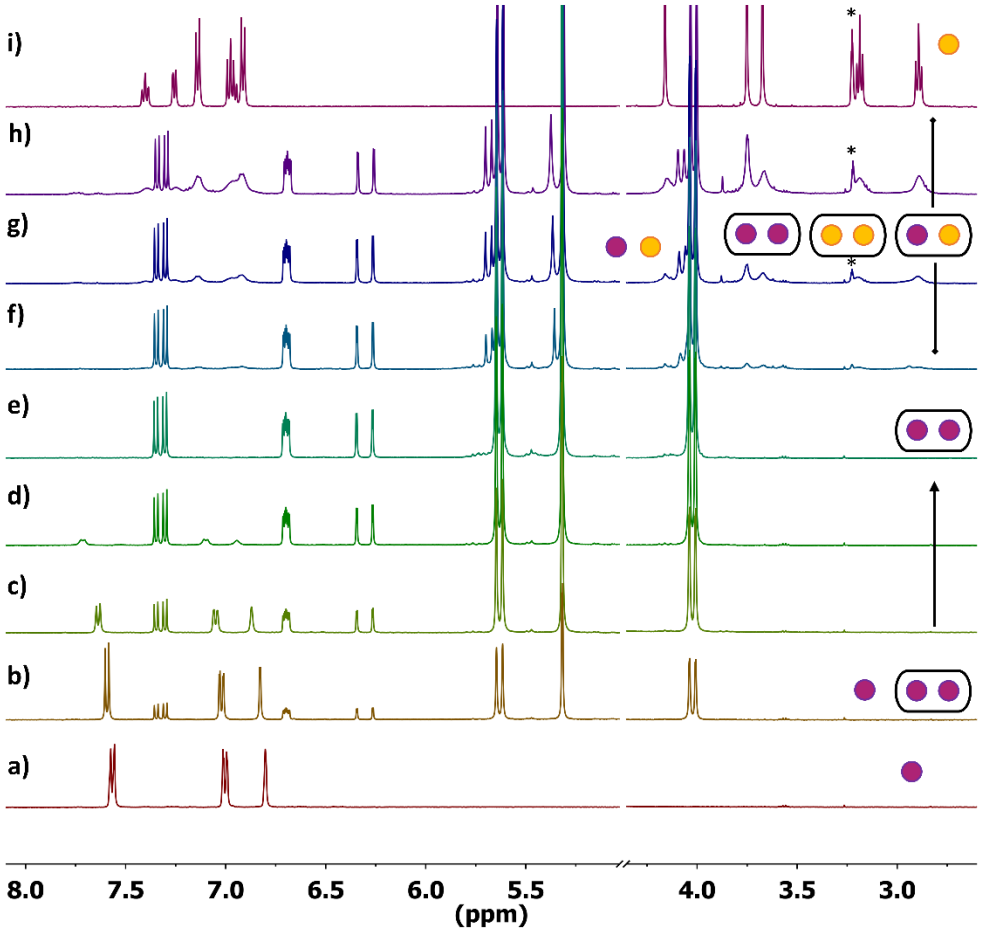

Figure 5.19. ^{1}H-NMR spectra in D_2O 10 mM pD= 5.5 of: a) TH 2 mM; b) TH 2 mM and CB[8] 0.25 mM; c) TH 2 mM and CB[8] 0.5 mM; d) TH 2 mM and CB[8] 0.75 mM; e) TH 2 mM and CB[8] 1 mM corresponding to the spectrum of CB[8]@TH_2; f- h) spectra with increasing concentrations of 1 (0.5, 1, 2 mM); i) **1** 1 mM.

This confirms the formation of CB[8]@TH_2 complex, in slow exchange regime, were the symmetry of the TH is not present anymore, because of the paring in the cavity with a second TH molecule. At the same time, the signals of the free TH, experience a down-field shift and a pronounced broadening as the amount of cucurbituril added increases. This could suggest the presence of also the CB[8]@TH complex, with 1:1 stoichiometry, but this is apparently in fast exchange with the free form. In the spectrum e, only the signals of the CB[8]@TH_2 are present in the spectrum. When molecule **1** is added, a new set of broad signals as if in solution would be present CB[8]@TH_2 and a second specie, probably CB[8]@$\mathbf{1}_2$. At the same time, some TH is pushed out from the cavity because the signals of the free specie are again visible. Interestingly, the signals of **1** (reported in spectrum i) undergo significant broadening when added to the CB[8]@TH_2

solution. This means either that the complexation is not in slow exchange on the NMR timescale or that some rotational modes of **1** are hampered when complexed in CB[8]. The latter hypothesis is suggested also from the fact that not all the signals of **1** experience the same broadening. As the free TH is not fully restored even after of excess of **1** (spectrum h), this suggest that mixed species as CB[8]@TH@**1** can be formed. To understand better the stoichiometry of the possible complexes formed some ESI mass analysis have been performed. From the Figure 5.20 it is possible to see clearly the formation of the double charged species CB[8]@TH_2, CB[8]@$\mathbf{1}_2$, CB[8]@TH@1, as well as CB[8]@**1**. No considerations can be made about the relative amounts of these species in solution.

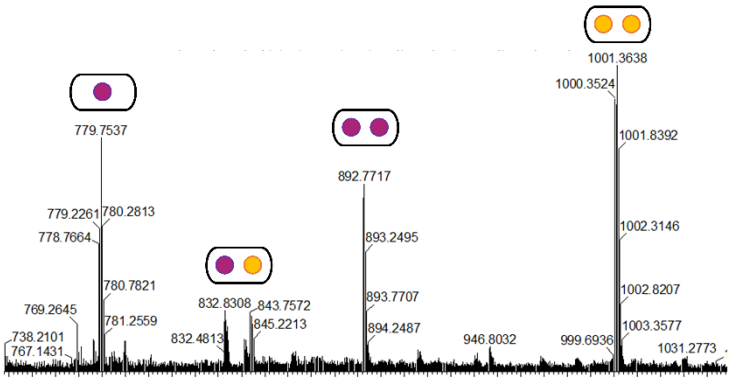

Figure 5.20. ESI-mass spectrum D_2O of a mixture of CB[8]@TH_2 50 μM and **1** 0.5 mM. With the yellow dot is schematized the analyte **1**, with the purple one, the thionine TH.

Subsequently, I performed the same experiments with OX: in this case as well the signals of the free dye are split in two sets and undergo high field shift. However, after addition of **2**, a second set of cucurbituril signal appeared, suggesting the formation of the complex CB[8]@OX_2. This is confirmed also from the fact that the signals of free OX appear again, with no shift compared to the ones of the free molecule. So, with this system the stoichiometry appears simpler than in the previous case (*Figure 5.21*).

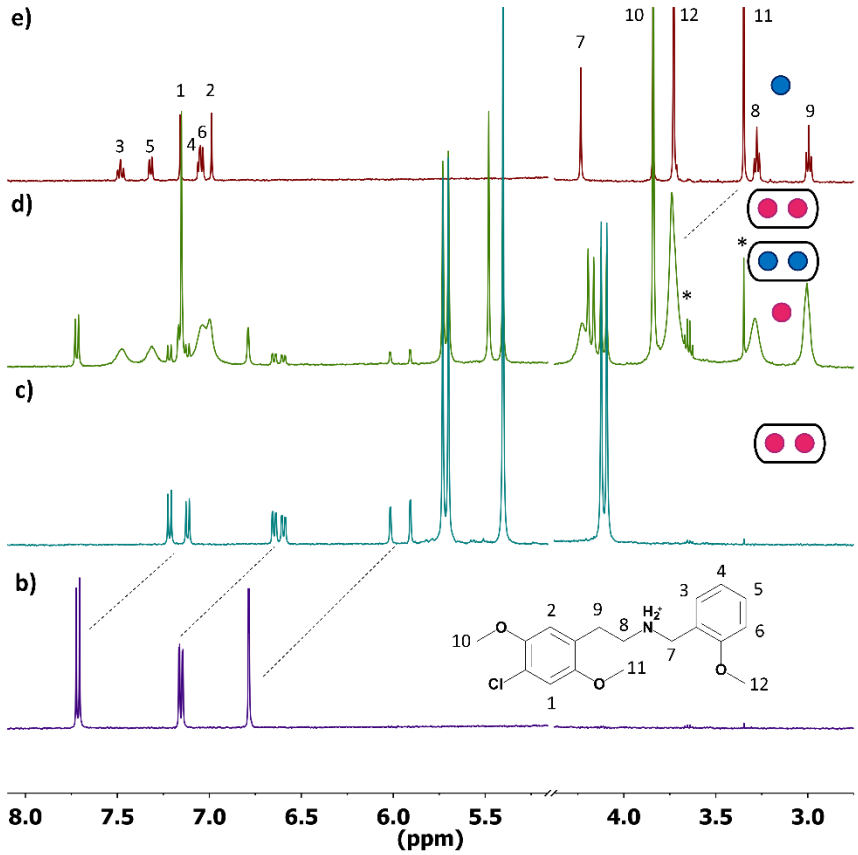

Figure 5.21. ^{1}H-NMR spectra in D_2O 10 mM pD= 5.5 of: a) OX 2 mM; b) OX 2 mM and CB[8] 1 mM corresponding to the complex CB[8]@OX2; c) OX 2 mM and CB[8] 0.5 mM and **2** 1 mM; d) **2** 2 mM and CB[8] 0.75 mM;

The ESI mass analysis confirms in this case the absence of the mixed complexes. The most relevant ones (double charged) are CB[8]@**2** (also with a Na^+ adduct) and CB[8]@$\mathbf{2}_2$.

Probably the difference in the complexation equilibria is the reason of the difference in selectivity in the two presented tests. Further investigations are needed to understand exactly the dynamics of the TH-CB[8] system.

Figure 5.22. ESI-mass spectrum D_2O of a mixture of CB[8]@OX_2 50 μM and **1** 0.5 mM. In yellow is reported the 25C-NBOMe.

5.13 Paper test

The variation of absorbance takes place in the visible region; moreover, at the concentrations used, the change from purple to blue can also be detected by naked eye. For this reason, I decided to support the sensor on a paper strip, so as to have a handy device that could give a visible colour change when exposed to NBOMes. If we think about it, colorimetric pH indicator papers are widely used for quick detection of pH variations when a fast and qualitative response is needed, even if more accurate methods (pH-meter) are available.

To create the test paper, I prepared a buffered 100 μM solution of the CB[8] complex, and soaked some small pieces of filter paper in it. After removal of the excess solution, I dried them with absorbent paper and let them dry at room temperature for 15 minutes. The test of the drug is as simple as exposing the paper to a small drop (1 μl) of a 10 mM aqueous solution of the drug. The response is considered positive when the wetted region of the paper turns immediately to light blue. The colour change persists even when the paper dries again. In *Figure 5.23* I reported the pictures of the paper after the deposition of different analytes and interferents.

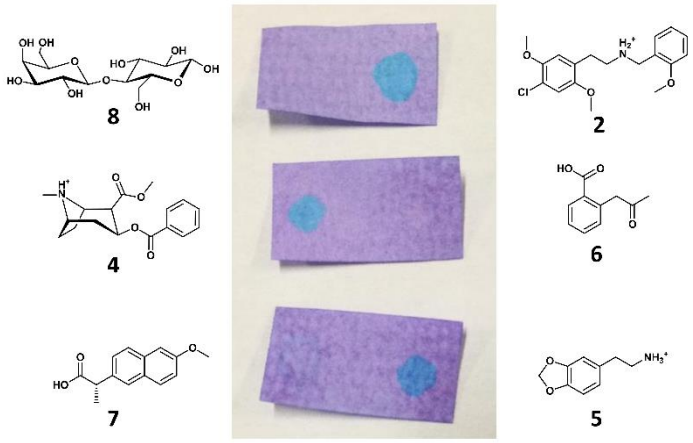

Figure 5.23. Picture of the strips exposed to different analytes.

The selectivity found in solution is not matched by the strip test, so the colorimetric paper is not able to discriminate among different drugs, but it's an effective way to understand if the suspected analyte is a drug or not, since the colour change is not generated by the addition of the interferents. The test gives positive response to 25C-NBOMe, LSD, cocaine, MDMA and various amphetamine and methamphetamine analogues. It's not sensitive to variations of pH and it gives negative response to acetylsalicylic acid, paracetamol, sugars (lactose, sucrose…), nicotinamide. The reason of the lower selectivity loss due to the operating concentrations: in the spectrophotometric experiments, micromolar analyte solutions were used. In the case of the strip test, the local concentration in the region wetted by the drop is 10 mM and probably higher, as the water is diffusing freely on paper, but the same does not happen for organic molecules (in a TLC fashion). So, even molecules that in solution need a higher concentration to displace the TH from CB[8] give positive response to the strip test. Any attempt to decrease the concentration of the analyte solutions to get back the selectivity failed: 2 to 10-fold dilutions were tried, but all the drugs still gave the positive signal, just with a lower intensity. So, 10 mM appears to be the best compromise between the amount of illicit substance needed, and the easiness of detection of the colour variation. I performed a stability test, keeping the strips for four months at room temperature in a sealed plastic jar (to prevent dust deposition) and the reactivity was not perturbed.

There are some caveats for the use of the test. First of all, the analyte must be dissolved in water (or methanol), otherwise the paper could give a false negative response. This could have a two reasons: paper is highly hydrophilic, so polar protic solvents are needed to effectively wet the strip, and bring the analyte close to the CB[8]·TH_2 complexes trapped between the paper fibres. Second, as the complexation equilibrium is dynamic, to get the displacement of the TH from the CB[8] cavity, not only the analyte but also the CB[8]·TH_2 complex must be solvated. Methanol and water can dissolve it, but, for example, acetonitrile cannot. The strip test can't be exposed to heat sources, otherwise the background colour is not homogeneous, and the interpretation could be difficult.

5.14 The real sample

I tested the sensor on a sample of what we suspected was NBOMe, seized by the police from the illegal market. The sample presents itself as a small piece of blotter paper (5mm square) with a smiling face of the comic character "Felix the cat" printed on it (*Figure 5.24 a*). I extracted the active principle as follows: I placed the blotter paper in a vial with 2 ml of ethanol and left it in ultrasound bath for ten minutes; then I centrifuged (1 min, 10k rpm). I then removed the ethanol and rinsed the blotter paper again with another millilitre of ethanol. After evaporation of the ethanol, I obtained 1 mg of colourless sticky residue. The blotter paper remains intact after the treatment, no paper fibres are left in the solution after centrifugation and no colour from the picture is transferred to the ethanol. I considered the so obtained residue as 100% active principle and I dissolved it in a 50:50 solution of D_2O:MeOD, so to have a 10mM solution. The displacement titration reported in *Figure 5.24 d* shows that the trend is basically the same that for 25C-NBOMe. Some scattering is present for concentrations above 100 μM, probably due to different substances (glue) extracted from the blotter paper.

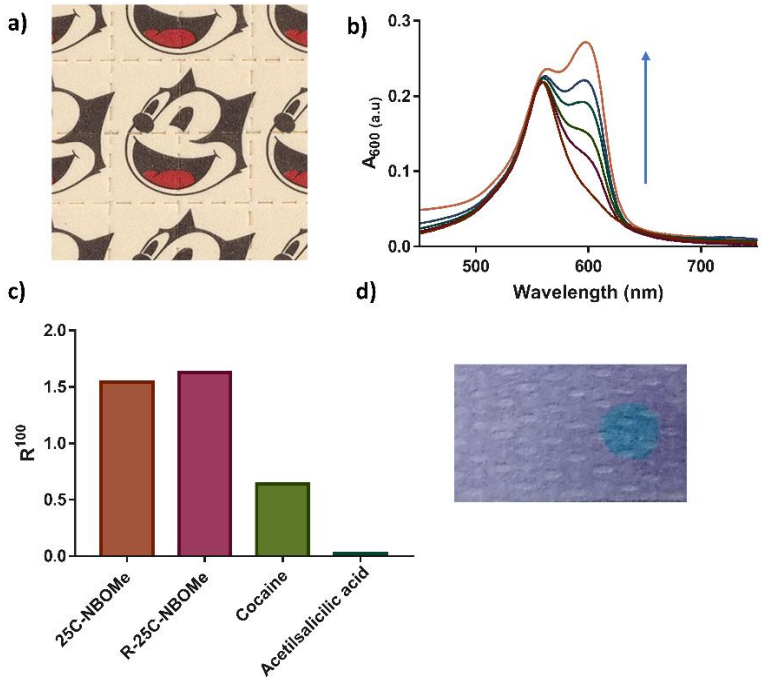

Figure 5.24. a) real retail sample of NBOMe absorbed on blotter paper; b) displacement titration; c) response factor histogram d) strip test exposed to 1µl of the NBOMe solution

The response value of 1.63, it's really close to the one of the standard molecule **2** (1.54). In *Figure 5.24 c* I reported the histogram with the values of **2**, **4**, and **6** for comparison. A strip test exposed to the real sample gives, as expected, a positive response (*Figure 5.24 d*).

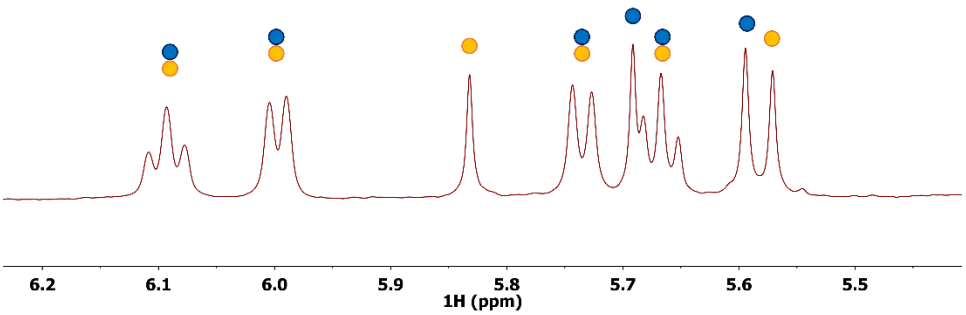

Figure 5.25. detail of the aromatic region peaks of ^{1}H-NMR spectrum of the seized NBOMe sample in MeOD. The colourful circles show the presence of two different NBOMe molecules in solution.

Analysis by ^{1}H-NMR spectrum confirmed that the substance on the blotter paper was indeed NBOMe (*Figure 5.25*). As two sets of signals are visible, a mixture of two different analogues in different proportions was absorbed on the blotter paper

most probably, 25C (blur circles) and 25B-NBOMe (yellow), judging from the chemical shifts

5.15 Conclusions

Considered the increasing importance that new hazardous drugs of abuse, in the form of designer drugs, are gaining in the illegal market, new sensing devices are needed to contrast this phenomenon. The sensing systems need to be easy to use, safe, not expensive and they need to be up to date with the drugs available on the illegal market. For on-field detection, a point-of-care detection method is as important as precise analytical techniques, because it can discriminate if a suspicious material is a drug or not in little time. Some sensors that use the properties of complexes between tricyclic dyes and cucurbiturils have been already reported in the literature, even for the sensing of drugs of abuse. This kind of sensors take advantage of arrays that discriminate the analytes according to their response in different conditions (size of cucurbituril, dye, solvent, concentration). As already stated in the beginning of this chapter, the aim of this section was to develop a simple, non-toxic method for the selective detection of NBOMes that can be used by non-trained personnel. Considered the portable dimensions of spectrophotometers nowadays, I thought that a colorimetric sensor could be the election technique. Moreover, for the exact characterization of a colour, new smartphone apps are available. Combined with the smartphone camera, they can extrapolate the wavelength of a colour by simply filming it. To this purpose, I have shown that the complex CB[8] ▪ TH_2 can be used as colorimetric indicator for 25C-NBOMe (**2**) detection in buffered water. In a displacement essay, the intensity increase of the absorption band of free TH can be used to discriminate if the drug under analysis is 25C-NBOMe. The reactants are cheap and easy to find, they are not harmful, and the analysis is quick and easy to perform, the amount of illicit substance needed is really small (less than 0.1 mg). The system is capable to discriminate 25C-NBOMe from other drugs of abuse, with the only possible interferents being cocaine (**4**) and LSD (**3**), that give a partial positive response. Amphetamine and methamphet-

amine analogues, as well as common excipients, don't give a positive signal. In addition to this, since the variation of absorbance is in the visible region and since at the concentrations used the colour variation is clear also by naked eye, I explored the possibility to immobilize the system on paper to create a drug strip test. The paper test shows a colour change from violet to light blue when exposed to a drug solution. In this test the selectivity is not retained, but it can discriminate drugs from common legal substances such as painkillers or sugars. I have shown an analogous sensor working in emission. It is based on the complex CB[8]@OX_2 and in this case it is not selective for 25C-NBOMe, but it can still discriminate the drugs from common legal substances.

Supplementary information

General

Solvents were purified by standard methods. Thionine acetate, CB[7], CB[8], and all the reagents needed for the synthesis of oxonine were commercially available and were used as received.

Standards of psychotropic drugs, were purchased from Cerilliant, through Sigma-Aldrich, as 1mg/ml solution of the drug hydrochloride. 25C-NBOMe and LSD were available as methanol solutions, cocaine as acetonitrile solution. The cocaine standard has been evaporated and dissolved in methanol. All the samples were treated under the authorization of Italian Ministero della Salute granted to Prof. Fabrizio Mancin for research purposes (SP/001, 10/01/2019).

TLC analyses were performed using Merck 60 F254 precoated silica gel. Column chromatography was carried out on Macherey-Nagel silica gel 60 (70-230 mesh).

NMR spectra were recorded using a Bruker AV III 500 spectrometer operating at 500 MHz for ^{1}H, 125.8 MHz for ^{13}C. Chemical shifts are reported relative to internal Me_4Si. Multiplicity is given as follow: s = singlet, d = doublet, t = triplet, q = quartet, qn = quintet, m = multiplet, br = broad peak.

ESI-MS mass spectra were obtained with an Agilent Technologies LC/MSD Trap SL mass spectrometer.

Fluorescence spectra were recorded on a Perkin Elmer LS50B fluorimeter with thermostated cell holder (25°C), using quartz cuvettes l=1cm.

UV-Vis spectra were recorded on a Varian-Agilent Cary 50 with thermostated cell holder (25°C), using quartz cuvettes l=1cm.

Cobaltocene solution

The cobaltocene solution has been prepared dissolving 3.3 mg of $CobPF_6$ in 50 ml of ultrapure water to obtain a 200 μM solution (MM = 334,08 g mol^{-1}). The exact concentration of the solution has been calculated using the value of ε reported in literature (ε_{261} = 34200 cm^{-1} M^{-1})

Synthesis of oxonine

The synthesis of oxonine has been performed with little modifications of a literature procedure by Maas et al.

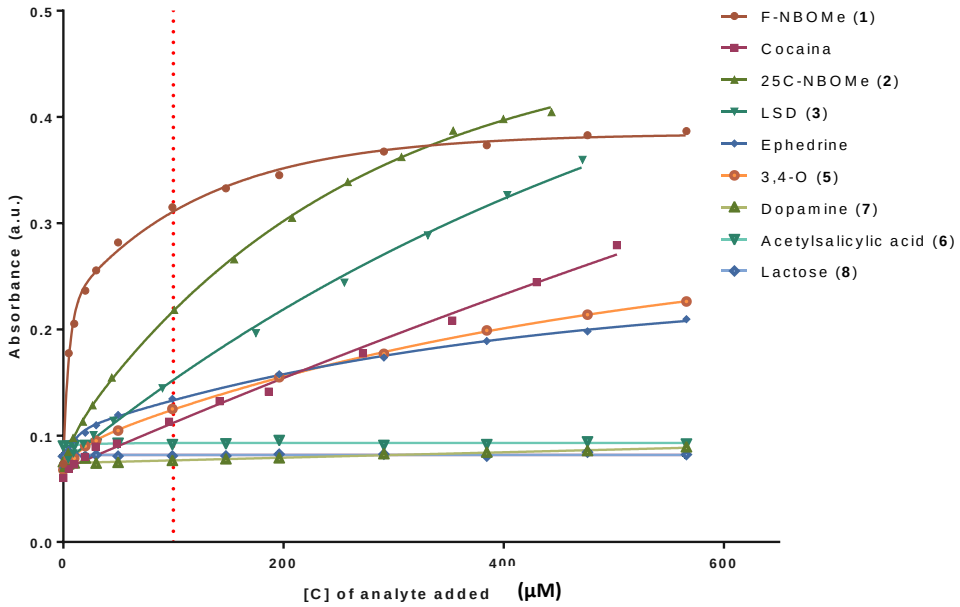

Figure 5.26. Plot of displacement titrations, obtained with different molecules for the system CB[8]@OX_2.

The titration of all the analytes have been done adding increasing amounts of the analyte solutions to a 5 μM solution of CB[8]·TH_2.For the analytes **5**, **6**, **7**, **8**, **9** we used a solution 10 mM in water, for analyte **1** a solution of the chlorhydrate 10 mM in water and methanol 50:50. Analyte **2** was used as purchased, in a standard solution 2.98 mM in methanol. Analytes **3** and **4** sold respectively as a 3.09 and 3.30 mM solution in acetonitrile where dried and dissolved in the same amount of methanol. R-BOME was dissolved in a mixture of water and methanol 50:50 to get a solution 10 mM. The ab-

sorbance at 599 nm obtained from the titration curves was corrected for the dilution and plotted against the concentration of analyte added.

Dilution an methanol effect on the stability of CB[8]·TH_2

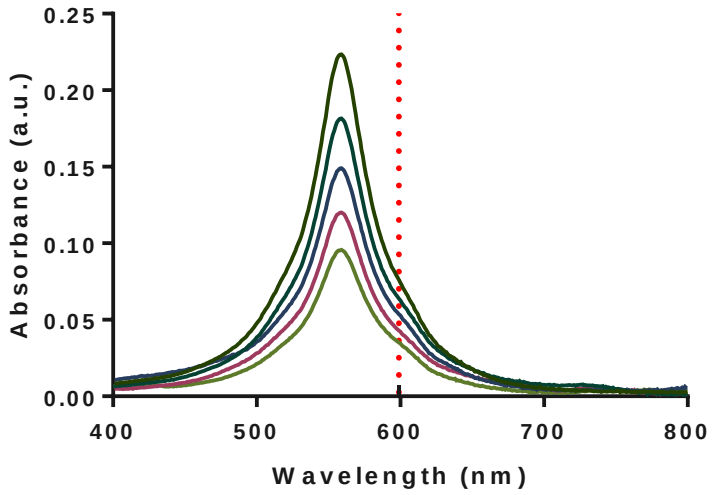

Figure S6. Spectra obtained after addition of 0, 200, 400, 600 and 800 µl of water to 1 ml solution of 5 µM CB[8]·TH_2

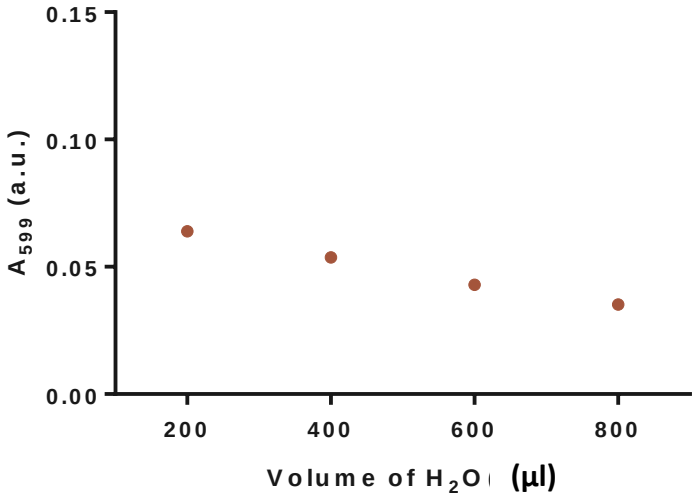

Figure S7. Plot of the absorbance at 599 nm obtained from the spectra shown in Fig. S6. As the plot is linear with the additions of water, there is only a dilution effect and the complexation equilibrium of CB[8]·TH_2 is not affected.

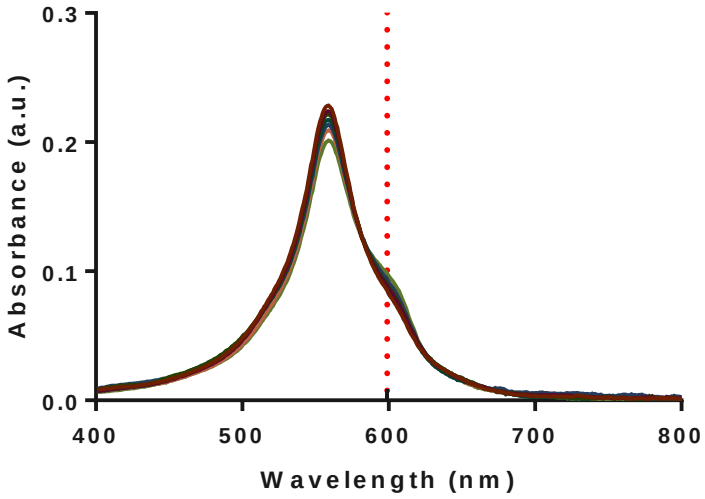

Figure S8. Spectra obtained after addition of 0, 20, 40, 60, 80 and 100 µl of water to 1 ml solution of 5 µM CB[8]·TH_2

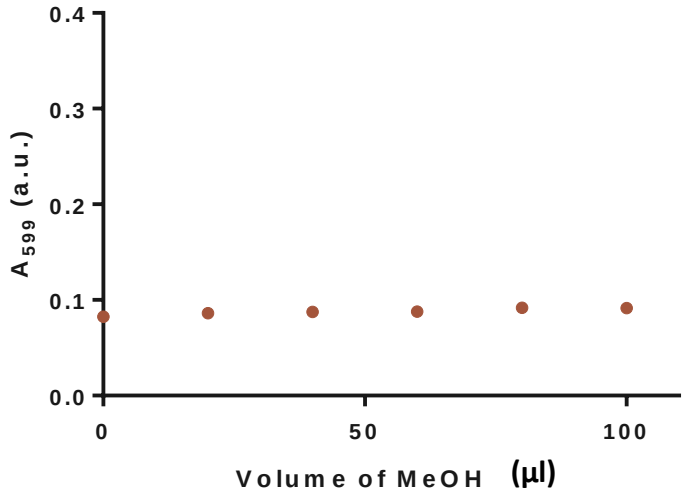

Figure S8. . Plot of the absorbance at 599 nm obtained from the spectra shown in Fig. S6. The complexation equilibrium of CB[8]·TH_2 is affected in a negligible way by the addition of MeOH

The complex CB[8]·TH_2 is stable upon dilution with water and the effect of the addition of methanol is negligible at the concentrations use in this work.

Bibliography

(1) Gabrielli, L.; Rosa-Gastaldo, D.; Salvia, M. V.; Springhetti, S.; Rastrelli, F.; Mancin, F. Detection and Identification of Designer Drugs by Nanoparticle-Based NMR Chemosensing. *Chem. Sci.* **2018**, *9* (21), 4777–4784.

(2) Baudot, P.; Andre, J. C. A Low-Cost Differential Fluorimeter for the Detection and Determination of LSD in Illicit Preparations. *J. Anal. Toxicol.* **1983**, *7* (2), 69–71.

(3) Morris, J. A. Modified Cobalt Thiocyanate Presumptive Color Test for Ketamine Hydrochloride. *J. Forensic Sci.* **2007**, *52* (1), 84–87.

(4) Argente-García, A.; Jornet-Martínez, N.; Herráez-Hernández, R.; Campíns-Falcó, P. A Passive Solid Sensor for In-Situ Colorimetric Estimation of the Presence of Ketamine in Illicit Drug Samples. *Sensors Actuators, B Chem.* **2017**, *253*, 1137–1144.

(5) Matsuda, K.; Fukuzawa, T.; Ishii, Y.; Yamada, H. Color Reaction of 3,4-Methylenedioxyamphetamines with Chromotropic Acid: Its Improvement and Application to the Screening of Seized Tablets. *Forensic Toxicol.* **2007**, *25* (1), 37–40.

(6) Masseroni, D.; Biavardi, E.; Genovese, D.; Rampazzo, E.; Prodi, L.; Dalcanale, E. A Fluorescent Probe for Ecstasy. *Chem. Commun.* **2015**, *51* (64), 12799–12802.

(7) Garrido, E.; Pla, L.; Lozano-Torres, B.; El Sayed, S.; Martínez-Máñez, R.; Sancenón, F. Chromogenic and Fluorogenic Probes for the Detection of Illicit Drugs. *ChemistryOpen*. Wiley-VCH Verlag May 1, 2018, pp 401–428.

(8) Shi, Q.; Shi, Y.; Pan, Y.; Yue, Z.; Zhang, H.; Yi, C. Colorimetric and Bare Eye Determination of Urinary Methylamphetamine Based on the Use of Aptamers and the Salt-Induced Aggregation of Unmodified Gold Nanoparticles. *Microchim. Acta* **2014**, *182* (3–4), 505–511.

(9) Behrend, R.; Meyer, E.; Rusche, F. I. Ueber Condensationsproducte Aus Glycoluril Und Formaldehyd. *Justus Liebigs Ann. Chem.* **1905**, *339* (1), 1–37.

(10) Freeman, W. A.; Mock, W. L.; Shih, N. Y. Cucurbituril. *J. Am. Chem. Soc.* **1981**, *103* (24), 7367–7368.

(11) Assaf, K. I.; Nau, W. M. Cucurbiturils: From Synthesis to High-Affinity Binding and Catalysis. *Chemical Society Reviews*. Royal Society of Chemistry January 21, 2015, pp 394–418.

(12) Barrow, S. J.; Kasera, S.; Rowland, M. J.; Del Barrio, J.; Scherman, O. A. Cucurbituril-Based Molecular Recognition. *Chemical Reviews*. American Chemical Society 2015, pp 12320–12406.

(13) Day, A.; Arnold, A. P.; Blanch, R. J.; Snushall, B. Controlling Factors in the Synthesis of Cucurbituril and Its Homologues. *J. Org. Chem.* **2001**, *66* (24), 8094–8100.

(14) Pemberton, B. C.; Singh, R. K.; Johnson, A. C.; Jockusch, S.; Da Silva, J. P.; Ugrinov, A.; Turro, N. J.; Srivastava, D. K.; Sivaguru, J. Supramolecular Photocatalysis: Insights into Cucurbit[8]Uril Catalyzed Photodimerization of 6-Methylcoumarin. *Chem. Commun.* **2011**, *47* (22), 6323–6325.

(15) Walker, S.; Oun, R.; McInnes, F. J.; Wheate, N. J. The Potential of Cucurbit[n]Urils in Drug Delivery. *Israel Journal of Chemistry*. May 2011, pp 616–624.

(16) Gürbüz, S.; Idris, M.; Tuncel, D. Cucurbituril-Based Supramolecular Engineered Nanostructured Materials. *Org. Biomol. Chem.* **2015**, *13* (2), 330–347.

(17) Jang, Y.; Jang, M.; Kim, H.; Lee, S. J.; Jin, E.; Koo, J. Y.; Hwang, I. C.; Kim, Y.; Ko, Y. H.; Hwang, I.; et al. Point-of-Use Detection of Amphetamine-Type Stimulants with Host-Molecule-Functionalized Organic Transistors. *Chem* **2017**, *3* (4), 641–651.

(18) Baumes, L. A.; Sogo, M. B.; Montes-Navajas, P.; Corma, A.; Garcia, H. A Colorimetric Sensor Array for the Detection of the Date-Rape Drug γ-Hydroxybutyric Acid (GHB): A Supramolecular Approach. *Chem. - A Eur. J.* **2010**, *16* (15), 4489–4495.

(19) Poklis, J. L.; Raso, S. A.; Alford, K. N.; Poklis, A.; Peace, M. R. Analysis of 25I-NBOMe, 25B-NBOMe, 25C-NBOMe and Other Dimethoxyphenyl-N-[(2-Methoxyphenyl) Methyl]Ethanamine Derivatives on Blotter Paper. *J. Anal. Toxicol.* **2015**, *39* (8), 617–623.

(20) Oiye, É. N.; Midori Toia Katayama, J.; Fernanda Muzetti Ribeiro, M.; de Oliveira, M. F. Electrochemical Analysis of 25H-NBOMe by Square Wave Voltammetry. *Forensic Chem.* **2017**, *5*, 86–90.

(21) Chung, H.; Lee, J.; Kim, E. Trends of Novel Psychoactive Substances (NPSs) and Their Fatal Cases. *Forensic Toxicol.* **2016**, *34* (1), 1–11.

(22) Botch-Jones, S.; Foss, J.; Barajas, D.; Kero, F.; Young, C.; Weisenseel, J. The Detection of NBOMe Designer Drugs on Blotter Paper by High Resolution Time-of-Flight Mass Spectrometry (TOFMS) with and without Chromatography. *Forensic Sci. Int.* **2016**, *267*, 89–95.

(23) Carvalho, T. C.; Oliveira, I. F.; Tose, L. V.; Vanini, G.; Kill, J. B.; Neto, A. C.; MacHado, L. F.; Ambrosio, J. C. L.; Lacerda, V.; Vaz, B. G.; et al. Qualitative Analysis of Designer Drugs by Paper Spray Ionisation Mass Spectrometry (PSI-MS). *Anal. Methods* **2016**, *8* (3), 614–620.

(24) Boumba, V. A.; Di Rago, M.; Peka, M.; Drummer, O. H.; Gerostamoulos, D. The Analysis of 132 Novel Psychoactive Substances in Human Hair Using a Single Step Extraction by Tandem LC/MS. *Forensic Sci. Int.* **2017**, *279*, 192–202.

(25) Montes-Navajas, P.; Corma, A.; Garcia, H. Complexation and Fluorescence of Tricyclic Basic Dyes Encapsulated in Cucurbiturils. *ChemPhysChem* **2008**, *9* (5), 713–720.

(26) Yi, S.; Kaifer, A. E. Determination of the Purity of Cucurbit[n]Uril (n = 7, 8) Host Samples. *J. Org. Chem.* **2011**, *76* (24), 10275–10278.

(27) Ong, W.; Kaifer, A. E. Unusual Electrochemical Properties of the Inclusion Complexes of Ferrocenium and Cobaltocenium with Cucurbit[7]Uril. *Organometallics* **2003**, *22* (21), 4181–4183.

Overall conclusion and perspectives

In this work I described the development of the NMR-chemosensing method for the detection of designer drugs and biologically relevant amines. This technique is based on the combination of gold nanoparticles with a core diameter of about 2 nm and specific ^{1}H-NMR experiments. AuNPs are coated with specific functional thiols that allow their interaction with the target analyte. I showed that a thiol terminated with a negative charge (sulfonate) or with a crown ether allows the AuNPs to interact with phenethylamine derivatives that at physiological pH feature a positively charged amine in their structure. The studies performed confirmed that ion pairing is not the only driving force of recognition, but the hydrophobic effect plays a crucial role as well. Moreover, also the conformation of the monolayer can affect the interaction capability of the AuNPs, so when designing a sensor is important to consider these interactions not individually, but as a whole.

Few key points still need to be better understood and optimized. In particular we still do not control the influence of the thiol chemical structure on the organization of the monolayer, and, consequently, the sensing capabilities of the AuNP. A deeper insight on how a functional group (length of alkyl chain, amide, charge…) influences the properties of the monolayer, could allow a more effective sensor design, avoiding the trials and errors approach substantially followed so far.

A second point to understand is which is the optimal value of K_a that allows the best NMR response of the system. Indeed, in the case of NMR chemosensing, the common sense "the greater the better" may not be correct, since the intensity of the signal produced depends not only from the fraction of analyte bound but also from the residence time and magnetization/saturation transfer efficiency. Once all this is settled, it will be possible, in principle, just combining different binding blocks, to adapt the sensing system to any class of small molecule analytes. This way, the practical use of the NMR chemosensing can be expanded, making the technique also commercially appealing for screening or analytical purposes.

As last, the possibility to have different chemosensors that work together in same sample would allow the simultaneous screening of different classes of compounds.

I have shown also how this technique is not limited to the sensing of organic compounds but it can be used, using organic reporters, also for the sensing of inorganic species.

The other improvements that can be done concern the sensitivity of the NMR chemosensing that is not yet at the instrumental limit. As I described, more than one sequence is available for the NMR chemosensing. If NOE-pumping is the most general and reliable experiment as it can't yield false positive responses, using STD (or water-mediated STD, w-STD) it is possible to reach lower detection limits. To this aim I showed as well how increasing the dimension of the sensing system (Ludox®) without affecting the sensing properties of the AuNPs leads to sensing of concentrations as little as 10 μM. Using higher field magnets and cryoprobes could lower even more this limit. Currently in our research group are under investigation signal enhancement techniques (monolayer hyperpolarization) that could, in theory, improve the detection limit.

As, for now, NMR-based sensing techniques suffer of the limitations of the NMR instruments, so they are not portable, costly and they need periodical maintenance and trained personal, I explored the possibility to use a different supramolecular approach to obtain a colorimetric test for the detection of designer drugs. I have shown how a complex of cucurbit[8]uril and thionine shows a remarkable selectivity towards N-benzyl substituted phenethylamines (N-BOMEs) and it can be used to produce a strip test for qualitative on-site and real-time detection of illicit substances. This point of care test could be further improved to get better discrimination, exploring different dyes and other analytes.

Ringraziamenti

Grazie al mio supervisore, il prof. Fabrizio Mancin, per l'opportunità che mi ha dato e per la libertà che mi ha lasciato in questi tre anni trascorsi in laboratorio. Grazie al prof. Federico Rastrelli per l'NMR e grazie a Luca. Grazie ai miei genitori, a Laura, ai nonni e alla zia Loredana. Grazie a Miina per il sostegno, per Mustu, per la transiberiana e per tutte le altre cose fatte insieme. Grazie a Federico, per i caffè, gli spritz e per i lavori condivisi. Grazie a Lucia, per essere stata la prima studente che ho seguito in laboratorio, e per le chiacchierate nei due anni trascorsi assieme in lab 207. Grazie a Giordano per i consigli sulle sintesi e per le piante carnivore. Grazie a Sun. Grazie all'altra Lucia, a Joanna, a Yanchao per aver condiviso con me questa esperienza. Grazie a Giuliano, Emil, Angelo, Claudia, Federica, Marco, Lorenzo e Nicole per avermi insegnato un sacco di cose. Grazie a tutte le altre persone passate in laboratorio in questi tre anni. E grazie a Giulia, senza neanche bisogno di dire perché.